Catalytic Inhibition of Laminar Flames by Metal Compounds

Gregory T. Linteris[1], Marc D. Rumminger[2] and Valeri I. Babushok[3]

[1]Building and Fire Research Laboratory
Fire Research Division
National Institute of Standards and Technology
100 Bureau Dr. Stop 8652
Gaithersburg MD 20899-8665

[2]Cleaire Advanced Emission Controls, LLC
14775 Wicks Blvd.
San Leandro, CA 94577-6779

[3]Chemical Science and Technology Laboratory
National Institute of Standards and Technology
100 Bureau Dr. Stop 8652
Gaithersburg MD 20899-8652

July 2007

[1] Corresponding author. Phone: 301-975-2283; fax: 301-975-4052; email: linteris@nist.gov

Abstract

Some of the most effective flame inhibitors ever found are metallic compounds. Their effectiveness, however, drops off rapidly with an increase of agent concentration, and varies widely with flame type. Iron pentacarbonyl, for example, can be up to two orders of magnitude more efficient than CF_3Br for reducing the burning velocity of premixed laminar flames when added at low volume fraction; nevertheless, it is nearly ineffective for extinction of co-flow diffusion flames. This article outlines previous research into flame inhibition by metal-containing compounds, and for more recent work, focuses on experimental and modeling studies of inhibited premixed, counterflow diffusion, and co-flow diffusion flames by the present authors. The strong flame inhibition by metal compounds when added at low volume fraction is found to occur through the gas-phase catalytic cycles leading to a highly effective radical recombination in the reaction zone. While the reactions of these cycles proceed in some cases at close to collisional rates, the agent effectiveness requires that the inhibiting species and the radicals in the flame overlap, and this can sometimes be limited by gas-phase transport rates. The metal species often lose their effectiveness above a certain volume fraction due to condensation processes. The influence of particle formation on inhibitor effectiveness depends upon the metal species concentration, particle size, residence time for particle formation, local flame temperature, and the drag and thermophoretic forces in the flame.

Keywords: flame inhibition, halon replacement, fire suppression, nanoparticles, fuel additives, transition metals.

Table of Contents

1. Introduction

The behavior of metals in flame systems has been of interest with regard to engine knock, flame inhibition, soot suppression, rocket nozzle afterburning, and fire retardancy in solids. Recently, high temperature metal chemistry has been useful in the areas of nanoparticle synthesis, pollutant formation in power plant exhaust streams, diesel emission control, and NO_x reduction techniques. This present review focuses on flame inhibition by transition metals with regard to the search for replacements of ozone-destroying halon fire suppressants.

In this review we do not discuss the studies of flame inhibition by alkali metal (primarily sodium and potassium) compounds, which are well known effective flame inhibitors and fire suppressants. Hence, in the present review, the word *metal* more accurately refers to *transition metals*. Potassium and sodium are widely used in different mixture compositions in fire suppression applications, and their mechanism of inhibition has been relatively well documented and is not covered here. The known compounds of Na and K are solids at ambient and flame pre-heating zone temperatures. Delivery to the flame zone is usually performed via finely divided particles. The relatively high saturated vapor pressures of alkali metal-containing species facilitate gas-phase inhibition processes in the flame reaction zone, and avoids the condensation/re-evaporation processes upstream of the flame reaction zone observed in experiments with the transition metals as described below. Recent studies of inhibition mechanisms by K- and Na-containing compounds can be found in references [1-7].

Although the work reviewed below represents a range of fields, the primary motivation for much of the work has been the production ban on the widely-used and effective halon fire suppressants [8]. Metal containing compounds have attracted attention for use in unoccupied spaces, or as benign additives to water, because of the extraordinary effectiveness shown in some laboratory experiments. For example, when added at low concentration [9], $Fe(CO)_5$ has been found to be up to eighty times more effective than CF_3Br at reducing the burning velocity in premixed methane-air flames. Another example is methylcyclopentadienlmanganese tricarbonyl (MMT) [10], which was forty times more effective. In other tests [11,12], chromium and tin were even more effective than iron at accelerating the recombination of radicals. Until recently, the mechanism of flame inhibition by these metal compounds was uncertain. Furthermore, there exist some flame experiments [13] in which the metal additives were nearly ineffective at influencing the extinction properties.

Here, we present the work of numerous researchers in varied areas relevant to flame inhibition by metal compounds, organized mainly by the type of experimental configuration of combustion system. Detailed experimental and numerical investigations of the inhibition mechanisms of iron-containing compounds are then described, followed by a review of related studies of flame inhibition by manganese- and tin-containing compounds. To address the loss of effectiveness which occurs with the increase of additive concentration, we next present results of studies of particle formation accompanying the increase of agent concentration. In particular, we discuss in detail why the inhibition effect occurs to varying extent in different flame systems. Finally, the properties of highly effective catalytic flame inhibitors are outlined, based on the current understanding of the behavior of metals in flames.

Note that there was a much lower publication rate for flame inhibition in general, and transition metal inhibition in particular during the time period of 1975 to 1996. Hence, the review here has less to cite for that time period. Much of the more recent material of this review represents a summary of work performed by the authors.

2.   Background

2.1.   Overview

There has been much research concerning the effect of metal compounds on the high-temperature oxidation reactions of hydrocarbons in a number of different applications. The interest in the present work is on their potential as fire suppressants, as well as evidence for and mechanisms of a loss of inhibition effectiveness that they might demonstrate in some fire suppression applications. Since flame inhibition effectiveness, as well as any loss of effectiveness, may be governed by similar mechanisms occurring in the different phenomena, we explore several relevant combustion processes that might have bearing on the performance of metals as fire suppressants.

In directly relevant work, metal compounds have been added to flames in screening tests aimed specifically at assessing their potential as fire suppressants. Screening tests have been performed to understand their influence on flame speed (premixed flames) and extinction (diffusion flames), as well as their effect on ignition. Beyond the screening tests, flame studies have also been used to understand the detailed mechanism of inhibition of metal agents, either by providing direct experimental data on species present in the flame zone, or by validating numerical models which are then used to calculate the flame structure. Studies of engine knock suppression by metals provided much early data on metal behavior in flames. Since engine knock is known to occur from the rapid pressure rise (and subsequent homogeneous autoignition of the end gases inside an engine cylinder), the mechanisms of engine knock reduction may have relevance to fire suppression—in which the goal is to reduce the overall reaction rate with the addition of the suppressing agent. In engines—as well as in heating applications—research has also been directed at understanding the efficacy of metals for soot reduction. Since both soot formation and the overall reaction rate of flames are known to be related to the location and concentration of radicals, the effects of metals on soot formation may provide insights into the flame inhibition effects of metals.

Other configurations have been used to understand metal chemistry in flames. A large amount of fundamental work has been done using premixed atmospheric-pressure flat flame burners. In this system, the flat flame provides a nearly one-dimensional system, and the region above the flame (i.e., downstream of the main reaction zone) provides a long residence time, high temperature region for radical recombination. The H-atom concentration typically is measured with the Li-LiOH method (described below), and the additive's effect on the radical recombination rate is determined. Ignition studies using flames for screening tests have been reported. In addition, much detailed fundamental understanding has come from shock-tube studies and flash-photolysis studies in reaction vessels. Some studies of fire retardants are also relevant to fire suppression mechanisms of metals. For example, when the fire retardant works by suppressing the gas-phase reactions (and the subsequent heat release and heat feedback to the

5

solid sample), the mechanisms are directly relevant to fire suppression. Finally, after-burning in rocket nozzles provided motivation to understand metal-catalyzed radical recombination reactions, and modeling studies have been performed for those systems.

It should be noted that much of the present understanding of flame inhibition by transition metal compounds is based largely on the seminal work of Rosser and co-workers [14], [15,16]Dixon-Lewis et al.[17,18], Biordi et al. [19-21], and Westbrook [22-24]. Similarly, important early contributions for other radical recombination cycles involving SO_2 were made by Smith et al. [25] and [26]

It is clear that metals can have a profound effect on flame chemistry. Their effectiveness in these varied applications may well be related. In any event, data from each of the applications can provide insight into possible metal-containing compounds for application to fire suppression as well as provide fundamental data useful for predicting their performance in a range of applications. Work investigating the effect of metals for each of the applications is described below.

2.2.   Engine Knock

Many agents that reduce engine knock (e.g., lead-, iron-, and manganese-containing compounds) are also effective flame inhibitors, and it is useful to examine the literature of engine knock to search for possible moieties (keeping in mind that the engine knock involves ignition chemistry, which is different from that of flame propagation)[27]. Engine knock is the onset of detonation waves in an engine cylinder brought about by the homogeneous ignition of the end-gas region of highly compressed and heated fuel and air. The effect of some agents in reducing knock has been known since the 1920s [28]. Compounds used at the time included those containing fbromine, iodine, tellurium, tin, selenium, iron, and lead, as well as aniline [29]. Tetraethyl lead (TEL, $Pb(C_2H_5)_4$) very early became the anti-knock agent of choice. While much subsequent research was performed to understand the mechanism of knock[30,31], the exact mechanism for this agent remains an unsolved problem in combustion research (perhaps because leaded fuel was eventually banned due to its toxicity and poisoning effect on catalytic converters). Although much progress was made, the researchers divided into two camps: those endorsing a heterogeneous mechanism [32,33] and those promoting a homogeneous gas-phase radical recombination mechanism [34,35].

Several known effects of lead in engines support the heterogeneous mechanism. Muraour [36] appears to have been the first to propose chain-breaking reactions on the surface of a colloidal fog formed from TEL. The particle cloud was subsequently shown to be composed of PbO, which is the active species [37]. Since a strong influence of PbO coatings on reaction vessel walls has also been observed [37], a heterogeneous mechanism of PbO was assumed. Although other results support the heterogeneous mechanism, the evidence is somewhat circumstantial. The known *metallic* antiknock compounds (tetraethyl lead, tellurium diethyl, iron pentacarbonyl, nickel tetracarbonyl, [32,35]) all produce a fog of solid particles. The alkyls of bismuth, lead, and thallium are anti-knocks, but those of mercury (which does not form particles) are not [38]. Richardson et al. [39] showed that carboxylic acids increase the research octane number of TEL in engines, and argued that they reduced agglomeration of the PbO particles in the engine end-

6

gas, but acknowledged that their arguments were qualitative. Zimpel and Graiff [40] used a fired engine to provide end-gas samples for transmission electron microscopy (TEM). They claimed that 1000 nm diameter particles formed prior to the arrival of the flame, proving that the effect of TEL was heterogeneous. Commenters to the paper pointed out, however, that the particles could be forming in the sampling system, that the effect of lead extenders was not captured in the particle morphology. Even if particles form, the gas-phase species can still be present, and it is thus not precluded that they are responsible for the inhibition. It has recently been shown [41] that even if particles form, they can re-evaporate in the hot region of the flame if they are small enough. Finally, as described by Walsh [32], a confounding factor in work with TEL is that TEL itself is easily absorbed on tubing surfaces on the way to the reaction vessel, so that it is difficult to know how much TEL actually makes it to the flame. This is of particular significance since, as subsequently described, the efficiency [9,10,42-44] and particle formation [41,45] as a result of decomposition of organometallic agents are strongly affected by the volume fraction of the metal compound.

Later, Kuppo Rao and Prasad [46] claimed to prove the heterogeneous mechanism of lead anti-knock agents. They inserted copper fins coated with PbO into the cylinder of an engine, or injected 30 μm particles into the air stream, and found antiknock effects. They interpreted these results as evidence that the mechanism is heterogeneous. Nonetheless, they did not measure for the presence of gas-phase lead compounds, so a homogeneous mechanism cannot be ruled out. For the eleven lead compounds tested, they found the effectiveness to vary by a factor of about six, and found similarly sized particles of CuO_2, CuO, $CuCl_2$, $NiCl_2$, and $SnCl_2$ to have equal effectiveness, which was less than any of the lead compounds.

Pitz and Westbrook [47] modeled engine knock with and without TEL. Using numerical calculations which include detailed chemical kinetics for n-butane/air mixtures and measured temperatures and (or) pressures for the end gas in an engine cycle, they assumed that the anti-knock properties of lead compounds arise from species destruction via collisions with PbO particle surfaces. Through estimations of the collision rate of important intermediate species with the particles, they found that H_2O_2 and HO_2 removal by the particles can account for an 11 % and 23 % increase in the autoignition time.

The early evidence for a homogeneous gas-phase inhibition mechanism of TEL was suggested by Norrish [34]. Using flash photolysis of mixtures of acetylene, amyl nitrite, and oxygen in a reaction vessel, with and without TEL, the absorption and emission spectra of amyl nitrate, OH, Pb, PbO, NO, CN, CH, and TEL were obtained as a function of reaction progress. The reactants were chosen since, in the absence of anti-knock compounds, they showed the strong homogeneous detonation characteristic of engine knock. The researchers found that the induction time increased linearly with TEL addition at low TEL partial pressures, but that the effectiveness dropped off at higher pressures (a result described subsequently for the flame inhibitors $Fe(CO)_5$ [9,48], $SnCl_4$, [10,49], and methylcyclopentadienlmanganese tricarbonyl MMT [10]). After decomposition of TEL, Pb was present in low concentration, followed by large amounts of PbO and OH , which subsequently dropped off. With TEL addition, the formation of OH was retarded, and the increase in OH emission was smoother. No particles were reported. Norrish et al. described the action of TEL as a two-stage homogeneous gas-phase reaction mechanism. In the first stage, TEL reacts with the peroxide and aldehyde intermediates (characteristic of the end

of the cool flame regime of alkane combustion), thus reducing the availability of these species for initiating the well-known second stage of the combustion. Gas-phase PbO from the TEL then reacts with the chain-carrying intermediates to reduce the rate of heat release, slow the temperature rise, and reduce detonation. It is noteworthy that many of the features subsequently described [50] for flame inhibition by iron compounds (decreasing effectiveness with higher inhibitor concentration, the key role of the metal monoxide species, the necessary coexistence of OH and metal monoxide species, and loss of effectiveness as particles form) were shown in the 1950s by Norrish and co-workers to be necessary for effective knock reduction by TEL. The significant findings of their work predated most of the important flame inhibition work of the 1970s by 20 years. More recently, Benson [33], discussed the effects of TEL on the chemistry of hydrocarbons relevant to engine knock and suggested a "chain de-branching" mechanism. In it, a catalytic cycle involving PbO and PbOH results in the net reaction: $HO_2 + H => H_2O + O_2 + OH$, and represents an overall termination step (de-branching), decreasing the radical reservoir.

2.3. Soot Formation

Soot formation in flames is a complicated multi-step process and is affected by metal additives. While they are usually considered good soot suppressants in combustion processes with hydrocarbons [51-53], metal additives can also increase the yields of both poly-cyclic aromatic hydrocarbons (PAHs) and soot in flames. The overall effect of the additive depends upon the additive concentration [54,55], as well as by the addition location in the flame [56]. In various studies, enhanced soot formation was found to be caused by earlier nucleation induced by metal oxide particles [57-59], and the soot destruction was found to be caused by incorporation of metal oxide particles into the soot which acts to catalyze soot oxidation [52,58-60]. Metal additives to reduce soot emissions from diesel engines have been studied in the past, and currently diesel vehicles are using fuel-borne catalysts to assist with emission controls [61]. Future work to understand the effect of metal additives for soot reduction in DI diesel engines will no doubt benefit from the recent work of Dec. et al. [62].

It is generally recognized that reactions involving the formation of PAHs represent the most likely pathway to soot formation. Enhanced soot formation with metal additives has been postulated to occur due to catalysis of the PAH formation by metal oxide particles either in isolation [63]or incorporated on growing soot particles [64].

Effective soot reducing additives containing Fe and Mn are also effective flame inhibitors [54,65]. The mechanism of flame inhibition involves reduction of the radical pool. This leads to a decrease in the overall reaction rate and an increase in the thickness of the reaction zone. It is interesting to speculate on possible effects arising from reductions in the concentration of the radical pool. Two main effects of radical scavenger compounds (e.g., metal-containing flame inhibitors) on PAH and soot production are expected. First they will decrease the contribution of abstraction pathways for fuel decomposition, and the unimolecular routes will become more important. Thus it is possible that there will be some increase of unsaturated hydrocarbon production leading to an increase in the concentration of the important precursors (C_2H_2, C_3H_3, etc.) for the production of aromatic compounds. On the other hand and in accord with accepted mechanisms of PAH growth processes, decreases in hydrogen atom abstraction rates by radicals will lead to decreases in the destruction of PAHs.

Modeling results have demonstrated [66] that for premixed flames and stirred reactors, radical scavenger effects are important for increasing PAH concentrations for near stoichiometric conditions. For richer conditions, the relative effect of such additives decreases, and at very high equivalence ratios (near the sooting limit), the gas phase influence of radical scavenger additives disappears. Kinetic models demonstrate that the gas phase effect of radical scavenger additives (on flame radical pool) is to enhance PAH formation. The results of [66] support the suggestion of earlier works, that the observed decrease of particulate formation is possibly the result of heterogeneous reactions of iron oxides that increase the soot oxidation rate [52,58,59].

2.4. Flame Screening Tests

As a prelude to the description of the flame screening tests, it is useful to describe the different terminology often used to describe the extinguishing of a flame. *Flame inhibition* usually refers to a weakening of a flame, that is, a lowering of the overall exothermic reaction rate in the flame. This weakening may or may not lead to extinguishment, depending upon the flow field in which the flame exists. In contrast, the terms *fire suppression*, *flame extinguishment*, and *flame extinction* are often used to refer to the case in which the flame has been weakened to the point where it can no longer stabilize in the relevant flow field. Flame quenching refers to flame extinguishment for which heat losses to a surface was a precipitating factor.

Papers describing the results of screening tests clearly demonstrated the superior effectiveness of some metals as flame inhibitors. The seminal work of Lask and Wagner [49] investigated the efficiency of numerous compounds for reducing the burning velocity of premixed Bunsen-type hexane-air flames stabilized on a nozzle burner. They found the metal halides $SnCl_4$ and $TiCl_4$ to be quite effective at low volume fraction (and $GeCl_4$ about a factor of two less then these). In unpublished work, cited by others [67], Lask and Wagner provide the measured flame speed reduction with addition of $SbCl_3$ to hexane-air flames, showing it to be about twice as effective as CF_3Br. They tested iron pentacarbonyl ($Fe(CO)_5$), tetraethyl lead, and chromyl chloride (CrO_2Cl_2) and found these to be extraordinarily effective, with volume fractions of only 170 µL/L and 150 µL/L required for the first two to reduce the burning velocity the hexane-air flames by 30 % (although not quantified, they believed the effectiveness of CrO_2Cl_2 to be even higher). They categorized the compounds they tested into two classes: halogens and transition metals. In general, transition metals were much more effective.

Miller et al [68], using a burner which produced conical flames, measured the effect of eighty compounds on the burning velocity of premixed hydrogen-air flames (fuel-air equivalence ratio ϕ of 1.75). They found the most effective to be tetramethyl lead (TML, $Pb(CH_3)_4$), $Fe(CO)_5$, $TiCl_4$, $SnCl_4$, $SbCl_5$, and TEL (in that order), with TEL only slightly better than CF_3Br, and TML about 11 times better than CF_3Br. A limitation of this work, however, is that the agents were tested at only a single volume fraction. Since the efficiency of many agents is known to vary with their concentration [9], such an approach can skew the relative performance rankings. It should also be noted that in the hotter, faster-burning hydrogen flames, the propensity to form particles from the metal oxides and hydroxides will be lower than in the slower, cooler hydrocarbon-air flames of other studies (see Rumminger et al. [41]). An additional flame screening test was performed by Miller [69], who tested fifteen compounds added to low-pressure (1.01 kPa) premixed and diffusion flames, and found tin (as $SnCl_4$), phosphorus (as

9

POCl₃), titanium (as TiCl₄), iron (as Fe(CO)₅), tungsten (as WF₆), and chromium (as CrO₂Cl₂) to have some promise.

Two screening tests involved the inhibition of propagating premixed flames through clouds of small solid particles of inhibitor. Rosser et al. [70] added metal salts as dispersions of fine particles (2 μm to 6 μm diameter) to premixed methane-air flames. They used the reduction in upward flame propagation rate through a vertical tube as a measure of the inhibition effect. From their data, they calculated the effects of flame speed and particle diameter on the particle heating rate, and together with the volatilization rate for each compound, assessed the fraction of the particle which was vaporized. They quantified the effect of particle size on inhibition effectiveness, and showed that while additional agent decreased the flame speed, the effectiveness eventually saturated (i.e., beyond a certain additive mass fraction, additional inhibitor had far less effect on the flame speed). They postulated a homogeneous gas-phase inhibition mechanism involving H, O, and OH radical recombination reaction with the metal atom and its hydroxide. This mechanism had many of the features of subsequently described mechanisms [10-12,71]. They also noted that catalytic radical recombination relies upon a super-equilibrium concentration of radicals (commonly present in premixed flames and diffusion flames), and that this provides an upper limit to the chemical effect of catalytically acting agents. Finally, they suggested that adding an inert compound as a co-inhibitor can overcome this limitation. A number of alkali metal sulfates, carbonates, and chlorides were tested, as well as cuprous chloride CuCl, which was found to be about twice as effective as Na_2CO_3 (after correcting for the larger size of the CuCl particles).

A later study involving premixed flames with particles was performed by deWitte et al. [72]. Relatively large particles (100 μm diameter) were electrostatically suspended in a tube and then injected into a downward facing premixed Bunsen-type flame, and their effect on the flame temperature, burning velocity, and extinction condition was measured. Various barium, sodium, and potassium compounds were tested, as well as $AlCl_2$, $CuCl_2$, and PbO. The authors noted a thermal and chemical effect of the particles, and assumed that the chemical effect was due to recombination of chain-carrying radicals on the particle surfaces. The authors estimated that for these large particles, the vaporization rate was negligible. Nonetheless, it is not possible to separate the heterogeneous and homogeneous inhibition effects from their data. The authors found particles of $CuCl_2$ and PbO to be about two and eight times as effective as particles of Na_2CO_3, and surprisingly, found $AlCl_3$ to be about three times as effective.

A series of flame screening tests incorporating many compounds was also performed by Vanpee and Shirodkar [73] to test the relative effectiveness of metal salts. The metal acetonates and acetylacetonates were dissolved in ethanol, and fine droplets of the metal salt solutions were sprayed into the air stream of a counterflow diffusion flame over an ethanol pool. The inhibition effect was quantified, at a given air flow velocity (i.e., strain rate) as the change in the oxygen volume fraction at extinction caused by addition of the inhibitor, normalized by the inhibitor volume fraction (mole merit number = $(X_{O_2,ext} - X_{O_2,ext,i})/X_i$, in which $X_{O_2,ext,i}$ and $X_{O_2,ext}$ are the oxygen volume fractions required for extinction, with and without added inhibitor, and X_i is the volume fraction of inhibitor in the oxidizer stream). Their results are depicted in Fig. 1[2], which

---

[2] Note: the uncertainties in the measurements are provided in original reference.

shows the metal compounds tested, listed from most effective to least. The maximum and minimum values of the mole merit number are listed for the range of oxidizer velocities of the tests (50 cm/s to 60 cm/s). As the figure shows, the metal salts of Pb, Co, Mn, Fe, and Cr all show some inhibition effect. Interestingly, $Fe(CO)_5$ was not as effective as iron acetylacetonate, and for lead, the acetonate was about twice as effective the acetylacetonate. It should be noted, however, that the interpretation of the present data is complicated by several effects. First, changing the oxygen mole fraction changes the temperature, which can change the effectiveness of an agent, as subsequently described in refs. [9,42,43,74,75]. Since the air-stream velocity is changed while holding the nebulizer flow constant, the ethanol concentration changes in these partially premixed diffusion flames. Adding changing amounts of a fuel species (i.e., the carrier ethanol) in the air stream, changes the flame location and the scalar dissipation rate for a given strain rate (i.e., air flow velocity); thus, the extinction condition is modified (as discussed in [76] and [77]). The size of the residual particle (which will vary from agent to agent) could affect its ability to vaporize in the flame, influencing the indicated efficiency. Finally, for metal agents that condense, their effectiveness is a very strong function of the concentration at which they are added. Hence, without knowing what the additive mole fraction is, it is difficult to cross compare the effectiveness of the different agents.   For these reasons, it seems appropriate to consider the results shown in Fig. 1 as qualitative, rather than quantitative. For example, subsequent studies [78] have rated iron as about ten times as effective as sodium (in contrast to the results of Vanpee and Shirodkar, which show the acetylacetonate of iron to be only about 20 % more effective than that of sodium).

2.5.   Radical Recombination in Post-flame Region of Premixed Flames

Much of the understanding of the homogeneous gas-phase flame inhibition by metals came from studies of H-atom recombination rates above premixed, fuel rich, $H_2 - O_2 - N_2$ burner-stabilized premixed flames (postflame zone). The techniques, pioneered by Sugden and co-workers [79-81], involve absorption spectroscopy for OH, and the Li/LiOH technique for H atom. (In the latter technique, the strong absorption lines of Li and Na are simultaneously measured above a flat flame. With the assumptions that Na is present in the flame only in atomic form and that Li is present only as Li and LiOH, the measured ratio of the Li to Na absorption together with the known equilibrium constant for the reaction $Li + H_2O = LiOH + H$ provides the hydrogen atom concentration. In early work they determined the dominant metal species in H_2-O_2-N_2 premixed flames above Meker burners with added dilute sprays from aqueous salts of copper and manganese. Copper was found to exist mostly as Cu in the flame, and the dissociation constants of CuH [82]and CuOH [81] were determined from their concentrations above the flame at different temperatures. Similar results were subsequently obtained for MnO and MnOH [83].

In a detailed study of chromium-catalyzed recombination processes, Bulewicz and Padley [84] added μL/L levels of Cr (from either chromium carbonyl or aqueous sprays of chromium salts) to a premixed, fuel rich, flat-flame burner of $H_2\pm$-/O_2/N_2, and measured the catalytic radical recombination by the chromium compounds. They identified the active chromium species as Cr, CrO, CrO_2, and $HCrO_3$ and also detected solid particles, which appeared to have equivalent black-body temperatures up to 500 K higher than the gas. They estimated an upper limit for the rate of heterogeneous radical recombination on the particle surfaces, and estimated that, at an upper limit, it was the same order as the natural un-catalyzed recombination rate in the flame. They also found that Cr showed measurable catalytic radical recombination even when added at

volume fractions of about 1μL/L—at which heterogeneous particle catalysis cannot be contributing. They cite Jenkins [85] as first showing the catalytic effect of metals (Ca, Sr, Ba) on radical recombination in flames. Interestingly, their data show a saturation effect in the catalytic radical recombination by Cr species, and their analyses show that it is due, not to condensation of the active gas-phase Cr-containing species to particles, but to reduction in the available radicals to recombine.

In continuing work, Bulewicz and coworkers [11,12] studied the catalytic effects of twenty-one metal species on recombination of chain-carrying flame radicals present at super-equilibrium levels in the post-flame zone of premixed, fuel rich, flat flames of $H_2/O_2/N_2$ at 1860 K. Table 1 shows the ratio of the catalyzed to un-catalyzed recombination rate for H atom caused by each of the metals, added at 1.3 μL/L. The cut-off value for this ratio was arbitrarily set to 1.1, and those above that value were described as having a strong catalytic effect (Cr, U, Ba, Sn, Sr, Mn, Mg, Ca, Fe, and Mo, in that order). Those species having lesser but still measurable effect were Co, Pb, Zn, Th, Na, Cu, and La, while V, Ni, Ga, and Cl (included for comparison purposes) had no effect at these volume fractions. The possibility of heterogeneous recombination on particles was admitted, but at these low volume fractions, the authors argued for a homogeneous gas-phase mechanism involving H or OH reaction with the metal oxide or hydroxide (attributed to Jenkins [85]).

$$H + MO + (X) = HMO + (X) \tag{1}$$

$$HMO + OH \text{ (or H)} = MO + H_2O \text{ (or } H_2), \tag{2}$$
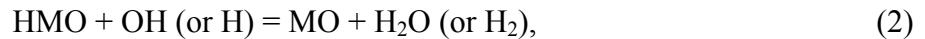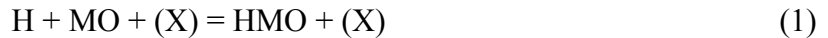
in which M is a metal, and X is a third body.

In concurrent work with the alkaline earth metals, Cotton and Jenkins [71] showed that Ca, Sr, and Ba added as a fine mist of a salt solution to premixed $H_2/N_2/O_2$ flat flames catalyzed the radical recombination for additive volume fractions in the range of 1 μL/L to 10 μL/L. By estimating the reaction rates with the use of possible recombination mechanisms, they suggested the radical recombination mechanism:

$$MOH + H => MO + H_2 \tag{3}$$
$$MO + H_2O(+X) => M(OH)_2(+X) \tag{4}$$
$$M(OH)_2 + H \leftrightarrow MOH + H_2O . \tag{5}$$

Jenkins and co-workers extended their studies of metal-catalyzed radical recombination in premixed flames to study soot formation in diffusion flames. The strong effect of metals on soot formation in flames is well-known [52]. Cotton et al. [86] added forty metals to co-flow diffusion flames of propane and N_2/O_2 mixtures and measured their effect on soot emissions and the smoke point. They postulated a mechanism for soot reduction whereby the catalytic reaction scheme listed above runs backwards, promoting dissociation of H_2O and H_2 into OH and H, which then oxidize the soot particles.

The contribution of heterogeneous processes versus homogeneous gas-phase chemistry was investigated by Bulewicz et al [87]. Through examination of the variation of the intensity of emitted radiation as a function of wavelength from particles formed above a premixed $H_2/O_2/N_2$ flat flame with added spray of aqueous uranium salt, they determined that the temperature of the particles (presumably composed of uranium oxide) was up to 500 K above the gas temperature. They interpreted the particle temperature rise to be caused by the catalytic recombination of H and OH on the particle surfaces. Nonetheless, Tischer and Scheller [88] pointed out that the spectral variation of the particle emissivity is unknown, and the gray-body assumption of Bulewicz is probably unjustified. They also argued that the excess temperature may be due to surface reactions other than radical recombination.

In similar work with premixed, fuel rich, flat flames of $H_2/O_2/N_2$, Jensen and Jones [89] extended the classic $Li + H_2O \leftrightarrow LiOH + H$ photometric method to include the equilibrium for the reaction $Sr^+ + H_2O \leftrightarrow SrOH^+ + H$, in which $[SrOH^+]/[Sr^+]$ is measured mass-spectrometrically. Using both this technique as well as the LiOH photometric method, they studied the catalytic flame radical recombination by tungsten and molybdenum, as well as confirmed the strong effect of tin. Using flames at temperatures of 1800 K to 2150 K, and with metal addition from 1 µL/L to 110 µL/L, they collected data on the rates of radical recombination in the presence of the metal catalysts (added as tetramethyl tin, or hexacarbonyls of tungsten or molybdenum), and measured the major species present in flames inhibited by W and Mo. By analogy with the mechanisms they developed for calcium [71]and iron [90] in flames, they suggested reaction mechanisms for W and Mo, and estimated the rates for the reactions in the catalytic cycles. For the conditions of their flames, the radical recombination cycles, for either W or Mo, were about five times faster then those of tin (this translates to an effectiveness about ten times that of CF_3Br, or about one fifth that of $Fe(CO)_5$ [10]).

Continuing their investigations with premixed flames, Jensen and Jones [91] used similar techniques to study the radical recombination by cobalt added to a premixed, fuel rich, flat flame of $H_2-N_2-O_2$. With Co added as cyclopentadienylcobalt dicarbonyl ($C_7H_5CoO_2$) at volume fractions of about 0.03 µL/L to 145 µL/L, and flame temperatures ranging from 1800 K to 2615 K, they spectroscopically identified the dominant cobalt-containing species to be Co, CoO, CoOH, and $Co(OH)_2$, with most of the cobalt being present in the flame as free Co atoms. By analogy with the Ca and Fe mechanisms, and based on reactions (3) to (5), they developed a kinetic mechanism for radical recombination by Co. The rates of the catalytic steps were again inferred from the experimental data. Cobalt appeared to be about 2/3 as effective as tin at these conditions.

Hastie [92] used mass spectrometry to study the effect of inhibitors on premixed flames. He studied the effects of $SbCl_3$ and $SbBr_3$, and detected the intermediate species in the premixed $CH_4-O_2-N_2$ flame using a Bunsen-type burner. This work is described below.

2.6. Flame Retardant Additives to Polymers

Insight into mechanisms of metal flame inhibition can also be gleaned from studies of metal species added to polymers as fire retardants (when their mode of action has been found to be in the gas phase). One such system is the antimony - halogen combination. Fenimore and coworkers [93-96] showed that the relevant species act in the gas phase; they suggested that the

antimony moieties poisoned the flame, much as do brominated species. Similarly, Martin and Price [97] observed that the addition of triphenylantimony to certain polymer substrates provided fire retardancy, even in the absence of halogen, and believed the mechanism involved antimony species in the gas phase. In a series of detailed experiments, Hastie and co-workers determined the mechanism of flame inhibition in the antimony-halogen system. Using a Knudsen effusion cell containing Sb_2O_3 over which passed HCl, they showed that $SbCl_3$ was evolved through a series of halogenation steps involving successive oxychloride phases [98]. With a molecular beam mass spectrometer, they studied both the pyrolysis products of polyethylene retarded by antimony-oxide/halogen, as well as intermediate species profiles in premixed $CH_4/O_2/N_2$ flames with added $SbCl_3$ and $SbBr_3$ [99]. For the pyrolysis studies, the major effused species from the polymer were $SbCl_3$ and SbOCl. In the flame studies [92], they found that $SbCl_3$ reacts readily to SbOCl, which then reacts with H to form SbO. They measured the major intermediate species of $SbBr_3$ flame inhibition to be SbO, Sb, HBr, and Br, measured the decrease in the hydrogen atom volume fraction with addition of $SbBr_3$, and developed a reaction sequence for the formation of the intermediate species and for the gas-phase inhibition reactions. They argued that the inhibition effect of antimony-oxide/halogen system is predominantly from the reaction sequence (similar to reactions (1) and (2)):

$$SbO + H \rightarrow SbOH^*$$
$$SbOH + H \rightarrow SbO + H_2$$
$$\overline{\hspace{3cm}}$$
$$net: H + H \rightarrow H_2$$
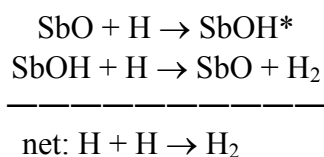
with a smaller effect from the usual bromine sequence, and an even smaller contribution from the equivalent chlorine cycle.

2.7.   Ignition Studies

The effect of metals on ignition has been studied in both shock tubes and flames. Morrison and Scheller [67] investigated the effect of twenty flame inhibitors on the ignition of hydrocarbon mixtures by hot wires, and found that $SnCl_4$ was the most effective inhibitor tested for increasing the ignition temperature; whereas the powerful flame inhibitors CrO_2Cl_2 and $Fe(CO)_5$ had no effect on the ignition temperature. Dolan and Dempster [100] studied the effect of small particles of metal compounds (5 μm to 10 μm diameter) on suppressing the spark ignition of premixed natural gas-air mixtures in a vertical 7 cm diameter tube. They found that barium hydroxide octahydrate, barium chloride, and copper acetate monohydrate were each about three times less effective than were sodium bicarbonate particles in their tests, while cuprous oxide and cobaltous chloride hexahydrate were each about 20 % less effective than $NaHCO_3$. Several studies have shown that metals can actually speed the ignition process in some chemical systems. In shock-tube studies, Matsuda and co-workers [101]found that $Cr(CO)_6$ *reduced* the initiation time for reaction of CO or C_2H_2 with O_2 in shock-heated gases. The metal carbonyl was present at 0 μL/L to 50 μL/L, so the presence of any particles was precluded. The mode of action was believed to be gas-phase reactions involving CrO, CrO_2, and CrO_3. In later shock-tube work with $Fe(CO)_5$ in mixtures of $CO-O_2-Ar$, Matsuda [102] found that a volume fraction of $Fe(CO)_5$ of few hundred μL/L greatly accelerated the consumption of CO. They postulated the effect to be due to oxidation of CO by metal oxides via: $FeO + CO => Fe + CO_2$, and noted that these

14

reactions may be of importance since the mixtures were quite dry ($X_{OH} \approx 5\ \mu L/L$). Interestingly, such accelerating oxidation pathways were also found to be important in the dry reaction of CO with N_2O in flames [103]. In recent shock-tube studies of CH_4-O_2-Ar mixtures, Park et al. [104] found that with 500, 1000, or 2000 $\mu L/L$ of $Fe(CO)_5$, the ignition time was shorter than without the additive, again indicating a promotion effect of the metal additive; however, they did not determine the cause of the promotion for this moist system. On the other hand, with similar conditions, but *ethane* as the fuel, Shin et al. [105] found that 1000 $\mu L/L$ or 2000 $\mu L/L$ of $Fe(CO)_5$ had a distinct inhibition effect on the ignition delay time. Finally, in flash photolysis studies, Erhard and Norrish [34] found that $Pb(C_2H_5)_4$ and $Te(CH_3)_2$ retarded hydrocarbon combustion, where as $Ni(CO)_4$, $Fe(CO)_5$, and $Cr(CO)_6$ had a promotion effect.

2.8. Radical Recombination in Rocket Nozzles

Jensen and co-workers were motivated to study radical recombination involving metal species with the intention of suppressing afterburning in rocket nozzle exhausts. Using mechanisms developed for K, Ba, Fe, Mo, W, Cr, and Sn, Jensen and Webb [106] calculated the amount of inhibitor required to suppress afterburning in the exhaust plume of a double-base propellant (probably a homogeneous mixture consisting of nitrocellulose and nitroglycerine). The products of the propellant reactions consist of a fuel-rich mixture—principally CO and H_2, much like the recombination region above the fuel-rich premixed H_2-O_2-N_2 flames laboratory flames used to study the metal-catalyzed radical recombination. Their calculations (which do not include the effects of condensation) indicate that W and Mo are about a factor of five less effective than Fe, Cr about a factor of six less effective, and Sn more than seven times less effective. These results are consistent with those of the flat flame measurements described above.

Particle formation was discussed by Jensen and Webb [106]. Although they did not measure particles or calculate the degrading effects of particle formation on the suppression of afterburning in rocket motors, they did estimate the upper limit for radical recombination by the heterogeneous reactions on the particle surfaces. Their calculations indicated that while significant, the heterogeneous reactions could not suppress the afterburning, even for the smallest particle diameters assumed (10 nm). They also estimated that even though the inhibiting species were probably volatilized in the combustion chamber, the characteristic times for condensation were probably of the same order as the residence time in the nozzle, indicating the possibility for condensation. Their conclusions were that the metals held good promise for afterburning suppression in rocket motors, and that further work was necessary to estimate the rates of the catalytic cycle reactions and the condensation rates of the metal derivatives at the conditions of their system.

2.9. Other Relevant Investigations of Metals Compounds in Flame Systems

There have been a number of more recent papers dealing with metals in flames. Crosley and co-workers [107] added MMT to premixed flames with the purpose of studying its effect on NO formation. Adding MMT at volume fractions of about 0.5 $\mu L/L$ to near-stoichiometric premixed low-pressure (522 Pa) propane-air flat flames in a McKenna burner, they measured the temperature and the relative concentrations of OH, H, O, CH, NO, and CO through the flame. While they observed no discernable effect of the MMT, this may have been due either to the low concentration of the additive, or the low pressure, both of which could limit the influence

[10,108]. They did, however, suggest a kinetic model for MMT behavior in flames which served as a basis for future efforts [10].

Chromium reaction in an atmospheric pressure, premixed hydrogen-air flame flat flame was studied by Yu et al. [109]. Using microprobe gas sampling in the region downstream from the main reaction zone, they collected chromium species in the gas and condensed phase. The particle size distribution and the fraction of Cr as Cr(VI) was determined as a function of position. In addition, they assembled a kinetic mechanism for Cr reactions in flames through analogy with boron and aluminum combustion, and used the mechanism, together with the measured temperature profile, to calculate the fraction of hexavalent Cr in the downstream region from the flame zone. They also modeled the growth of the particles. For both particle growth and Cr(IV) formation, the calculations were able to predict the experimental trends. They concluded that further kinetic model development was necessary for accurate treatment of Cr speciation in flames. In later work, Kennedy et al. [110] studied the morphology of the particles formed in a hydrogen–air–nitrogen co-flow diffusion flame with added chromium nitrate or chromium hexacarbonyl. They found that the morphology of the particles varied with the temperature of the flame and the source of the chromium.

Kellogg and Irikura [111] performed theoretical calculations to predict the heats of formation as well as the enthalpies and free energies of reaction for the FeO_xH_y species thought to be important in iron inhibition. They found that nearly all of the reactions involving these species (and potentially contributing to flame inhibition) are exergonic at 1500 K. Hence, they suggested that further refinement of the inhibition mechanisms of iron would require knowledge of the actual kinetic rates of the inhibition reactions to improve upon the kinetic model suggested in Rumminger et al. [42]. It is of note that the plethora of possible iron intermediates in catalytic cycles is a consequence of the multiple oxidation states of iron, as has recently been noted for phosphorus compounds as well.

In a comprehensive review of possible chemicals for use as halon alternatives, Tapscott et al. [112] suggested that the metals Cu, Fe, Mn, and Sn, were worthy of further study. Since that time, premixed [10] and co-flow diffusion flame [113] studies have been performed for Fe, Mn, and Sn. No additional work has been reported for copper as a fire suppressant.

2.10. Flame Studies with Iron-containing Compounds

After the potential effectiveness of iron as a flame inhibitor was indicated in the 1950s [32,38], the behavior of iron pentacarbonyl was investigated in detail in the 1960s. The extraordinary flame inhibiting effectiveness of iron was first quantified by Lask and Wagner [49] in their screening study involving methane-, hexane-, and benzene-air premixed Bunsen-type flames with numerous additives. In continuing work, Bonne et al. [108] described the superior effectiveness of $Fe(CO)_5$ for reducing the burning velocity of hydrocarbon-air flames in nozzle burners. They found that an $Fe(CO)_5$ volume fraction of 100 μL/L reduces the burning velocity by 25 % when added to stoichiometric methane-air flames at atmospheric pressure. With oxygen as the oxidizer, or at reduced pressure, they found the effectiveness to be lowered. For hydrogen-air flames, $Fe(CO)_5$ was again much more effective than Br_2. They noted that at low volume

fractions, the decrease in the burning velocity was proportional to the concentration of $Fe(CO)_5$, whereas for increasing concentrations of $Fe(CO)_5$, the relative influence seems to decrease. They postulated a homogeneous radical recombination mechanism at low volume fraction, and a heterogeneous one at higher concentration.

To understand the mechanism of $Fe(CO)_5$, Bonne et al. [108] spectroscopically investigated premixed flat flames of methane with air or O_2. Unfortunately, at the low pressures for which the flame zone was expanded sufficiently to optically probe the flame (8 kPa), the kinetic effect of $Fe(CO)_5$ was very small. For $Fe(CO)_5$ volume fractions up to 100 µL/L they observed that the peak OH volume fraction X_{OH} was unchanged and shifted slightly downstream from the burner. Nonetheless, the decay rate of X_{OH} was increased in the presence of $Fe(CO)_5$, clearly indicating the effect of $Fe(CO)_5$ on radical concentrations in the flame. They measured FeO and Fe emission, as well as Fe absorption, and found that Fe and FeO emission peaked in the main high-temperature reaction zone, implicating these species in the radical recombination reactions. Although FeO had a double peak, with a minimum at the location where the rate of OH recombination was greatest, the authors did not feel that the decrease in FeO emission was correlated with a decrease in FeO concentration. They noted that solid particles were forming.

Skaggs et al. [114] performed the first measurements of OH concentration reduction in low-pressure counterflow diffusion flames inhibited by $Fe(CO)_5$, using laser-induced fluorescence (LIF). They found that increasing the amount of N_2, CF_3Br or $Fe(CO)_5$ in the air stream lead to lower values of OH LIF, and that $Fe(CO)_5$ was far more effective than CF_3Br at reducing OH.

2.11. *Summary of Demonstrated Flame Inhibition Potential by Transition Metal Compounds*

Based on the results presented above, we can assemble a list of transition metals which demonstrated inhibitory effects in flame systems (Table 2).   The metallic elements which have shown flame inhibition potential in experimental studies are listed down the left column, and the type of flame system used to determine the effectiveness is listed across the top. Under each category of flame system, the reference is listed. The elements are listed in the approximate order of demonstrated or expected effectiveness based on the above discussion. Note that there is a large uncertainty in this ranking and the ranking might be different for different experimental configurations.

A comprehensive ranking of the inhibition efficiency for a wider range of inhibitors has also been conducted. Such an effort is difficult since the experimental data in the literature was obtained from different flame systems with different fuels, as well as agents added at different concentrations in different chemical forms. Nonetheless, a ranking has been performed for hydrocarbon fuels with air [78]. Experimental data were compiled on the influence of different additives on burning velocities, flammability limits, extinction strain rates, suppression concentrations and other combustion properties, for different fuel compositions. The most reliable of these were considered to be the burning velocity measurements, and hence, a ranking was developed based on relative reduction in the laminar burning velocity, in the range of 10 % to 30 %, caused by addition of the metallic agent. Consideration was limited to hydrocarbon-air flames (typically alkanes), under near stoichiometric conditions. As described by Babushok and Tsang [78], since alkane-air burning velocities are controlled by the same reactions of the hydrocarbon fragments , ranking and relative flame inhibitor behavior across hydrocarbon fuel

17

types is mostly preserved. Normalizations were made for the different fuel, experiment type, and stoichiometry, and the results are presented on a molar basis, for stoichiometric methane-air flames at ambient initial conditions. Agents were added as gases, finely divided powders, or mists. The nature of these estimates makes it impossible to give uncertainties, especially in an absolute sense, but the relative order of inhibitor efficiency is believed to be representative.

Fig. 2 presents the estimated flame inhibition efficiency for metallic and non-metallic compounds (relative to CF_3Br). Approximately 60% of presented results are based on direct experiments, while the remainder is estimates based on experimental data obtained for different conditions (fuel system, equivalence ratio, etc.). Metallic compounds containing Fe, Pb, and Cr, are the most effective, followed by the alkali compounds containing Rb, K, and Na. The relative independence of inhibition effectiveness on the attached ligand was observed for highly effective metal inhibitors containing Fe, Na, K, Mn, Sn. Bromine- and iodine-containing additives also demonstrate that inhibition effectiveness is mostly determined by the number and type of halogen atom present in the compound [78]. Similarly relatively close flame inhibition effectiveness was observed for different phosphorus containing additives [115-118].

3. Gas-Phase Mechanisms of Flame Inhibition by Metallic Compounds

The flame inhibition by metal compounds was clearly too strong to be accounted for only by physical effects (dilution, increased heat capacity, etc.). Nonetheless, prior to the recent work, controversy still existed as to whether the catalytic action was due to homogeneous gas-phase chemistry or heterogeneous chemistry on particle surfaces. Since significant evidence existed that a gas-phase mechanism dominated, that avenue was pursued first. More detailed experimental data were required, from which the gas-phase chemical mechanisms could be developed and validated. This section describes the experiments, gas-phase kinetic mechanisms, and the results of numerical simulations of flame inhibition by the metal compounds. Results are presented for iron-, tin-, and manganese-based organometallic compounds in premixed and counterflow or co-flow diffusion flames, with methane or CO as the fuel, and are based on previous studies [9,10,41-45,74,103,113,119].

3.1. Iron-Containing Compounds

3.1.1. Experimental Results

Because iron pentacarbonyl was the most effective flame inhibitor ever found [49], and since its mechanism of inhibition had not been determined [120], $Fe(CO)_5$ was studied first [9]. One-dimensional codes were available to solve the transport equations with full chemistry for both premixed and non-premixed combustion. Thus the flame systems approximating these conditions were selected. The organometallic agents were added to the oxidizer stream in two- or three-stage saturators in controlled-temperature baths. For the premixed flames, the laminar flame speed S_L was determined with a Bunsen-type flame using the total area method [121,122]. Although corrections for hydrodynamic stretch and preferential diffusion were not made, only near-stoichiometric methane-air flames (Le near 1) were used, the flame height was maintained constant with and without inhibitor, and the flame speeds with the metal additives were normalized by the uninhibited flame speeds, all of which reduced the error due to stretch. Unlike

18

other inhibitors, metallic agents were required only in trace quantities, so the effective equivalence ratio was unaffected by inhibitor addition. For the counterflow diffusion flame experiments [9], opposing tubes (2.2 cm diameter, with flow-straightening screens) injected the fuel and oxidizer, and the momentum of these two streams was balanced. A global expression provided an estimate of the strain rate [123]. Inhibitor was added to either the fuel or air stream, while the flame was positioned either on the fuel or air side of the stagnation plane (by varying the N_2 dilution). For all of the experiments, there was an orange-colored deposition on surfaces, which did not occur without $Fe(CO)_5$ addition (the flames were all non-soot emitting). It was inferred that the deposition was the result of particle formation in the flames.

Experiments with a premixed Bunsen-type nozzle burner over a small range of ϕ and $X_{O_2,ox}$ verified iron pentacarbonyl's strong inhibition at low volume fraction, but also revealed a loss of marginal (i.e., additional) effectiveness for volume fractions above 100 µL/L. For example, the normalized burning velocity as a function of the volume fraction of $Fe(CO)_5$ for stoichiometric methane flames with varying oxygen volume fraction in the oxidizer ($X_{O_2,ox}$) is shown in Fig. 3, while that for $X_{O_2,ox}$= 0.21 with ϕ=0.9, 1.0, and 1.1 is shown in Fig. 4 [9]. (Note that the figures also include lines showing the results of numerical calculations that will be discussed later.) As the figures show, there is a strong initial inhibition at low $Fe(CO)_5$ volume fraction, but at 100 µL/L to 300 µL/L, the incremental effect of the additive becomes much smaller. For leaner flames and flames with lower oxygen volume fraction, the initial inhibiting effect was stronger, and the point at with the inhibitor became less effective was at lower inhibitor volume fraction. Thus, there are at least three phenomena to be explained: 1.) very strong inhibition at low volume fraction (almost two orders of magnitude higher than CF_3Br), 2.) variation of this strong inhibition with flame properties, and 3.) dramatic loss of effectiveness at volume fractions near 100 µL/L to 300 µL/L.

The variation of the inhibition effectiveness with flame properties can be investigated, to some extent, through examination of the properties of the *uninhibited* flames. Since the action of iron pentacarbonyl was believed to be catalytic radical recombination (either in the gas phase or on particle surfaces), it requires radical volume fractions in excess of the equilibrium values. As a first step in understanding the higher effectiveness for some flames, the inhibitor effectiveness at low volume fraction was compared with the radical super-equilibrium [9]. One measure of the inhibition effect is the inhibition parameter of Fristrom and Sawyer [124]
$\Phi_0 = (\delta S_L / S_{L,0})/(X_i / X_{O_2})$ in which X_i is the inhibitor volume fraction and $S_{L,0}$ is the laminar burning velocity. In the present case, Φ_0 is evaluated at X_i=0, and is essentially the slope of the normalized burning velocity curve at the lowest inhibitor volume fraction, divided by the oxygen volume fraction. Fig. 5 shows the inhibition parameter Φ_0 as a function of the degree of radical super equilibrium (defined here as the ratio of the peak H-atom concentration $[H]_{peak}$ to the local equilibrium value to $[H]_{eq}$); as indicated, Φ_0 varies from 500 to 1600, and increases as the radical super equilibrium increases. (For comparison, the value of Φ_0 for CF_3Br is about 20.)

Results for methane counterflow diffusion flames were similar when the inhibitor was added to the oxidizer stream [9]. Fig. 6 shows the normalized extinction strain rate with added $Fe(CO)_5$ for three values of $X_{O_2,ox}$ in the oxidizer stream. The diluted flames are again inhibited more strongly, and the marginal effectiveness decreases as X_i increases (although not as drastically as

in the premixed flames described above). Conversely, when the inhibitor is added to the fuel stream (Fig. 7), there is no inhibition, and perhaps even a slight bit of promotion. The stronger inhibition for the lower-strain flames can again be explained by the properties of the uninhibited flames; for example, in Fig. 8, the super-equilibrium of H-atom is shown to be larger for flames at higher strain. The promotion effect for fuel-side $Fe(CO)_5$ addition to counter-flow diffusion flame, as well as the promotion or inhibition effects of the metals on the shock tube and flash-photolysis ignition studies discussed in section 2.7. may also highlight the reversible nature of catalytic cycles. As discussed above regard to soot formation, Cotton et al. [86] found that promotion can occur if the catalyst is present in systems in which radicals are present in sub-equilibrium. That is, the catalytic cycle can run backwards to more rapidly bring radical concentrations up to equilibrium levels. More detailed kinetic calculations are necessary to test this hypothesis.

In order to vary the conditions for particle formation and flame inhibition, other fuels and oxidizers were tested. In the methane-air flames described above, the degree of inhibition was influenced by the size of the radical pool (and its departure from equilibrium); hence, moist CO flames with increasing H_2 content were used to vary the size of the radical pool, while maintaining a nearly constant final flame temperature (which could affect the tendency to form condensed particles). The burning velocity of moist $CO/O_2/N_2$ flames with added $Fe(CO)_5$ is shown for varying $X_{O_2,ox}$ for $X_{H_2}= 0.01$ in Fig. 9, and for varying X_{H_2} with $X_{O_2,ox}=0.24$ in Fig. 10. The overall trends were similar to the methane results: the lower O_2 or H_2 volume fraction cases (which both have smaller radical pools and larger radical overshoot) gave stronger initial inhibition, but the loss of effectiveness again occurred, and it was more severe for the flames that were inhibited more strongly at low volume fraction. As described below, however, for the CO flames, the temperature of the flames was not the cause of any differences.

Tests with oxidizers which produce non-branching systems for radical chemistry have proven useful in past research on the mechanisms of flame inhibitors [15,17]. Consequently, N_2O was used as the oxidizer in dry and moist CO flames inhibited by $Fe(CO)_5$ [103]. Contrary to expectations, addition of iron pentacarbonyl promoted rather than inhibited the combustion, and the effect was larger for the dryer flames. As Fig. 11 shows, with $Fe(CO)_5$ added at 100 µL/L, the normalized laminar burning velocity of a premixed CO-N_2O flame was increased by 17 % for bone-dry flames, and 7 % for flames with $X_{H_2} = 0.002$. Numerical modeling results revealed that the metal oxide, in an example of chemical looping combustion [125], served to oxidize the CO, and the resulting metal was then oxidized by the N_2O, completing the cycle: $N_2O + M = N_2 + MO$ and $CO + MO = CO_2 + M$ (where M is Fe, FeO, or FeOH). This oxidation route for CO supplemented the usual routes (which are faster under moist conditions).

To test the uniqueness of $Fe(CO)_5$ as the source of iron, tests were also conducted for premixed methane-air flames with added ferrocene [44]. These tests and calculations showed that, on a mole basis, ferrocene was equal in effectiveness as $Fe(CO)_5$. Furthermore, tests with combinations of CO_2 and ferrocene hinted that blends of inert and chemically active species might be an effective combination. Fluorinated hydrocarbons, however, were shown to be poor choices for the carrier of $Fe(CO)_5$, since their decomposition can lead to reactions of the iron with F to form FeF, FeF_2, FeF_3, etc, which are effective sinks for iron in the system.

20

To interpret the experimental results presented above, flame simulation studies with detailed kinetic models were conducted .

3.1.2. Kinetic Mechanism

A gas-phase mechanism for the iron-catalyzed radical recombination in flames was developed by Jensen and Jones [90], and later, expanded by Rumminger et al. [42]. In both, the main catalytic cycle leading to radical recombination was:

$$FeOH + H \leftrightarrow FeO + H_2$$
$$FeO + H_2O \leftrightarrow Fe(OH)_2$$
$$Fe(OH)_2 + H \leftrightarrow FeOH + H_2O$$
$$\overline{}$$
$$(net: H + H \leftrightarrow H_2).$$
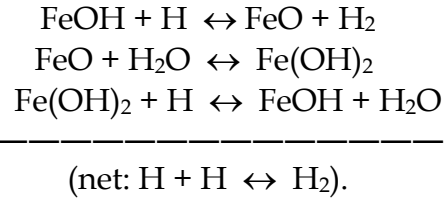
This mechanism is shown schematically on the right side of Fig. 12, in which the arrows connect reactants and products, and reaction partners are next to the arrow. Although the mechanism described in Rumminger et al. also included other catalytic cycles besides the two shown Fig. 12, they were not found to be particularly important in methane-air flames, either premixed or diffusion [43]. In work with premixed CO-N_2-O_2–H_2 flames, however, the new O-atom cycle:

$$Fe + O_2 + M \leftrightarrow FeO_2 + M$$
$$FeO_2 + O \leftrightarrow FeO + O_2$$
$$FeO + O \leftrightarrow Fe + O_2$$
$$\overline{}$$
$$net: O + O \leftrightarrow O_2 .$$
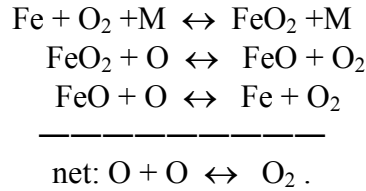
(shown on the left side of Fig. 12) was found to be much more important than the H-atom cycle.

Recent computations of iron compound thermochemistry at flame conditions support the possibility of many additional radical recombination cycles [111]. In that study, seven iron species thought to exist at flame temperature were considered: Fe, FeH, FeO, $FeOH$, FeO_2, $FeO(OH)$, $Fe(OH)_2$ [42], and the heat of reaction at 0 K and the change in Gibbs free energy at 1500 K were calculated. Based on the results, however, very few of the considered reactions and cycles could be eliminated based on the thermodynamics. The complexity of the situation is illustrated in Fig. 12, (from Kellogg and Irikura, [111]), which shows schematically the possible inhibition cycles of iron. (Note that in the figure there are on the order of 50 possible cycles since [Fe] can be replaced by Fe, FeH, FeO, or FeOH.)

3.1.3. Numerical Modeling Results

The calculated flame structure based on the gas-phase kinetic mechanism was able to reproduce many of the trends in the experimental data for low iron pentacarbonyl volume fractions. For example, the predicted burning velocity reduction caused by addition of iron pentacarbonyl to premixed $CH_4/O_2,N_2$ flames with varying $X_{O_2,ox}$ in the oxidizer stream is shown by the solid lines in Fig. 3. At low X_i, the model captures the mildly decreasing slope, as well as the stronger inhibition at lower $X_{O_2,ox}$ (although the experiment shows a stronger effect for varying $X_{O_2,ox}$ than

21

do the calculations). Similarly, the predictions for ϕ=0.9, 1.0, and 1.1 (for $X_{O_2,ox}$=0.21) in Fig. 4 show the correct variation with ϕ, but again, the experiments show a somewhat larger effect of ϕ on the initial inhibition effectiveness than is predicted by the calculations. Most important, however, is that in all cases, the experiments show a much stronger reduction in the inhibition effectiveness at higher Fe(CO)$_5$ volume fractions than predicted by the gas-phase model.

Some of the reduction in the calculated inhibition effectiveness with added inhibitor was shown to be caused by movement of the radical populations nearer to equilibrium conditions after inhibitor addition [42]. For example, Fig. 14 shows the ratio of the peak and to equilibrium values of the H-atom concentration, as a function of X_i, for $X_{O_2,ox}$= 0.20, 0.21, and 0.24. As X_i increases, the departure from equilibrium also decreases; that is, the driving force for catalytic radical recombination is lower, and the catalyst is less effective. The variation in the effectiveness of the catalytic cycle (at low inhibitor volume fraction) with radical super-equilibrium is likely due to changes in the flame temperature with the different flame conditions. This effect has also subsequently been demonstrated for CF$_3$Br by Lott et al. [126] and for organic phosphous containing compounds by Fisher and co-workers [77][75].

For counterflow diffusion flames, the model performed similarly. As shown in Fig. 7, the calculated (lower solid line) extinction strain rate for CH$_4$-air flames with Fe(CO)$_5$ added to the air stream agrees reasonably well with the experimental results at low Fe(CO)$_5$ volume fraction. Again, the loss of effectiveness at higher Fe(CO)$_5$ volume fraction (which is not as dramatic as in the premixed flames) is not captured by the gas-phase model. For agent added to the fuel stream (upper curves in Fig. 7), the overall lack of effectiveness is captured; however, the small amount of promotion observed experimentally was not reproduced in the simulations. Examination of the numerical results [43] indicated that Fe(CO)$_5$, when added to the fuel stream, does not inhibit the counterflow diffusion flames because the flame is located on the air side of the stagnation plane, and the iron-containing intermediate species do not effectively diffuse to the H- and O-atom locations on the air side of the stagnation plane. That is, the inhibiting species and radicals are not co-incident in the flame due to gas-phase transport limitations. Nonetheless, if the counterflow flame characteristics are modified to move the flame location closer to the stagnation plane (by nitrogen dilution to the fuel and air streams), different results are obtained. In some cases [42], the flame (and hence the peak [H]) are nearer to the stagnation plane, and sufficient diffusion of the active gas-phase iron species could occur. Thus there should be sufficient overlap of the inhibiting species and the radicals. Nonetheless, much less flame inhibition occurred than was expected based on the gas-phase model. Discussion of this anomalous behavior is presented below.

Although the gas-phase model does not include condensed-phase iron compounds, it can still be used to investigate their possible formation. For example, using the gas-phase numerical flame structure results, the predicted volume fraction of iron intermediates can be estimated throughout a flame. Fig. 15 shows the temperature and supersaturation ratio (actual partial pressure divided by the saturation vapor pressure at the local temperature) for Fe or FeO through a premixed CH$_4$-air the flame, with Fe(CO)$_5$ added at 100 μL/L or 500 μL/L [42]. As indicated, large super saturation ratios exist; for condensation to occur, values between 10 and 1000 are often needed for iron compounds, and these ratios are exceeded in the cooler parts of the flame [127].

The kinetic mechanism for $Fe(CO)_5$ inhibition was also tested using data from other flames. Numerical simulations were performed for the moist $CO-O_2-N_2$ flames with $Fe(CO)_5$ which were described above. As Fig. 9, for X_{H_2} =0.01 and varying $X_{O_2,ox}$, and Fig. 10 for $X_{O_2,ox}$=0.24 and varying X_{H_2} show, the numerical model is able to predict the trends in the experimental data well, although the magnitude of the inhibition with added $Fe(CO)_5$ is not perfectly captured. From the numerical results, several new insights regarding the gas-phase mechanism were obtained. As described above and shown in Fig. 12, a new catalytic cycle (involving O atoms) was found in the moist CO flames, and it was shown to cause the faster loss of effectiveness in the CO flames with increasing agent volume fraction. The numerical modeling was essential for explaining the promotion effect of $Fe(CO)_5$ when added to N_2O-CO flames.

It is important to note that even for iron compounds, for which the most research has been performed, the mechanism is in an early stage of development. For example, the rates of the most important reaction steps in the mechanism were selected (within the uncertainty bounds suggested by Jensen and Jones [90]) to provide agreement with experiments. The mechanism has been tested only for near stoichiometric premixed $CH_4-N_2-O_2$, $CO-N_2-O_2$, and $CO-N_2O$ premixed flames, $CH_4-O_2-N_2$ counterflow diffusion flames, and CH_4-air cup-burner flames. Although at low Fe-containing additive mole fraction the agreement was usually good, there were some conditions for which the predicted inhibition deviated significantly. These cases include lean premixed CH_4-air flames (ϕ=0.9), $CH_4-O_2-N_2$ flames with an oxygen volume fraction in the oxidizer of 0.20, and cup-burner flames with added CO_2 (at very low $Fe(CO)_5$ volume fraction). Reaction rates in the mechanism required to provide agreement with the experiments were at the upper end of the uncertainty, and are close to gas-kinetic rates. Hence, it was of interest to determine if natural limits exist for homogeneous gas-phase chemical inhibition of flames.

3.2. Chemical Limits to Flame Inhibition

Initial efforts to determine if gas-phase reactions alone could account for the extreme effectiveness of $Fe(CO)_5$ at low volume fraction [9,119] lead to the development of a "perfect inhibitor," an idealized flame inhibitor that represents an upper limit for chemical inhibition of hydrocarbon flames. Hence, it can be used to explore the mechanisms of flame inhibition by highly effective fire suppressant agents such as iron pentacarbonyl, and investigate such effects as the extreme effectiveness at low concentration as well as the reduced marginal effectiveness (saturation effect) as the concentration is increased. In the course of this work it became apparent that iron pentacarbonyl may be approaching the natural limit of chemical effectiveness.

Chemical inhibition arises from the lowering of the concentration of chain-carrying radicals in the flame reaction zone through their reaction with the inhibitor. Inherent in this picture is not only the reaction of the radicals with the scavenging species but also the regeneration of the latter, so an amplifying effect is observed [17,128]. Thus, effective inhibition mechanisms contain two important types of reactions: reactions scavenging chain carriers and reactions regenerating inhibitor agent.

A variety of analogous processes have been invoked to cover the action of chemicals such as HBr, CF_3I, $Fe(CO)_5$, etc. In all cases they involve catalytic cycles leading to the destruction of chain carriers. There are essentially no limitations on the type of reactions that may lead to the

23

inhibition or the regeneration of the inhibiting agent. The catalytically active species can be the inhibitor itself or some reaction intermediate. The regeneration reactions can take the form of chain propagation ($Br + CH_2O = HCO + HBr$) or termination ($CH_3 + I + M = CH_3I + M$, $I + HO_2 -> HI + O_2$). Generalizing from the possible types of inhibition reactions [119], we can write the simplest mechanism for inhibition as :

$$X + Inh\ (+M) = InhX\ (+M),\ \ and$$

$$X + InhX = X_2 + In,$$
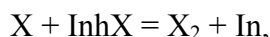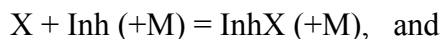
where X is the major chain carrier (H, O, or OH), Inh is the inhibiting species, and M is a third body. In this mechanism, both scavenging and regeneration reactions are termination processes. Thus this catalytic recombination cycle is the most effective one due to termination of a chain carrier at each reaction step of the catalytic cycle. Further simplification can be brought about by noting that at atmospheric pressure, rates of termolecular reactions are usually much slower than for bimolecular processes. Therefore the more effective cycle will be one with bimolecular scavenging of the chain carrier, or $X + Inh = InhX$. Obviously, the inhibitor must also be inert with respect to the other species in the system. Then, if one assigns a collisional rate constant for these processes, any decrease in the calculated flame velocity with added Inh will be the maximum achievable. This mechanism is termed the "perfect inhibitor" model.

The efficiency of the perfect inhibitor was studied by modeling its influence on the laminar burning velocity of premixed methane/air mixtures. In addition, calculations were also performed using the mechanism suggested by Jensen and Jones for iron pentacarbonyl [90], with the addition of two reactions: $Fe(CO)_5 = Fe + 5CO$ and $Fe + O_2 = FeO + O$ (note that this mechanism has slower rates for the key iron reactions as compared to the mechanism of Rumminger et al. [42]). Finally, for comparison, calculations were performed with a CF_3Br inhibition model [129].

Table 3 lists the results of simulations. The volume fraction of inhibitor (Inh, $Fe(CO)_5$, or CF_3Br) required to achieve a 30 % or a 50 % decrease in the flame velocity is listed for each mechanism. Particularly interesting is the close match between the experimental results for $Fe(CO)_5$ and the perfect inhibitor model. In contrast and in accord with experimental observations, CF_3Br is much less effective.

The dependence of burning velocity on perfect inhibitor concentration is non-linear, and the inhibition effect decreases with increasing inhibitor concentration. This may be related to the saturation effect, which is caused by a lowering of the super-equilibrium radical concentration in the presence of inhibitor. For example, Table 4 shows the calculated H, O, and OH volume fractions in a methane-air flame with 0 μL/L and 1900 μL/L of $Fe(CO)_5$; results are given for the radicals at the reaction zone location and far downstream (i.e., the equilibrium value). As indicated, with 1900 μL/L of $Fe(CO)_5$, the radical super-equilibrium is essentially eliminated, so the driving force for the catalytic recombination is gone, and additional $Fe(CO)_5$ will have little effect. Nonetheless, for $Fe(CO)_5$, the reduced effectiveness in the experiments is much larger than expected based on the reduction in the radical super-equilibrium predicted by the gas-phase kinetic mechanism. It is believed that the larger reduction in efficiency of $Fe(CO)_5$ may be due

24

to loss of iron-containing species to condensed-phase particles (since the vapor pressure of the iron compounds can be low, even at flame temperatures).

With the perfect inhibitor model, one can select which chain-carrying radical is terminated (for example, H, O, OH, or all three). With Inh added at 100 µL/L, and the mechanism acting only on O-atom, the reduction in burning velocity is 52 % of the reduction with all three radicals involved, while for H-atom it is 82 %. Since the concentrations of H, O and OH are related by partial equilibrium relationships in the flame zone, reducing the concentration of one species leads to a reduction in the others. Hence, the higher efficiency of the cycle recombining one radical instead another is smeared by the shuffle reactions.

Efficient radical scavenging was shown to require effective regeneration of the inhibiting species. The regeneration properties of an inhibitor can be characterized by a regeneration coefficient, K_{reg} , defined as the effective number of catalytic cycles involving the inhibitor in flame zone [130], normalized by the initial volume fraction of the inhibitor $K_{reg} = [Inh]_{total}/[Inh]_0$. Here, $[Inh]_{total}$ can be determined by integration of the rates of reactions in which Inh is consumed

$$Inh_{total} = \int \Sigma W_{Inh,i} \, dt,$$

Where $W_{Inh,i}$ is the reaction rate of the "i"-th reaction consuming Inh. At a volume fraction X_{Inh} of 100 µL/L, the calculated regeneration coefficient for the perfect inhibitor is 104. To produce the same degree of inhibition requires about 1 % of CF_3Br or CF_3I, which yields regeneration coefficients for HBr and HI of 7 and 3, respectively. Thus a perfect inhibitor is very effective in regenerating itself. In the cases of a perfect inhibitor versus CF_3Br, an additional factor is that regeneration reactions of the former involve termination processes. It should be noted that modeling results for iron pentacarbonyl-inhibited flames using the original rate constants suggested by Jensen and Jones [90] gives an underestimate of the reduction in burning velocity as compared to the experimental observations. A reasonable adjustment of the rate constants [42] leads to agreement with experimental results.

There are a number of interesting consequences derived from studies with the perfect inhibitor model. First, there is a natural limit to the extent that neutral ground state chemistry can inhibit flames. This is somewhat obvious since reactions cannot proceed faster than the collisional rate. This places lower limits on the concentration of a perfect inhibitor for which there are pronounced effects on the combustion processes, typically in the 10 µL/L to 100 µL/L range of additive volume fraction. The experimental results for the metal systems suggest that they are very close to this limit, and thus it is not likely that one can obtain much more efficient inhibitors. Second, an important result is that for these metal systems, it is highly unlikely that surface processes are making contributions, since these would be inherently less efficient (due to lower surface area) than the gas-phase reactions considered here. Third, the key role of regeneration steps in the catalytic cycle have been demonstrated. Finally, the simulations have illustrated that a saturation effect occurs due to reduction of the radicals towards their equilibrium levels, and that this is probably a property of all catalytically acting inhibitors.

3.3. Tin- and Manganese-Containing Compounds

Iron pentacarbonyl was shown to be up to two orders of magnitude more effective than CF_3Br as a flame inhibitor; however, it loses its effectiveness when added at higher concentrations. Consequently, it was of interest to determine if other metals caused similar strong flame inhibition while not suffering from the loss of effectiveness. Since there was early evidence that tin and manganese might be effective flame inhibitors [49,67-69,73], they were studied in more detail [10]. Also, because manganese- and tin-containing species have higher vapor pressures than those of iron species, they might not lose effectiveness due to condensation as badly as iron compound do. Using techniques developed for $Fe(CO)_5$, methylcyclopentadienlmanganese tricarbonyl (MMT) and tetramethyl tin (TMT) were added to premixed Bunsen-type flames at increasing volume fraction, and their effect on flame speed was observed. Detailed kinetic models for the behavior of Sn and Mn in hydrocarbon flames were developed, and the predicted reduction in normalized flame speed with metal additive was compared to the experimental values. Finally, the detailed inhibition mechanisms predicted by the models were interpreted and compared for the different metals. Note that some metallic compounds tested are too toxic to be used directly as fire suppressants. The organometallic compounds, however, provided a convenient means to deliver the gas-phase metals to the flame so that their inhibition mechanisms could be studied.

3.3.1. Experimental Results

The laminar flame speed S_L was determined using a Bunsen-type flame [122] as described above. Since the vapor pressure of MMT is somewhat lower than that of the other agents previously tested, experiments with it were conducted at a slightly elevated temperature (80 °C). Although the absolute value of the burning velocity is quite sensitive to the inlet temperature, the performance of the agents can be compared across this range of differing gas inlet temperatures, since the *reduction* in the *normalized* burning velocity with agent addition is relatively insensitive in T_{in} for the range of $298 \text{ K} \leq T_{in} \leq 353 \text{ K}$.

Fig. 16 compares the experimentally determined inhibition effectiveness of $Fe(CO)_5$, MMT, TMT, $SnCl_4$, CF_3Br, and CO_2 in the premixed methane-air flames. For agent volume fractions providing burning velocity reduction of up to 40 %, TMT is three times, MMT forty times, and $Fe(CO)_5$ is about eighty times as effective as CF_3Br at reducing the overall reaction rate of these stoichiometric, premixed methane-air flames. Data for $SnCl_4$ from ref. [49] show that tin tetrachloride is as effective in n-hexane/air flames as TMT is in methane/air flames. For all agents at lower volume fractions, the flame speed reduction is linear with additive volume fraction. For TMT, MMT, and $Fe(CO)_5$, however, the curves start to flatten out, indicating loss of marginal effectiveness at higher loadings. As discussed above and previously [130,131], most inhibitors lose their effectiveness at higher mole fractions, but the decrease in inhibition effectiveness is much more dramatic for the organometallic compounds, indicating a different mechanism. Nonetheless, the mechanisms of inhibition in the gas phase were compared for each of these metals at volume fractions below those for which condensation is important, and the numerical results were used to interpret differences in the kinetic mechanisms of tin, manganese, and iron.

3.3.2. Kinetic Mechanisms

Kinetic models for highly effective flame inhibitors can be considered to consist of three sub-models. The first sub-model is the methane combustion mechanism itself. The second includes reactions for the agent decomposition and formation of the active inhibiting species, while the third includes the inhibition reactions. In previous work, it has been shown that for the phosphorus-containing compound DMMP and for ferrocene, the decomposition reactions have a small influence on the predicted inhibitor efficiency as long as the overall activation energy of decomposition is less than 250-335 kJ/mol [44,132]. In the present work, this was also found to be true for TMT and MMT decomposition. Of course, the thermodynamics of the metal compound must allow it to decompose in the flame (e.g., the very stable compound Fe_2O_3 would not be effective).

Kinetic mechanisms were developed for tin and manganese inhibition of methane-air flames [10]. The reaction sets were developed based on consideration of possible reactions of tin- or manganese-containing species with the radical pool and with the main species of methane combustion. The mechanism for tin had five species and 37 reactions, and the mechanism for manganese had nine species and 61 reactions. The manganese mechanism was based upon an earlier one of Smith and co-workers [107]. The most important reactions in the mechanisms were determined based on sensitivity analysis, and those rates were adjusted within their uncertainties to yield agreement with the experimental flame speed measurements.

3.3.3. Numerical Modeling Results

Numerical calculations of flame speed for TMT- and MMT-inhibited flames were performed based on the gas-phase mechanism. The calculations were made for a small range of oxygen volume fraction and equivalence ratio. Fig. 17 shows the measured and predicted flame speeds for stoichiometric methane-air flames with added TMT for $X_{O_2,ox}$, = 0.20, 0.21, and 0.244, while Fig. 18 shows the results for added MMT for ϕ=0.9, 1.0, and 1.1. As shown, the numerical predictions are reasonable in the linear region of burning velocity decrease. For the TMT-inhibited flames with $X_{O_2,ox}$=0.21 (not shown), however, the inhibition was under-predicted for lean flames and over-predicted for rich flames, and reasonable adjustment of the rates did not yield improvement. Nonetheless, the performance of the mechanism is reasonable for a first effort. With TMT or MMT addition, as with iron, there is a volume fraction above which the marginal effectiveness of added agent is much smaller. This decrease in effectiveness is likely due to condensation of the metal compounds, and comparison of the three mechanisms of inhibition are made only in the regime where loss-of-effectiveness is not occurring. Hence, the present simulations can be used to gain insight into the mechanisms of inhibition of Fe, Sn, and Mn and their differences.

3.3.4. Comparative Performance of Fe, Sn, and Mn

The flame structure (i.e., the stable species volume fractions, reaction rate data, and temperature through the flame) predicted by the numerical model was used to understand and compare the mechanism of inhibition of the three metallic agents. A premixed methane-air flame was used, to which TMT, MMT, or $Fe(CO)_5$ was added at an amount required to produce a 30 % reduction of flame speed, (1963, 128, or 105) μL/L, respectively. This level of inhibition was selected because it provides a significant weakening of the flame (a factor of two reduction in overall

27

reaction rate) while still residing in the linear region flame speed reduction with inhibitor concentration (i.e., away from the region of loss of effectiveness). The most important reactions of the catalytic cycle for flame inhibition by TMT, MMT, and $Fe(CO)_5$ are shown in parallel format in Fig. 19, The reactions shown were based on consideration of the reaction fluxes and sensitivities. In Fig. 19, the pathway for consumption of each species is shown, with arrows connecting the relevant reactant and product species, while the number next to each arrow gives the fraction of the total consumption flux for that reactant which proceeds through that particular reaction.

There are several common elements in the inhibition mechanisms. The monoxide species crucial in the catalytic cycle is formed in each from metal atom reaction with O_2 (in a binary reaction for Sn and three-body one for Fe and Mn). The key inhibition step in each mechanism is the metal hydroxide species reaction with a radical (and reaction with H is always very important). Regeneration of the metal hydroxide occurs primarily from its reaction with H, although for Mn and Fe, this proceeds first through an intermediate step involving formation of the metal di-hydroxide by reaction with H_2O. The main difference in the cycles involves the lack of a comparable di-hyroxide species for Sn, so that the Sn inhibition proceeds through the slow three-body reaction $SnO + H + M$.

As has been discussed previously for other compounds (and discussed below for transition metals), thermodynamic constraints can, to some extent, determine the level of metal species participation in catalytic inhibition cycles. For Sn, Mn, and Fe, the efficiencies of the catalytic cycles were found to be influenced strongly by the thermodynamic equilibrium distributions of the intermediates in the cycle. The importance of constraints on equilibrium concentrations as they relate to inhibitor efficiency is illustrated in Fig. 20, which shows the fraction of all metal species in the flame. For these equilibrium calculations, the metallic element (Sn, Mn, or Fe) is present at a volume fraction of 1.0×10^{-4}, and methane and air are present at stoichiometric proportions. Note that since the flames of Fig. 19 all have equivalent levels of inhibition, the flux of each radical recombining catalytic cycle is about the same; e.g., SnOH, MnOH, and FeOH must be present at about the same mole fraction since their rates of reaction with H-atom are close, and the rates of reactions forming the hydroxide are approximately the same. In the case of Sn inhibition, [SnO] at equilibrium is about 1000 times greater than [SnOH] for flame conditions, so correspondingly higher levels of total tin in the system are required for equivalent flame inhibition as compared to Mn or Fe (since adequate levels of SnOH are required for the cycle to complete itself). Similarly, the equilibrium volume fraction of $Mn(OH)_2$ drops off in the range 1800 K < T < 2000 K as compared to $Fe(OH)_2$, so that Mn will be less effective at these higher temperatures (but is predicted to be more effective at temperatures lower than this range).

Note that Sn, Mn, and Fe demonstrate multiple oxidation states. For flame inhibition by phosphorus compounds, Jayaweera et al. [117] and Korobeinichev et al. [116] demonstrated that the multiple oxidation states of phosphorus leads to multiple recombination cycles by phosphorus-containing compounds. It would be of interest to study the possible influence of the multiple oxidation states of metals on their inhibition effectiveness.

3.3.5. Blends of Metals

The loss of effectiveness at higher inhibitor mole fractions for tin, manganese and iron limit the utility of these elements for fire suppression. It is important to understand the reasons for the loss of effectiveness. Two mechanisms have been proposed: radical depletion towards equilibrium which renders the catalytic cycles inoperative, and metal oxide condensation which serves as a sink for the gas-phase intermediate metal species in the gas-phase catalytic cycle. One approach for overcoming the loss of effectiveness that has been proposed is to add non-condensing amounts of several inhibitors. However, if the loss of effectiveness were due to radical concentrations, which were already driven towards equilibrium, adding a second inhibitor would not further reduce the burning velocity. Fig. 21 shows the flame speed with pure MMT, pure $Fe(CO)_5$, or a blend of MMT and $Fe(CO)_5$, added at a molar ratio of 2:1, respectively. (The data for the combination of MMT and $Fe(CO)_5$ are plotted as a function of the mole fraction of the abundant agent, MMT). The numerical model, which includes both the reactions of manganese-containing species and the iron-containing species from ref. [42] predicts well the normalized flame speed reduction. The results show that MMT added to the flame at the point where $Fe(CO)_5$ is losing its effectiveness provides additional flame speed reduction over that from $Fe(CO)_5$ alone. Hence, the loss of effectiveness is not likely due to radical depletion.

4. Effects of Particle Formation

4.1. Particle Formation in Flames Inhibited by Iron Pentacarbonyl

At the time of the measurements and modeling described in ref [42], the role of particles in flame inhibition by metals was not understood. The gas-phase kinetic mechanisms for Fe, Sn, and Mn described above are reasonably successful for describing many of the important features of inhibited premixed and counterflow diffusion flames at low inhibitor volume fraction. Nonetheless, in both premixed and counterflow diffusion flames, as the inhibitor loading is increased, the dramatic loss of marginal effectiveness of these metals is not described by the gas-phase models. (This is particularly important for fire suppressants since it is usually desired to apply them at concentrations which completely extinguish the strongest existing or expected flame.) Further, there are some configurations in the counterflow diffusion flames in which flame inhibition was expected to occur, but it did not.

A "somewhat lower effectiveness" at higher concentrations of $Fe(CO)_5$ was mentioned briefly by Jost and co-workers [48], who surmised that a particle inhibition mechanism may be at work at high concentration. Given the experimental evidence of particle formation, the high super-saturation ratio for some of the iron intermediates, and the existing controversy concerning the role of particles in the flame inhibition, there existed a need to measure the particle properties in the inhibited flames.

Additional motivation to understand the role of particles in flame inhibition by metals came from practical efforts to harness their potential. Based on the encouraging results from ferrocene and CO_2 in premixed flames [44], large-scale experiments were performed for extinction of a flame in an enclosure. Ferrocene was deployed together with an inert compound generated by a solid propellant gas generator (SPGG) [13]. Unfortunately, the combination did not demonstrate the intended high efficiency. Although it was not possible to extract fundamental information

concerning the lack of effectiveness for those experiments, the results of Holland and co-workers [13] provide important evidence for a loss-of-effectiveness for iron, and motivate a search for an explanation.

In order to measure particles, a laser scattering and extinction experiment was designed for application to the premixed, counterflow diffusion, and cup-burner flames [41]. Light scattering by particles was measured, and the particle size and number density (for the counterflow diffusion flame configuration) were determined and used to interpret the formation and destruction rates of particles and their influence on the flame inhibition. Note that the premixed, counterflow diffusion, and cup-burner (which had added N_2 to the air stream) flames were all non-sooting, and the scattering signal in the presence of inhibitor at low volume fraction is very close to that of air[41,45,113]. The absence of scattering from soot facilitates measurement of particles formed with $Fe(CO)_5$ addition . To obtain information on the particle morphology, a thermophoretic sampling system was also applied to the flames, and the samples were analyzed with transmission electron microscopy.

4.1.1.   Premixed Flames

4.1.1.1.   Laser Scattering Measurements

In the premixed flames, a laser beam was passed across the top portion of the conical Bunsen-type methane-air flame seeded with $Fe(CO)_5$. (Full experimental details are in [41,45].) Scattered light at 90° indicated the presence of particles in this horizontal slice through the flame at a height about midway up Bunsen cone. The flame showed a scattering signal which varied greatly with the position in the flame [41]. Fig. 22 shows the scattering signal as a function of distance from the burner centerline along a horizontal profile 7 mm above the burner base. At this height, the Bunsen cone has a radius of about 2.3 mm (the diameter of the burner exit nozzle is shown at the base of the figure). As the figure shows, there are two scattering peaks within the flame region (one for each side of the Bunsen cone). Far outside the flame region (i.e., downstream of the flame in the product gases), the scattering signal is two orders of magnitude larger than the in-flame signal, indicating very large or numerous particles. These downstream particles have little consequence for the flame inhibition by iron species, and we concentrate our discussion on the in-flame particles which might have effects on the flame reactions.

Comparison of particle measurements and numerically generated chemical species profiles implies that particles are present near the region of peak reaction rate of H-atom, which is also near the region where the inhibiting species (FeO, FeOH, and $Fe(OH)_2$) are most active [133]. Hence, the particles can act as sinks for the inhibiting iron-containing intermediate species. As the particles are carried further into the flame, the temperature rises, and they disappear. Only very far downstream (r>6 mm) do the particles reappear, but this location is too far from the radical chain-branching region to have much effect on the burning velocity. For those large values of r, the velocity is decreasing, leading to a larger residence time, and the temperature is decreasing (due to heat losses and co-flow air entrainment); both of these effects can lead to the very large scattering signal at that location. Fig. 23 shows the in-flame particle region in more detail. Scattering data are shown for $Fe(CO)_5$ volume fractions in the reactant stream of (0, 50, 100, 150, 200, and 300) μL/L. The curve for 0 μL/L of inhibitor (the bottom curve in the figure) clearly shows the difference in Rayleigh scattering by the gaseous reactant and products species

(which have a different density and composition). The scattering signal increases with increasing amounts of $Fe(CO)_5$.

Since the loss of effectiveness in premixed flames inhibited by $Fe(CO)_5$ was postulated to be caused by condensation of iron-containing intermediate species to particles, it is of interest to compare how the loss of effectiveness correlates with the particle scattering signal. The presence of particles is characterized by the height of the scattering peak above the background scattering caused by the gas-phase species at the same physical location in the flame (approximately the height of the peaks in Fig. 23). Fig. 24 shows data for the normalized burning velocity (left axis), and the maximum value of the in-flame scattering (right axis), as a function of the volume fraction of added $Fe(CO)_5$. To provide variation in the manner in which the inhibitor loses its effectiveness, curves are provided for two values of the oxygen volume fraction in the oxidizer $X_{O_2,ox}$, 0.21 and 0.24. Referring to the two curves for $X_{O_2,ox} = 0.21$ in Fig. 24, the value of the volume fraction of added inhibitor X_{inh} at which the great loss of effectiveness occurs (i.e., the slope changes sharply) is about 100 μL/L, and this volume fraction also corresponds to the point at which the scattering signal starts to rapidly increase in magnitude. The curves for $X_{O_2,ox} = 0.24$ indicate that loss of effectiveness of $Fe(CO)_5$ occurs at a higher value of X_{inh} than for $X_{O_2,ox} = 0.21$, and that the increase in particle scattering is also retarded until a larger quantity of $Fe(CO)_5$ is added. The curves in Fig. 24 indicate that the formation of particles is correlated with a *loss* of effectiveness of $Fe(CO)_5$, rather than being associated with the strong inhibition itself.

As noted above, iron pentacarbonyl loses its effectiveness at a higher volume fraction for the flame which has a higher $X_{O_2,ox}$. Two features of the flames may be responsible—one thermodynamic and one kinetic. The larger value of $X_{O_2,ox}$ leads to a higher final temperature of the flame, which would hinder condensation (due to the thermodynamic effects on the inhibiting species vapor pressure), requiring a larger value of X_{inh} for an equivalent amount of scattering. Alternatively, the higher temperature flames have a higher flame speed, which provides a shorter residence time in the flame for particle inception and growth. In order to examine which of these effects is important for particle formation and loss of effectiveness of $Fe(CO)_5$, experiments with varying $X_{O_2,ox}$ and fuel type were conducted. Mixtures of $CO/O_2/N_2/H_2$ with varying hydrogen volume fraction produced flames with nearly identical adiabatic flame temperatures but varying residence times (i.e., flame speeds) [74]. The normalized burning velocity and peak in-flame scattering signal for flames with H_2 volume fractions X_{H_2} of 0.005, 0.010, and 0.015 are shown in Fig. 25. As the figure shows, the flames with less H_2 (slower flames, longer residence times) lose their effectiveness at lower values of X_{inh}, and these flames also have particle scattering signals which rise faster at lower values of X_{inh}.

The results of experiments having a wide range of burning velocity and peak adiabatic flame temperature show the importance of residence time for particle formation. Fig. 26 shows the peak in-flame scattering signal for CH_4 and CO flames with varying peak temperature, burning velocity, and $Fe(CO)_5$ loading. Each solid line is a linear least-squared fit to all of the data at a certain value of X_{inh}, namely (100, 200, and 300) μL/L of $Fe(CO)_5$., which are noted by circles, diamonds, and squares, respectively. Within each data set for an inhibitor loading, the points correspond to: (h)igh, (m)edium, and (l)ow temperature, and CH_4 flames (open symbols) and CO flames (closed symbols). As Fig. 26 shows, the scattering signal is clearly related to the burning

31

velocity, which is inversely related to the residence time. Similar plots investigating the importance of peak flame temperature did not show its correlation with the scattering signal. Hence, the residence time is the important parameter controlling particle formation in premixed flames inhibited by $Fe(CO)_5$.

4.1.1.2.   Particle Size and Morphology in Premixed Flames

Further insight into the particle properties were extracted from the scattering signals (e.g., Fig. 23) by using other information available [41]. For example, as a means of bounding the particle properties, one may assume that 50 % to 100 % of the iron in the feed stream condenses to particles. Previous calculations using a gas-phase only mechanism for the flame inhibition by $Fe(CO)_5$ were in good agreement for low volume fraction, but deviated once the inhibitor reached the volume fraction at which it lost its marginal effectiveness [42]. The amount of deviation corresponds to condensation of about 50 % of the available $Fe(CO)_5$ (X_{inh}=200 µL/L), and an upper limit of particle mass is obtained assuming 100 % condensation. Other reasonable assumptions (for estimation purposes) are that the particles are monodisperse Rayleigh scatterers composed of FeO. Using the scattering signals collected for 200 µL/L of added $Fe(CO)_5$, and assuming 50 % and 100 % condensation, the particles have, respectively, a volume fraction of 1.2×10^{-8} and 2.2×10^{-8}, diameter of 16 nm and 13 nm, and number density of 5.3×10^9 cm^{-3} and 2.1×10^{10} cm^{-3}. Using the optical and bulk properties of Fe instead of FeO increases the inferred diameter by 15 % and the number density by 9 %.

For the counterflow diffusion flames (for which particle measurements are described in more detail in a latter section), both laser scattering and laser extinction measurements were possible for some conditions. It was found [45], that for low strain rate flames, the particles have diameters between 10 nm and 30 nm, number densities of 10^8 cm^{-3} to 10^{10} cm^{-3}, and volume fractions of 10^{-7} to 10^{-8}. The mean diameter and volume fraction of the particles generally increased with increasing $Fe(CO)_5$ loading. Hence, these particle properties measured using scattering and extinction techniques in the counterflow flames are in the same range as the estimates from the premixed flames assuming 50 % to 100 % condensation.

Additional information on the particle properties was obtained from thermophoretic sampling of the flames. For the premixed flames, a 3 mm diameter TEM grid was inserted at a height of 7 mm above the burner rim, and at a location corresponding to the main reaction zone of the flame (r = (2.7 ± 0.3) mm). For a dwell time of 375 ms in a a premixed flame with X_{in} = 200 µL/L [41], the particles showed a moderate degree of agglomeration, with about 1 to 10 primary particles per agglomerate and primary particle sizes of under 20 nm. The primary particle diameters from the TEM images were in reasonable agreement with those estimated above from the scattering signal (assuming 50 % to 100 % of the iron species condense). These small diameters, 10 nm to 20 nm, support the possibility of particles evaporating as they convect to regions of higher temperature.

For the counterflow flames, the appearance of the particles extracted using thermophoretic sampling is similar. For those tests, the TEM grid was inserted perpendicular to the plane of the flame, at the centerline of the burner, into the center of the visible flame [45]. For a counterflow diffusion flame of methane and air with 300 µL/L or $Fe(CO)_5$ added to the air stream, the degree of agglomeration is much smaller than that in the premixed flame. Primary particle sizes range

from 5 nm to 25 nm in diameter, which is in reasonable agreement with the results of laser-based scattering measurements [45].

4.1.1.3. Estimate of Upper Limit of Heterogeneous Inhibition

Although the results presented above support a gas-phase inhibition mechanism of $Fe(CO)_5$, it is possible that heterogeneous chemistry also makes a contribution. The effects of walls on radical chain branching with regard to explosion limits are well documented [134], and heterogeneous iron and iron oxide catalysts are widely used in industrial processes. Further, iron oxide particles have recently been proposed as catalysts for NO_x reduction in stationary combustors [135], and iron catalysts are used to reduce emissions of soot and hydrocarbons from diesel engines [136].

With some assumptions, we can estimate the upper limit of radical recombination by collisions with particles, and determine the maximum effect of the particles on the burning velocity. To provide this upper limit, we assume: 1) a two-step heterogeneous inhibition mechanism (Langmuir-Rideal type) in which a radical is absorbed onto a particle surface $R+P \rightarrow RP$, followed by the reaction of the activated particle RP with another radical and the release of the stable species $RP+R \rightarrow R_2+R$; 2) all of the iron present condenses to particles; 3) the particles are spherical with a specified mean diameter d_m and log-normal size distribution; 4.) all collisions of radicals with particles lead to their recombination; 5.) only H-atom recombination is considered (the additional benefit of adding OH and O recombination is minor). The calculation is implemented using the PREMIX code and with the particles represented as fictitious species with the required rate parameters [41]. The results of the calculation are shown in Fig. 27 for particles of diameter 10 nm to 80 nm. Also shown for comparison are experimental data (points) for $Fe(CO)_5$ inhibition of the premixed methane-air flames [9], and the results of a calculation for a proposed perfect gas-phase inhibitor [119] (bottom curve). In the perfect gas-phase mechanism, collisions of a chain-carrying radical with <u>any</u> gas-phase intermediate species of the inhibitor result in trapping of the radical. As the figure shows, the heterogeneous mechanism does show significant flame inhibition, which increases as the assumed particle diameter decreases. Nonetheless, the inhibition from the heterogeneous mechanism is not as strong as that shown by the experiment or by the perfect gas-phase inhibition mechanism.

The results of the calculations presented in Fig. 27 support the primary contribution of a homogeneous inhibition mechanism of iron rather a heterogeneous one. The formation of particles essentially increases the number of inhibitor molecules per particle, and increases the particle mean diameter d_m. Since of the number of particles scales as $1/d_m^3$, but the collision cross section of particles with radical scales as $1/d_m^2$, the net effect of particle formation is to decrease the collision rate of radicals with inhibiting species. These idealized calculations support the proposals [9,119] that only gas-phase chemistry is fast enough to account for the extraordinary inhibition effect of $Fe(CO)_5$. A more realistic model of heterogeneous radical recombination would probably result in less inhibition by the particles. It is interesting to note that the residual inhibition of $Fe(CO)_5$ at $X_{in} > 300$ μL/L in Fig. 27, while small compared to values at $X_{in} < 100$ μL/L, is not zero. The magnitude is similar that calculated for 80 mm diameter particles in Fig. 27, which is also comparable to that of CF_3Br, and may be due to

heterogeneous inhibition. The relative contribution from homogeneous and heterogeneous mechanisms might explain the flame inhibition behavior of other metals.

4.1.2.   Counterflow Diffusion Flames

Laser scattering experiments to detect the presence of particles were also conducted in counterflow diffusion flames [45]. For these flames, the line-of-sight measurements were made along a vertical path at the centerline of the fuel and oxidizer tubes. Fig. 28 shows the scattering signal as a function of the distance from the center of the methane and air jets. The data points (connected by lines) correspond to values of $Fe(CO)_5$ volume fraction of (0, 50, 100, and 300) μL/L. The calculated gas temperature [43] as a function of distance from the center of the jets is shown by the top scale, and the calculated gas-flow stagnation plane is indicated by the vertical line. As the figure illustrates, the particles are formed in the low-temperature region on the air side of the flame, at temperatures below 500 K. Interestingly, as in the premixed flames, the particles are nearly completely consumed by the time they reach the location of the peak flame temperature (1961 K), and then re-form as they approach the stagnation plane. For this flow field, however, the residence time gets much longer as the particles approach the stagnation plane, allowing much time for particle growth. Further, as discussed below, thermophoretic forces cause the particles to cross the stagnation plane and reach an area of particle stagnation, which corresponds roughly to the location of the peak particle scattering signal, and occurs on the fuel side of the gas stagnation plane. As discussed in ref. [45], addition of increasing amounts of the $Fe(CO)_5$ to a methane-air counter-flow diffusion flame results in a larger particle volume faction and mean diameter, but lower number density.

The thermophoretic velocity of particles 5 nm in diameter [45] was calculated based on the gas-phase flame structure obtained from numerical calculations of uninhibited flames. Combining these with the gas-phase velocity and the distances traveled yielded the residence time of 5 nm particles injected from either the fuel or air jet. The hatched line near the top of Fig. 28 shows the particle residence time (as 10 ms intervals between the hatch marks). Near the particle stagnation region, the near-zero particle velocities create large uncertainties in the estimated residence time (caused in part by the limited spatial resolution of the numerical flame structure calculation); this region is indicated by the shaded bar on the line showing the residence time. The inclusion of the thermophoretic velocity of the particles shows that 5 nm particles are expected to cross the stagnation plane about at the location of the fuel-side scattering peak, explaining its existence.

Nonetheless, it is the particle formation on the *air* side of the gas stagnation plane that is the likely cause of the loss of inhibition. With addition of $Fe(CO)_5$ to the air stream, the air-side scattering signal increases, even for values of X_{inh} as low as 50 μL/L. The dotted line in Fig. 28 illustrates the calculated H-atom volume mole fraction in the uninhibited flame. The location of the peak particle scattering (about −1.75 mm) overlaps with the region of high H-atom mole fraction. Catalytic radical recombination cycles are most important in the regions where radical mole fractions are the highest (and iron species most strongly catalyze H-atom recombination). Hence, particles forming near the peak [H] can sequester the active gas-phase iron-containing species and thereby reduce the effect of the catalytic cycles.

34

The loss of effectiveness of $Fe(CO)_5$ in counterflow diffusion flames can be directly correlated with the formation of the air-side scattering peak from particles. Following the approach described above for premixed flames with $Fe(CO)_5$, the presence of particles is quantified by the height of the air side scattering peak (minus the scattering signal from the gas-phase species). Fig. 29 shows the normalized extinction strain rate (left axis) as a function of the $Fe(CO)_5$ volume fraction in the air stream. As in the premixed flames, the inhibitor is very effective at low values of X_{inh}, but loses its effectiveness faster as X_{inh} reaches a certain value (about 150 µL/L for these conditions). Similarly, the normalized extinction strain rate calculated using a gas-phase only kinetic mechanism [42] (solid line in Fig. 29) follows the experimental data reasonably closely for $X_{inh}<100$ µL/L, and then starts to deviate as X_{inh} increases. The measured scattering cross section (right axis; open squares connected by dotted lines) shows that the scattering signal increases noticeably when the $Fe(CO)_5$ reaches the point of lower marginal effectiveness (~150 µL/L). As in the premixed flames, the *loss* of effectiveness of the $Fe(CO)_5$ is correlated with particle formation.

Particle formation followed by flow-field effects can also *prevent* metallic inhibitors from entering into gas-phase catalytic radical scavenging reactions. To illustrate this, Fig. 30 shows the scattering cross section from a counterflow methane-air diffusion flame with $Fe(CO)_5$ added to the *fuel* side of the stagnation plane at various values of X_{inh}. The calculated temperature field, residence time estimate, and location of peak [H] are the same as in Fig. 29 for air-side agent addition. In the case of fuel-side $Fe(CO)_5$ addition shown in Fig. 30, the iron-containing species also start to condense at local gas temperatures less then 500 K. In this case, however, the thermophoretic forces *prevent* the iron-species particles from crossing the stagnation plane, and the scattering signal reaches its peak value near the calculated particle stagnation region for 5 nm particles. The scattering signal at the particle stagnation plane is two orders of magnitude larger for fuel-side agent addition than for air-side addition. Thus, fuel-side agent addition leads to particle formation, which together with thermophoretic and flow-field (i.e., drag) forces, effectively prevents the active species from reaching the location of peak [H]. For the methane-air flames of Fig. 30, however, the $Fe(CO)_5$ added to the fuel stream would not be expected to inhibit the flame, even if the particles did not form. This is illustrated in Fig. 31, which shows the reduction in the normalized extinction strain rate (left axis) with added $Fe(CO)_5$ to the fuel stream. For both the experimental data and the numerical predictions (based on a gas-phase only model), the inhibition of the flame is minimal. The increase in the scattering signal (right axis) with added $Fe(CO)_5$, however, is very large. As discussed previously [43], the $Fe(CO)_5$ added to the fuel stream is ineffective even if it remains in the gas phase; to be effective, the inhibiting species (or their precursors) must diffuse upstream into the oxidizer stream and reach the location of significant H-atom mole fraction. For these flames, however, the convective flow is larger than the diffusive flow, so the inhibitor (or its fragments) is unable to enter the reaction zone.

The importance of particle convection can be more clearly illustrated by considering a counterflow diffusion flame with the peak temperature and peak [H] closer to the stagnation plane, where gas-phase inhibiting species could diffuse. Such a flame is obtained from an oxidizer with volume fractions of 30 % O_2 / 70 % N_2 , and a fuel of 80 % CH_4 / 20 % N_2. The results of particle measurements for $Fe(CO)_5$ added to the air stream of that flame is shown in Fig. 32. For this flame, both the peak temperature and [H] are slightly on the fuel side of the gas

35

stagnation plane (vertical line), while the particle stagnation plane (shaded box on the residence time bar at the top) is slightly on the oxidizer side. Clearly, very large particle scattering signals are present, and as in Fig. 30 above, the particles do not appear to have significantly crossed the gas stagnation plane, and hence cannot deliver the active species to the region of high [H]. Unlike in Fig. 30, however, the gas-phase inhibiting species *can* diffuse to the region of high [H]. This is illustrated in Fig. 33, which shows the experimental measured and numerically calculated reduction in the normalized extinction strain and the particle scattering cross section for increasing amounts of $Fe(CO)_5$ in the air stream. Based on the experiments, adding $Fe(CO)_5$ has little effect on this flame. The calculations, however, which are based on a gas-phase model, predict that the added $Fe(CO)_5$ should have a significant effect (implying that the gas-phase species *can* diffuse to the location of the peak [H] (shown in Fig. 32). Nonetheless, the scattering measurements show prominent particle formation. Since, in Fig. 32, both the gas stagnation plane (vertical line) and the particle stagnation region (shaded box on residence time bar at top) separate the particles from the region of peak [H], the particles can effectively isolate the active intermediate species from the location of H-atom where they are required to inhibit the flame. Consequently, we see in Fig. 33 that while the gas-phase model (solid line) implies that inhibition should occur with addition of $Fe(CO)_5$, the experiments (points) do not show inhibition, and this is consistent with the large scattering signal (dotted line) observed with addition of the $Fe(CO)_5$.

The results presented for the counterflow diffusion flames with added $Fe(CO)_5$ illustrate that the following *physical* phenomena can influence the efficiency of the inhibitor: 1) Gas-phase transport of the active inhibiting species to the location of peak [H], either by diffusion or convection; 2) particle formation, which can reduce the availability of active gas-phase species. The latter, particle formation, can act either by directly reducing the gas-phase volume fraction of the active iron-containing intermediate species in the vicinity of the peak [H], or by physically separating the particles (and hence the active species) from the region of peak [H] by flow field and thermophoretic effects. These insights are essential for understanding the relevant phenomena affecting the action of metallic inhibitors when added to the more complex flow field of the cup-burner flames, as described below.

4.1.3. Cup-Burner Flames

The work on metal inhibition of premixed and counterflow diffusion flames was extended to include co-flow diffusion flames in the cup-burner configuration [137]. The tests included $Fe(CO)_5$, TMT, and MMT with methane or heptane as fuels and air as the oxidizer [113,138,139]. Based on the loss of effectiveness at higher $Fe(CO)_5$ concentrations that was demonstrated in premixed and diffusion flames, it was not expected that iron pentacarbonyl alone would be effective in cup-burner flames. Notwithstanding, there was much suggestion in the literature that a combination of a good catalytic agent and an inert agent would prove to be an effective combination. In this case, the overall reaction rate is lowered in part through radical recombination by the catalytic agent, and in part through the lower temperature caused by the added diluent. This approach has been discussed since the 1950s [15,70,74,126,130,140] which suggested that combinations of thermally acting and catalytic agents might prove beneficial. Hence, $Fe(CO)_5$, MMT, or TMT were added to a cup burner of fuel and air, and the amount of CO_2 required for extinction was determined [113]. This approach is conceptually the same as the classic oxygen index test used for assessing material flammability [94]. In that test, the oxygen

36

volume fraction in the air stream at blowoff (i.e., the oxygen index) is determined for solid, liquid, or gaseous fuels with chemical additives in either the fuel or oxidizer.

Surprisingly, the effectiveness of CO_2 combined with any of the metal agents was much less than anticipated. Fig. 34 shows the measured CO_2 volume fraction required for extinction as a function of the catalytic agent volume fraction in the air stream. Data are presented for Br_2, CF_3Br, $Fe(CO)_5$, MMT, and TMT. Although the metals are still more effective than CF_3Br at low concentration, they are not nearly as effective as expected from the results in premixed and counterflow diffusion flames (i.e., 10 to 100 times more effective than CF_3Br).

In order to understand the lower effectiveness of metals in cup-burner flames compared to premixed and counterflow diffusion flames, several steps were undertaken. First, particle measurements in the cup-burner flames inhibited by $Fe(CO)_5$ were made. The results (shown in Fig. 35) indicate that particles are present both inside and outside (but not coincident with) the luminous flame zone, and that higher $Fe(CO)_5$ loadings produced higher particle scattering signals. In order to understand the particle formation and chemical inhibition, numerical modeling of the cup-burner flames inhibited by $Fe(CO)_5$ were performed [113], using the gas-phase only numerical model developed previously. This model has predicted the blow-off condition of methane and air cup-burner flames with added CO_2 [141], Ar and He[142], CF_3H [143], and CF_3Br and Br_2 [144]. The temperature field and the velocity vectors for methane-air cup-burner flames with 10 % CO_2, and 0 and 100 μL/L of $Fe(CO)_5$ are shown in Fig. 36, while Fig. 37 shows the calculated blow-off behavior. As in other flame configurations, the loss of effectiveness of iron and a discrepancy between predicted (gas-phase model) and measured effectiveness were both correlated with the formation of particles (see Fig. 38). To understand the propensity for particle formation, the degree of super-saturation of some of the iron-containing intermediates was calculated through the flame, using the detailed flame structure obtained from the model, together with vapor pressure data available from the literature. For a height above the cup burner which passes through the flame kernel (i.e., the stabilization region), Fig. 39 shows the radial profile of temperature and volume fractions of iron species and radicals, as well as the supersaturation ratio (which is the ratio of the calculated species partial pressure to the planar vapor pressure at the local conditions). The supersaturation ratio is highest for FeO, followed by Fe and $Fe(OH)_2$, and the values decrease as the radial location of peak temperature is approached. Note that vapor pressure data for FeOH, FeOOH, and FeO_2 are not available, and their condensation potential has not been assessed. The condensation potential is strong since the temperature of the flame kernel is much lower than the relevant regions of premixed or counterflow diffusion flames.

Finally, the numerical model was extended to include calculation of the particle trajectory for inert particles added to the flame, including the effects of gravity, drag, and thermophoretic forces. This was done since early estimates [139] were that thermophoresis may have been driving the particles away from the flame region. The results of the calculations (Fig. 40) show that near the flame base, there is some deviation of the particles both up and down around the reaction kernel; however, examination of the estimated radial and axial thermophoretic velocities shows them to be much less than the gas velocity. Consequently, the particles still pass directly into the reaction kernel, so the effect of thermophoresis near this region is expected to be minor factor. Unfortunately, measurements of particle scattering were not performed in the reaction

kernel itself. Nonetheless, the other results described above provide evidence that the loss of effectiveness is due to particle formation.

4.1.4.   Effective Chemical Inhibition by Metal Compounds

Studies of particle formation in premixed, counterflow diffusion, and cup-burner flames inhibited by $Fe(CO)_5$ outlined the importance of the following physical factors with respect to effective chemical inhibition:

1.) The metal species must be added to the flame in a chemical form which allows it to enter the gas phase
2.) Gas-phase transport of the iron-containing species to the region of high H-atom concentration is necessary for efficient inhibition.
3.) Particle formation near the location of peak [H] can act as a sink for the iron-containing intermediate species and reduce the catalytic effect.
4.) The volume fraction of inhibitor determines both the concentration of radicals available to recombine and the propensity of the metal intermediates to condense. The inhibition effectiveness depends on the concentration of metallic agent.
5.) The available residence time affects particle growth.
6.) Convection and drag forces combined with the existing flow field in the flame can prevent particles from reaching the region of peak [H].
7.) Thermophoretic forces can be large in the flame and re-distribute particles away from peak [H].
8.) Particle size determines if the particles can re-evaporate upon passing into the high-temperature region of the flame.
9.) The flame temperature of the stabilization region of cup-burner flames is much lower than in premixed or counterflow diffusion flames. This leads to the increased condensation of the active species.

In order to assess the condensation potential of other flame inhibiting metals, it is necessary to know their concentrations in the flame, as well as their local vapor pressure.   The availability of these data for the metals listed in Table 2 is discussed below.

4.2.   Potential for Particle Formation in Flames Inhibited by Other Metal Compounds

There exist several approaches for estimating whether other metals will have a similar loss of inhibition effectiveness to that of iron. One approach is to have experimental data for flame systems in which the loss of effectiveness is evident. This requires that the inhibitor be added at volume fractions high enough to allow the loss of effectiveness. Unfortunately, many of the early experiments with metal compounds were not conducted with high enough volume fraction of the metal to show the loss of effectiveness [49], or the inhibiting effect was not presented as a function of additive volume fraction (so the decreasing effectiveness was not illustrated) [11,12,68,69,73,89,91].   Another clue that a loss of effectiveness may occur is a reported presence of particles in some flame system. Although the presence of particles will depend upon the temperature of the flame, the concentration at which the metal moiety is added, and the residence time for particle formation, the observed presence of particles in one flame system is an indication that it may be important in other flame systems as well. Finally, the *potential* for

condensation can be assessed by considering the local metal species volume fraction as compared to its local vapor pressure in the flame. A limitation of this procedure is that it relies upon knowledge of the metal species present in a flame system, the mechanism of inhibition, as well as the vapor pressure (or gas-phase and condensed-phase thermodynamic data). Often, this information is incomplete. Vapor pressures for some metal compounds can be found in [145-149]. Further, the kinetic rates of the formation of more stable oxides of the metal must be known to assess the contribution of those compounds to condensed-phase particles (since often, the vapor pressure of these oxides is very low; e.g., Fe_2O_3). For each metal species of interest, the available data have been examined to assess the potential for condensation and subsequent loss of effectiveness.

For the highly effective compounds containing Cr [84], Fe, Mn, and Sn, evidence for decreased inhibition effectiveness has been described by the following: 1) demonstrated loss of effectiveness at higher volume fraction; 2) experimental evidence of particle formation; and 3) low saturated vapor pressure of at least one important intermediate metal species at flame conditions. Hence, it is highly likely that these metals will experience loss of effectiveness in fire suppression due to condensation. For the highly effective metal species Pb, particles have been reported [29,32,38,46], as well as a loss of effectiveness [34]. The vapor pressure of Pb and PbO are high[148], but that for PbO_2 is low [147,149], although it is not known what species form in the inhibition cycle. For titanium, particles have been reported but experiments were not carried to high enough volume fraction to show a loss of effectiveness, and vapor pressure data are not available. For the metals W, Mo, and Cu, the inhibition mechanisms are not developed sufficiently to know the intermediate species and their reaction rates. For Co, the vapor pressure of CoO is relatively low at flame temperatures, so that condensation may limit its effectiveness. For the metal species Ni, Te, Tl, Bi, U, Zn, La, Th, Se and Ge, though they have some potential as flame inhibitors, there is insufficient data on both the inhibition mechanism and the vapor pressures of the relevant intermediate species to know if particle formation will limit their effectiveness in flames. The case of Sb is discussed below.

The only flame data for antimony inhibition [49] did not go to high enough concentrations to show loss of effectiveness; nevertheless, antimony may form condensed-phase particles in flames. In studies of polymers with added Sb_2O_3 and halogen, Fenimore and Marin [93] showed that the fire retardant effect increases linearly with Sb_2O_3 at low mass fractions of Sb_2O_3, but saturates at some value, above which further addition of Sb_2O_3 is ineffective. Hence, the fire retardancy effect of antimony shows a strong saturation, much like that for iron, manganese, and tin in cup-burner flames [150]. To illustrate this, the data in Fig. 34 (CO_2 required for extinction with metal species added) is re-plotted below in Fig. 41 in terms of the limiting oxygen index (based on N_2). The top of the figure shows the limiting oxygen index (LOI) for polyethylene/halogen blends as a function of the volume fraction of the metallic inhibitor in the gas phase. The curves for Sb_2O_3 were calculated based on data available in Fenimore and Martin [95]. The effectiveness of the antimony/halogen system saturates at Sb_2O_3 volume fractions near 400 µL/L (based on Sb). On the bottom of the figure, curves for Fe, Mn, and Sn added to the air stream of methane-air cup burner flames are also shown [150] (although those experiments were conducted with CO_2 added as the diluent, the data were converted to an equivalent LOI with nitrogen diluent by correcting for the difference in heat capacity between N_2 and CO_2).

Although the influence of Fe, Mn, and Sn on the LOI when added to the air stream of methane-air cup-burner flames is much weaker than that of Sb_2O_3 in halogenated polyethylene, a similar saturation behavior is observed. It would be of value to understand why saturation occurs in the antimony-halogen system, since it has not been explained in the literature.

The current state of understanding of the inhibition of flames by metal compounds is summarized in Table 5. The inhibition potential is summarized in terms of the known inhibition behavior, the detection of metal-containing species in flames, and the state of development of a kinetic description of the inhibition. The level of our knowledge of the potential for loss-of-effectiveness is characterized in terms of the demonstrated loss of effectiveness in flame systems, the presence of particles, and the availability of vapor pressure data for the condensed-phase metal-containing species. The availability of the information is rated as high, medium, low, and none. It should be noted however, that this is a relative scale. Even for elements such as iron, which is the most extensively studied, there are fragmented data on the gas-phase species in flames, the gas-phase kinetic mechanism includes estimated rate constants, and vapor pressure data for some of the important intermediates are not available. As the table illustrates, most of the information needed to accurately predict both the inhibition potential as well as the potential for loss-of-effectiveness is incomplete. (Note again that the rating in the Inhibition Potential column is the amount of *data* about the inhibition potential, not the inhibition ability itself.)

4.3. Possible Approaches for Overcoming Condensation

There may exist approaches for overcoming the loss of effectiveness of metal compounds due to condensation of metal oxides. For example, halogens could be used to attack the metal oxide and provide metal-halogen species in the gas phase. As described by Hastie and co-workers [99], the halogen in the antimony-halogen fire retardant system acts to release the antimony from the condensed phase through a series of halogenation steps involving successive oxychloride phases [98]. Bromine has been used in the past to etch off the lead oxide deposits on engine valves, and halogen is used to remove the oxide coating from the incandescent filament in quartz-halogen light bulbs. It is clear that halogens can release metals from solid oxides, and it may be possible to use this property to re-introduce the metals from the condensed oxide into the gas-phase where they can again inhibit the flame. Finally, the use of carboxylic acids as extenders of antiknock agents [39] (through the formation of metal salts which can persist in the gas phase) raises the possibility of such an approach for metal-based fire suppressants as well.

The driving force of these studies was to understanding the inhibition mechanisms by highly effective additives. As illustrated, metal compounds are up to two orders of magnitude more effective flame inhibitors at low volume fraction than is CF_3Br. If a metal can be found for which condensation of the active intermediate species does not occur, or some means can be devised to re-introduce the active species to the gas phase or prevent condensation in the first place, metals might be used for very effective flame inhibition in unoccupied spaces. Alternatively, if a non-toxic form of the relevant metal is available, use in occupied spaces might be possible.

5. Conclusions

A review of the literature on flame inhibition by metal-containing compounds has been performed, including an overview of recent work of the authors. Gas-phase kinetic models have

been described that explain the effects of highly effective inhibitors added to laminar flames at low volume fraction. Measurements of particles formed from the metal species have been analyzed, and the role of particles in the flame inhibition by metals is discussed. The following major points have been elucidated in this review:

1. Metal agents act via gas-phase catalytic cycles involving metal oxides and hydroxides.
2. The flame inhibition by highly effective additives containing a particular element (Fe, Mn, Na, K,Br, I, P, etc.) is relatively insensitive to the ligands to which it is attached, as long as the element can enter the gas phase.
3. The reaction rates in the inhibition cycle involving iron-containing species are near their collisional rates, and the effectiveness of iron pentacarbonyl may be reaching an upper limit of chemical influence. Multiple catalytic cycles for a given metal are likely.
4. Heterogeneous radical recombination may contribute to the inhibition effect, but it is expected to be much less important than the gas-phase reactions.
5. Effective flame inhibitors act on the super-equilibrium radical concentrations, and their influence is reduced for flames with lower radical super-equilibrium.
6. Above a certain volume fraction metal compounds typically experience a large loss of marginal inhibition effectiveness, which varies with each metal and is due mostly to condensation processes (and partly to reduced super-equilibrium radical concentrations).
7. For effective flame inhibition, the location of the relevant metal-species intermediates must overlap with the location of high concentration of chain-carrying radicals. Factors, that can prevent this overlap include:
    a.) Flow-field effects preventing efficient gas-phase transport.
    b.) Low saturated vapor pressures of metal species that will lead to particle formation with the increase of agent concentration (hence acting as a sink for the active metal species)
    c.) Presence of other species that can react with the metal intermediates to form stable metal-containing compounds, which are a sink for the active species.
    d.) Entrainment or thermophoresis that drive particles away from the flame reaction zone.
    e.) Long residence times and low temperature regions, which promote particle formation.
8. Small particles, generated as a result of decomposition of the metal compound, can re-evaporate in regions of high temperature and strong flame inhibition can still occur.
9. Condensation of active species can severely limit the potential benefit of combinations of inert and effective chemical agents, which were expected to be highly efficient.

In future work, in order to further confirm and develop the inhibition mechanisms developed here, it would be of great value to measure the metal-containing intermediates and chain-carrying radicals in the flame zone. Also, numerical simulations including the condensation process and surface reactions on the particles would be very useful.

6. Acknowledgements

7.   References

1. Babushok VI, Mcnesby KL, Miziolek AW, Skaggs RR. Modeling of synergistic effects in flame inhibition by 2-H heptafluoropropane blended with sodium bicarbonate. Combustion and Flame 2003;133:201-5.

2. Baratov AN, Dobrikov VV, Shamonin VG. Proceedings of IX All Union Symposium on Combustion and Explosion, (in Russian). Chernogolovka. pp. 37-40.

3. Baratov AN, Dobrikov VV, Shamonin VG. The role of gas-phase processes in inhibition of air-methane flame by powder. Chemical Physics (in Russian) 1988;7:827-31.

4. Chelliah HK, Lazzarini AK, Wanigarathne PC, Linteris GT. Inhibition of premixed and non-premixed flames with fine droplets of water and solutions . Proceedings of the Combustion Institute 2002;29:369-76.

5. Chelliah HK, Wanigarathne PC, Lentati AM, Krauss RH, Fallon GS. Effect of sodium bicarbonate particle size on the extinction condition of non-premixed counterflow flames. Combustion and Flame 2003;134:261-72.

6. Williams BA, Fleming JW. Suppression mechanisms of alkali metal compounds. In: Gann, RG, Burgess, SR, Whisner, KC, Reneke, PA, editors. Papers from 1991-2006 Halon Options Technical Working Conferences (HOTWC), CD-ROM, NIST SP 984-4. Gaithersburg, MD: National Institute of Standards and Technology; 2006.

7. Zamansky VM, Lissianski VV, Maly PM, Ho L, Rusli D, Gardiner WC. Reactions of sodium species in the promoted SNCR process. Combustion and Flame 1999;117:821-31.

8. Gann RG. FY2003 Annual report -- Next generation fire suppression technology program (NGP). Gaithersburg, MD: National Institute of Standards and Technology; 2004.

9. Reinelt D, Linteris GT. Experimental study of the inhibition of premixed and diffusion flames by iron pentacarbonyl. Proceedings of the Combustion Institute 1996;26:1421-8.

10. Linteris GT, Knyazev VD, Babushok VI. Inhibition of premixed methane flames by manganese and tin compounds. Combustion and Flame 2002;129:221-38.

11. Bulewicz EM, Padley PJ. Catalytic effect of metal additives on free radical recombination rates in $H_2+O_2+N_2$ flames. Proceedings of the Combustion Institute 1971;13:73-80.

12. Bulewicz EM, Padley PJ, Cotton DH, Jenkins DR. Metal-additive-catalyzed radical-recombination rates in flames. Chemical Physics Letters 1971;9:467-8.

13. Fallis S, Reed R, Lu Y-C, Wierenga PH, Holland GF. Advanced propellant/additive development for fire suppressing gas generators. In: Gann, RG, Burgess, SR, Whisner, KC, Reneke, PA, editors. Papers from 1991-2006 Halon Options Technical Working Conferences (HOTWC), CDROM, NIST SP 984-4. Gaithersburg, MD: National Institute of Standards and Technology; 2006.

14. Rosser WA, Wise H, Miller J. Mechanism of combustion inhibition by compounds containing halogen. Proceedings of the Combustion Institute 1959;7:175-82.

15. Rosser WA, Inami SH, Wise H. Study of the mechanisms of fire extinguishment of liquid rocket propellants. ASTIA Document No. AD 216355; 1959.

16. Rosser WA, Inami SH, Wise H. Study of the mechanisms of fire extinguishment of propellants. Wright-Patterson Air Force Base, OH: Aeronautical Systems Command; 1961.

17. Day MJ, Stamp DV, Thompson K, Dixon-Lewis G. Inhibition of hydrogen-air and hydrogen-nitrous oxide flames by halogen compounds. Proceedings of the Combustion Institute 1971;13:705-12.

18. Dixon-Lewis G , Simpson RJ. Aspects of flame inhibition by halogen compounds. Proceedings of the Combustion Institute 1977;16:1111-9.

19. Biordi JC, Lazzara CP, Papp JF. Flame structure studies of CF_3Br-inhibited methane flames. II-Kinetics and mechanisms. Proceedings of the Combustion institute 1975;15:917-32.

20. Biordi JC, Lazzara CP, Papp JF. Flame-structure studies of CF_3Br-inhibited methane flames. Proceedings of the Combustion Institute 1973;14:367-81.

21. Biordi JC, Lazzara CP, Papp JF. Inhibition of low-pressure quenched flames by CF_3Br. Combustion and Flame 1975;24:401-3.

22. Westbrook CK. Inhibition of hydrocarbon oxidation in laminar flames and detonations by halogenated compounds. Proceedings of the Combustion Institute 1982;19:127-41.

23. Westbrook CK. Inhibition of methane-air and methanol-air flames by HBr. Combustion Science and Technology 1980;23:191-202.

24. Westbrook CK. Numerical modeling of flame inhibition by CF_3Br. Combustion Science and Technology 1983;34:201-25.

25. Smith OI, Wang SN, Tseregounis S, Westbrook CK. The sulfur catalyzed recombination of atomic oxygen in a $CO/O_2/Ar$ Flame. Combustion Science and Technology 1983;30:241-71.

26. Glarborg P, Kubel D, Damjohansen K, Chiang HM, Bozzelli JW. Impact of SO_2 and NO on CO oxidation under post-flame conditions. International Journal of Chemical Kinetics 1996;28:773-90.

27. Westbrook CK. The chemistry behind engine knock. Chemistry & Industry 1992;562-6.

28. Midgley T, Boyd TA. The application of chemistry to the conservation of motor fuels. Industrial and Engineering Chemistry 1922;894-51.

29. Kovarik B. Charles F. Kettering and the development of tetraethyl lead in the context of alternative fuel technologies. In: Fuels and Lubricants. Baltimore MD.

30. Downs D, Walsh AD, Wheeler RW. A study of the reactions that lead to 'knock' in the spark-ignition engine. Philosophical Transactions of the Royal Society of London. Series A, Mathematical and Physical Science 1951;243:463-524.

31. Lovell WG. Knocking characteristics of hydrocarbons. Industrial and Engineering Chemistry 1948; 40:2388.

32. Walsh AD. The mode of action of tetraethyllead as an antiknock. In: Six lectures on the basic combustion process. Ethyl Corp.: New York, NY; 1954.

33. Benson S. The mechanism of inhlbition of knock by lead additives, a chain debranching reaction. J. Physical Chemistry 1988;92:1531-3.

34. Erhard KHL, Norrish RGW. Studies of knock and antiknock by kinetic spectroscopy. Proceedings of the Royal Society (London) A 1956;234:178-91.

35. Westbrook CK, Pitz WJ, Leppard WR. The autoignition chemistry of paraffinic fuels and pro-knock and anti-knock additives: a detailed chemical kinetic study. SAE 1991;91:2314.

36. Muraour H. La theorie des anti-detonants. Chem. et Industr. 1925;14:1911.

37. Chamberlain GHN, Walsh AD. The inhibiting effect of lead tetraethyl. 1. The effect of lead compounds on the vapour phase slow oxidation of diisopropyl ether and on the ignition of diethyl ether. Proceedings of the Royal Society A 1952;215:175-86.

38. Cheaney DE, Davies DA, Davis A, Hoare DE, Protheroe J, Walsh AD. Effects of surfaces on combustion of methane and mode of action of anti-knock containing metals. *Proceedings of the Combustion Institute* 1959;7:183-7.

39. Richardson WL , Ryason PR, Kautsky GJ, Barusch MR. Organolead antiknock agents--their performance and mode of action . Proceedings of the Combustion Institute 1962;9:1023-33.

40. Zimpel CF, Graiff LB. An electron microscopic study of tetraethyllead decomposition in an internal combustion engine. Proceedings of the Combustion Institute 1967;11:1015-25.

41. Rumminger MD, Linteris GT. The role of particles in the inhibition of premixed flames by iron pentacarbonyl. Combustion and Flame 2000;123:82-94.

42. Rumminger MD, Reinelt D, Babushok VI, Linteris GT. Numerical study of the inhibition of premixed and diffusion flames by iron pentacarbonyl. Combustion and Flame 1999;116:207-19.

43. Rumminger MD, Linteris GT. Numerical modeling of counterflow diffusion flames inhibited by iron pentacarbonyl. In: *Fire Safety Science: Proceedings of the Sixth International Symposium*. Poitier France. 289-300.

44. Linteris GT, Rumminger MD, Babushok VI, Tsang W. Flame inhibition by ferrocene and blends of inert and catalytic agents. Proceedings of the Combustion Institute 2000;28:2965-72.

45. Rumminger MD, Linteris GT. The role of particles in the inhibition of counterflow diffusion flames by iron pentacarbonyl. Combustion and Flame 2002;128:145-64.

46. Kuppu Rao V, Prasad CR. Knock suppression in petrol engines. Combustion and Flame 1972;18:167-72.

47. Pitz WJ, Westbrook CK. Chemical-Kinetics of the High-Pressure Oxidation of Normal-Butane and Its Relation to Engine Knock. Combustion and Flame 1986;63:113-33.

48. Jost W, Bonne U, Wagner HG. Iron carbonyl found to be powerful flame inhibitor. Chemical & Engineering News 1961;39:76.

49. Lask G, Wagner HG. Influence of additives on the velocity of laminar flames. Proceedings of the Combustion Institute 1962;8:432-8.

50. Linteris GT ,Rumminger MD. Particle formation in laminar flames inhibited by metals. In: Proceedings of the Western States Section Meeting. La Jolla, CA. 2002. Paper 030.

51. Tappe M, Haynes BS, Kent JH. The effect of alkali-metals on a laminar ethylene diffusion flame. Combustion and Flame 1993;92:266-73.

52. Howard JB, Kausch WJ. Soot control by fuel additives. Progress in Energy and Combustion Science 1980;6:263-76.

53. Lahaye J, Behm S, Ehrburger P. Bockhorn H, editor, Soot formation in combustion. Springer-Verlag, Berlin ; New York ; 1994.

54. Bulewicz EM, Evans DG, Padley PJ. Effect of metal additives on soot formation processes in flames. Proceedings of the Combustion Institute 1974;15:1461.

55. Salooja KC. Journal of Industrial Fuel 1972;45:37.

56. Salooja KC. Combustion control by novel catalytic means. Nature 1972;240:350.

57. Ritrievi KE, Longwell JP, Sarofim AF. The effects of ferrocene addition on soot particle inceptionand growth in premixed ethylene flames. Combustion and Flame 1987;70:17-31.

58. Hahn DW, Charalampopoulos TT. The role of iron additives in sooting premixed flames. Proceedings of the Combustion Institute 1992;24:1007-14.

59. Zhang J, Megaridis CM. Soot suppression by ferrocene in laminar ethylene/air nonpremixed flames. Combustion and Flame 1996;105:528-40.

60. Fenimore CP, Jones GW. Oxidation of soot by hydroxyl radicals. Journal of Physical Chemistry 1967;71:593.

61. Stanmore BR, Brilhac JF, Gilot P. The oxidation of soot: A review of experiments, mechanisms and models. Carbon 2001;39:2247-68.

62. Flynn PF, Durrett RP, Hunter GL, zur Loye AO, Akinyemi OC, Dec JE, Westbrook CK. Diesel combustion: An integrated view combining laser diagnostics, chemical kinetics, and empirical validation. Livermore, CA: Lawrence Livermore National Laboratory; 1999.

63. Kasper M, Siegmann K. The influence of ferrocene on PAH synthesis in acetylene and methane diffusion flames. Combustion Science and Technology 1998;140:333-50.

64. Feitelberg AS , Longwell JP, Sarofim AF. Metal enhanced soot and PAH formation. Combustion and Flame 1993;92:241-53.

65. Wei YL. Effect of potassium hydroxide on PAH formation during toluene incineration. Chemosphere 1998;37:509-21.

66. Babushok VI, Tsang W, Mcnesby KL. Additive influence on polycyclic aromatic hydrocarbon formation. Proceedings of the Combustion Institute 2003;29:2315-23.

67. Morrison ME, Scheller K. The effect of burning velocity inhibitors on the ignition of hydrocarbon-oxygen-nitrogen mixtures. Combustion and Flame 1972;18:3-12.

68. Miller DR, Evers RL, Skinner GB. Effects of various inhibitors on hydrogen-air flame speeds. Combustion and Flame 1963;7:137-42.

69. Miller WJ. Inhibition of low pressure flames. Combustion and Flame 1969;13:210-2.

70. Rosser WA, Inami SH, Wise H. The effect of metal salts on premixed hydrocarbon-air flames. Combustion and Flame 1963;7:107-19.

71. Cotton DH, Jenkins DR. Catalysis of radical-recombination reactions in flames by alkaline earth metals. Transactions of the Faraday Society 1971;67:730-9.

72. deWitte M, Vrebosch J, van Tiggelen A. Inhibition and extinction of premixed flames by dust particles. Combustion and Flame 1964;9:257-66.

73. Vanpee M, Shirodkar P. A study of flame inhibition by metal compounds. *Proceedings of the Combustion Institute* 1979;17:787-95.

74. Rumminger MD, Linteris GT. Inhibition of premixed carbon monoxide-hydrogen-oxygen-nitrogen flames by iron pentacarbonyl. Combustion and Flame 2000;120:451-64.

75. Macdonald MA, Gouldin FC, Fisher EM. Temperature dependence of phosphorus-based flame inhibition. Combustion and Flame 2001;124:668-83.

76. Fallon GS, Chelliah HK, Linteris GT. Chemical effects of CF_3H in extinguishing counterflow $CO/Air/H_2$ diffusion flames. Proceedings of the Combustion Institute 1996;26:1395-403.

77. MacDonald MA, Jayaweera TM, Fisher EM, Gouldin FC. Variation of chemically active and inert flame-suppression effectiveness with stoichiometric mixture fraction. Proceedings of the Combustion Institute 1998;27:2749-56.

78. Babushok VI, Tsang W. Inhibitor rankings for hydrocarbon combustion. Combustion and Flame 2000;123:488-506.

79. James CG, Sugden TM. Photometric investigations of alkali metals in hydrogen flame gases. 3. The source of the alkali metal continuum. Proceedings of the Royal Society A 1958;248:238-47.

80. Bulewicz EM, James CG, Sugden TM. Photometric investigations of alkali metals in hydrogen flame gases. 2. The study of excess concentrations of hydrogen atoms in burnt gas mixtures. Proceedings of the Royal Society A 1956;235:89-106.

81. Bulewicz EM, Sugden TM. Determination of the dissociation constants and heats of formation of molecules by flame photometry; Part 3.-Stability of gaseous cuprous hydroxide. Transactions of the Faraday Society 1956;52:1481-8.

82. Bulewicz EM, Sugden TM. Determination of the dissociation constants and heats of formation of molecules by flame photometry; Part 2.-Heat of formation of gaseous cuprous hydroxide.

Transactions of the Faraday Society 1956;52:1475-80.

83. Padley PJ, Sugden TM. Determination of the dissociation constants and heats of formation of molecules by flame photometry; Part 6.-stability of MnO and MnOH and their mechanisms of formation. Transaction of the Faraday Society 1959;55:2054-61.

84. Bulewicz EM, Padley PJ. Photometric investigations of the behavior of chromium additives in premixed $H_2+O_2+N_2$ flames. Proceedings of the Royal Society London A. 1971;323:377-400.

85. Jenkins, DR. Thornton Research Centre, Personal communication; 1969.

86. Cotton DH, Friswell NJ, Jenkins. The suppression of soot emission from flames by metal additives. Combustion and Flame 1971;17:87-98.

87. Bulewicz EM, Jones G, Padley PJ. Temperature of metal oxide particles in flames. Combustion and Flame 1969;13:409-12.

88. Tischer RL, Scheller K. The behavior of uranium oxide particles in reducing flames. Combustion and Flame 1970;15:199-202.

89. Jensen DE, Jones GA. Mass-spectrometric tracer and photometric studies of catalyzed radical recombination in flames. Journal of the Chemical Society-Faraday Transactions I 1975;71:149-60.

90. Jensen DE, Jones GA. Catalysis of radical recombination in flames by iron. Journal of Chemical Physics 1974;60:3421.

91. Jensen DE, Jones GA. Aspects of flame chemistry of cobalt. Journal of the Chemical Society-Faraday Transactions I 1976;72:2618-30.

92. Hastie JW. Mass spectroscopic studies of flame inhibition: analysis of antimony trihalides in flames. Combustion and Flame 1973;21:49-54.

93. Fenimore CP, Martin FJ. Flammability of polymers. Combustion and Flame 1966;10:135-9.

94. Fenimore CP, Jones GW. Modes of inhibiting polymer flammability. Combustion and Flame 1966;10:295-301.

95. Fenimore CP, Martin FJ. Candle-type test for flammability of polymers. Modern Plastics 1966;12:141-92.

96. Fenimore CP, Martin FJ. Burning of polymers. In: Wall LA, editor, The mechanisms of pyrolysis, oxidation and burning of organic materials. National Bureau of Standards: Washington, D.C.; 1972.

97. Martin FJ, Price KR. Flammability of epoxy resins. Journal of Applied Polymer Science 1968;12:143.

98. Hastie JW. Molecular basis of flame inhibition. Journal of Research of the National Bureau of Standards - A. Physics and Chemistry 1973;77A:733-54.

99. Hastie JW, McBee CL. Mechanistic studies of halogenated flame retardants: The antimony-halogen system. In: Gann RG, editor, Halogenated Fire Suppressants. American Chemical Society : Washington, DC; 1975.

100. Dolan JE, Dempster PB. The suppression of methane-air ignitions by fine powders. Journal of Applied Chemistry 1955;5:510-7.

101. Matsuda S, Gutman D. Shock-tube study of C_2H_2-O_2 reaction. Acceleration of reaction in the presence of trace amounts of $Cr(CO)_6$. Journal of Physical Chemistry 1971;75:2402-4.

102. Matsuda S. Gas phase homogeneous catalysis in shock waves. II. The oxidation of carbon monoxide by oxygen in the presence of iron pentacarbonyl. Journal of Physical Chemistry 1972;57:807-12.

103. Linteris GT, Rumminger MD, Babushok VI. Premixed carbon monoxide-nitrous oxide-hydrogen flames: measured and calculated burning velocities with and without $Fe(CO)_5$. Combustion and Flame 2000;122:58-75.

104. Park K, Bae GT, Shin KS. The addition effect of $Fe(CO)_5$ on methane ignition. Bulletin of the Korean Chemical Society 2002;23:175-6.

105. Shin KS. The inhibition effect of $Fe(CO)_5$ on the ignition of ethane. Bulletin of the Korean Chemical Society 2004;25:745-6.

106. Jensen DE, Webb BC. Afterburning predictions for metal-modified propellant motor exhausts. AIAA Journal 1976;14:947-54.

107. Westblom U, Fernandezalonso F, Mahon CR, Smith GP, Jeffries JB, Crosley DR. Laser-induced fluorescence diagnostics of a propane air flame with a manganese fuel additive. Combustion and Flame 1994;99:261-8.

108. Bonne U, Jost W, Wagner HG. Iron pentacarbonyl in methane-oxygen (or air) flames. Fire Research Abstracts and Reviews 1962;4:6-18.

109. Suyuan Y., Jones AD, Chang DPY, Kelly PB, Kennedy IM. The transformation of chromium in a laminar premixed hydrogen-air flame. Proceedings of the Combustion Institute 1998;27:1639-45.

110. Kennedy IM, Zhang Y, Jones AD, Chang DPY, Kelly PB, Yoon Y. Morphology of chromium emissions from a laminar hydrogen diffusion flame. Combustion and Flame 1999;116:233-42.

111. Kellogg CB, Irikura KK. Gas-Phase thermochemistry of iron oxides and hydroxides:portrait of a super-efficient flame suppressant. Journal of Physical Chemistry a 1999;103:1150-9.

112. Tapscott RE, Sheinson RS, Babushok V, Nyden MR, Gann RG. Alternative fire suppressant chemicals: a research review with recommendations. Gaithersburg MD: National Institute of Standards and Technology; 2001.

113. Linteris GT, Katta VR, Takahashi F. Experimental and numerical evaluation of metallic compounds for suppressing cup-burner flames. Combustion and Flame 2004;138:78-96.

114. Skaggs RR, Mcnesby KL, Daniel RG, Homan B, Miziolek AW. Spectroscopic studies of low pressure opposed flow methane/air flames inhibited by $Fe(CO)_5$, CF_3Br, or N_2. Combustion Science and Technology 2001;162: 1-17.

115. Shmakov AG, Korobeinichev OP, Shvartsberg VM, Yakimov SA, Knyazkov DA, Komarov VF,

Sakovich GV. Testing organophosphorus, organofluorine, and metal-containing compounds and solid-propellant gas-generating compositions doped with phosphorus-containing additives as effective fire suppressants. Combustion Explosion and Shock Waves 2006;42:678-87.

116. Korobeinichev OP, Shvartsberg VM, Shmakov AG, Bolshova TA, Jayaweera TM, Melius CF, Pitz WJ, Westbrook CK, Curran H. Flame inhibition by phosphorus-containing compounds in lean and rich propane flames. Proceedings of the Combustion Institute 2005;30:2353-60.

117. Jayaweera TM , Melius CF, Pitz WJ, Westbrook CK, Korobeinichev OP, Shvartsberg VM, Shmakov AG, Rybitskaya IV, Curran HJ. Flame inhibition by phosphorus-containing compounds over a range of equivalence ratios. Combustion and Flame 2005;140:103-15.

118. Jayaweera TM , Fisher EM, Fleming JW. Flame suppression by aerosols derived From aqueous solutions containing phosphorus. Combustion and Flame 2005;141:308-21.

119. Babushok VI, Tsang W, Linteris GT, Reinelt D. Chemical limits to flame inhibition. Combustion and Flame 1998;115:551-60.

120. Williams FA. A unified view of fire suppression. Journal of Fire and Flammability 1974;5:54-63.

121. Mache H, Hebra A. Sitzungsber. Österreich. Akad. Wiss. 1941;IIa, 150:157.

122. Linteris GT, Truett L. Inhibition of premixed methane-air flames by fluoromethanes. Combustion and Flame 1996;105:15-27.

123. Seshadri K, Williams FA. Laminar flow between parallel plates with injection of reactant at high reynolds number. Int. J. of Heat and Mass Transfer 1978;21:137-50.

124. Fristrom RM, Sawyer RF. Flame inhibition chemistry. In: AGARD Conference Proceedings No. 84 on Aircraft Fuels, Lubricants, and Fire Safety, AGARD-CP 84-71. North Atlantic Treaty Organization: Neuilly-sur-Seine, France; 1971.

125. Richter HJ, Knoche KF. Reversibility of combustion processes. ACS Symposium Series 1983;235:71-85.

126. Lott JL, Christian SD, Sliepcevich CM, Tucker EE. Synergism between chemical and physical fire-suppressant agents. Fire Technology 1996;32:260-71.

127. Frurip DJ, Bauer SH. Homogeneous nucleation in metal vapors. 3. Temperature dependence of the critical supersaturation ratio for iron, lead and bismuth. Journal of Physical Chemistry 1977;81:1001.

128. Lovachev. L. A., Gontkovskaya VT. Regenerative inhibition in hydrogen oxidation. Proceedings of the Russian Academy of Sciences 1972;204-379.

129. Babushok V, Noto T, Burgess DRF, Hamins A, Tsang W. Influence of CF_3I, CF_3Br, and CF_3H on the high-temperature combustion of methane. Combustion and Flame 1996;107:351-67.

130. Noto T, Babushok V, Hamins A, Tsang W. Inhibition effectiveness of halogenated compounds. Combustion and Flame 1998;112:147-60.

131. Linteris GT. Effect of inhibitor concentration on the inhibition mechanism of fluoromethanes in

premixed methane-air flames. In: Miziolek AW, Tsang W, editor, Halon Replacements. ACS Symposium Series 611, American Chemical Society: Washington, D.C.; 1995.

132. Babushok VI ,Tsang W. Influence of phosphorus-containing additives on methane flames. In: Proceedings of the joint meeting of the United States sections of the Combustion Institute. Washington, DC. 1999. pp. 587-590.

133. Rumminger MD , Babushok VI, Linteris GT. Temperature regions of optimal chemical inhibition of premixed flames. Proceedings of the Combustion Institute 2002;29:329–336.

134. Glassman I. Combustion, New York, NY: Academic Press; 1977.

135. Lissianski VV, Maly PM, Zamansky VM, Gardiner WC. Utilization of iron additives for advanced control of NOx emissions from stationary combustion sources. Industrial & Engineering Chemistry Research 2001;40:3287-93.

136. Skillas G, Qian Z, Baltensperger U, Matter U, Burtscher H. The influence of additives on the size distribution and composition of particles produced by diesel engines. Combustion Science and Technology 2000;154:259-73.

137. Hirst B, Booth K. Measurement of flame extinguishing concentrations. Fire Technology 1977;13:296-315.

138. Linteris GT, Chelliah HK. Powder-matrix systems for safer handling and storage of suppression agents. Gaithersburg, MD: National Institute of Standards and Technology; 2001.

139. Reinelt D, Linteris GT. Experimental study of the flame inhibition effect of iron pentacarbonyl. In: Gann, RG, Burgess, SR, Whisner, KC, Reneke, PA, editors. Papers from 1991-2006 Halon Options Technical Working Conferences (HOTWC), CD-ROM, NIST SP 984-4. Gaithersburg, MD: National Institute of Standards and Technology; 2006.

140. Lippincott ES, Tobin MCJ. The vibrational spectra and thermodynamic functions of lead tetramethyl, tin tetramethyl and germanium tetramethyl. Journal of the American Chemical Society 1953;75:4141-7.

141. Katta VR, Takahashi F, Linteris GT. Numerical investigations of CO_2 as fire suppressing agent. In: Fire Safety Science: Proceeding of the Seventh International Symposium. Worchester, MA. 531-542.

142. Takahashi F, Linteris GT, Katta VR. Extinguishment mechanisms of co-flow diffusion flames in a cup-burner apparatus. Proceedings of the Combustion Institute 2006;31:doi:10.1016/j.proci.2006.08.112.

143. Katta VR, Takahashi F, Linteris GT. Extinction characteristics of cup-burner flame in microgravity. In: 41st Aerospace Sciences Meeting and Exhibit. Reno, NV. AIAA Paper No. 2003-1150.

144. Linteris GT, Takahashi F, Katta VR. Cup-burner flame extinguishment by CF_3Br and Br_2. Combustion and Flame 2006;submitted:

145. Nesmeianov AN. Vapour pressure of the elements., New York, Academic Press: 1963.

51

146. Grimley RT, Burns RP, Inghram MG. Thermodynamics of the vaporization of Cr_2O_3: dissociation energies of CrO, CrO_2, and CrO_3. Journal of Chemical Physics 1961;34:664-7.

147. Gurvich LV, Glushkov VP. Thermodynamic properties of individual substances. Gaithersburg, MD: National Institute of Standards and Technology; 1998.

148. Barin I, Knacke O. Thermochemical properties of inorganic substances, Berlin, New York: Springer-Verlag; 1973.

149. Barin I, Knacke O, Kubaschewski O. Thermochemical properties of inorganic substances, Berlin, New York : Springer-Verlag; 1977.

150. Linteris GT. Extinction of cup-burner diffusion flames by catalytic and inert inhibitors. In: Second NRIFD Symposium - Science, Technology and Standards for Fire Suppression Systems. Tokyo, Japan. 269-282.

151. Rumminger, M.D., Unpublished data, 2000.

152. Linteris GT. Limits to the effectiveness of metal-containing fire suppressants. Gaithersburg MD: National Institute of Standards and Technology; 2004.

8.   Table Captions

9.   Figure Captions

Table 1 - Catalytic efficiency of different metals in promoting radical recombination .

Values of k_{obs}/k_{uncat} (T = 1860°K; X[M] = 1.3 μL/L; $H_2/O_2/N_2$ = 3/l/6).

Strong effect		Some effect		No effect	
Cr	2.8	Co	1.1	V	1
U	1.82	Pb	1.1	Ni	1
Ba	1.75	Zn	1.07	Ga	1
Sn	1.6	Th	1.06	Cl	1
Sr	1.35	Na	1.04		
Mn	1.3	Cu	1.04		
Mg	1.25	La	1.04		
Ca	1.25				
Fe	1.2				
Mo	1.16				

Table 2 – Metals which have shown flame inhibiting properties. The type of experiment is shown at the top, followed by the specific reference.

Element	Detailed Flame Studies					Engine Knock					Flame Screening Tests						Flat-Flame Radical Recombination						Ignition			FR
	[108]	[9]	[10]	[44]	[113]	[38]	[29]	[46]	[34]	[32]	[49]	[73]	[68]	[69]	[72]	[70]	[11]	[12]	[84]	[91]	[89]	[90]	[100]	[67]	[34]	[98]
Cr											X	X		X			X	X	X							
Pb						X	X		X	X	X	X	X		X		X									
Fe	X	X		X	X	X	X			X	X	X	X	X			X				X					
Mn			X		X																					
Ni								X		X																
W														X							X					
Mo																	X				X					
Cu								X							X	X	X						X			
Te							X		X	X																
Tl						X																				
Bi						X																				
U																	X	X								
Zn																		X								
La																		X								
Th																		X								
Se						X																				
Sn		X			X	X	X				X		X	X			X	X		X			X	X		
Ti											X		X	X												
Co													X				X		X				X			
Ge											X															
Sb											X		X													X

58
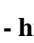
Table 3 . Inhibitor concentration required for 30 and 50 % decreases of burning velocity for different models and experimental data (stoichiometric methane/air flame, 0.101 MPa).
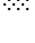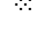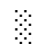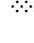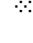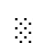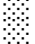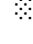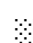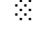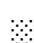
Model and Experimental Data	Reaction Rate Constant Pre-Exponential mol, cm^3 s units	Inhibitor, Volume Fraction μL/L required for:	
		30 % reduction	50 % reduction
Perfect inhibitor Model	5×10^{13}	100	200
	1×10^{14}	50	110
	2×10^{14}	30	60
Fe(CO)$_5$ model, Jensen and Jones [90]		400	800
CF$_3$Br model		5000	10000
Fe(CO)$_5$ Experiment[*], Lask and Wagner [49]		120	200
Fe(CO)$_5$ Experiment[*], Reinelt and Linteris [9]		70	130

[*] The data were obtained by linear extrapolation from experimental results.

Table 4. Calculated maximum and equilibrium radical volume fraction in methane-air flame.

Condition	Species		
	H	OH	O
Maximum (no inhibitor)	7.0×10^{-3}	7.8×10^{-3}	3.3×10^{-3}
Equilibrium (no inhibitor)	4.2×10^{-4}	3.0×10^{-3}	2.4×10^{-4}
End of flame reaction zone (1900 µL/L , $Fe(CO)_5$)	4.0×10^{-4}	2.0×10^{-3}	1.5×10^{-4}
Equilibrium (1900 µL/L $Fe(CO)_5$)	4.5×10^{-4}	2.5×10^{-3}	1.7×10^{-4}

Table 5 – Current state of knowledge relevant to inhibition potential of metals, and potential loss of effectiveness due to condensation. Key: ▓ - high, ▒ - medium, ░ - low, -none.

Element	Inhibition Information			Condensation Information		
	Inhibition Potential	Gas-phase Species Identified	Kinetic Mechanism State of Development	Demonstrated Loss-of-Effectiveness	Experimental Evidence of Particles	Experimental Vapor Pressure Data
Cr	high	low	low	high	high	low
Pb	high				high	
Fe	high	high	low	high	high	
Mn	high	high	low	high	low	low
Ni	low	high	low	high		
W	low		low			low
Mo	low		low			low
Cu	low	low				low
Te	low					
Tl	low					
Bi	low					
U	low					
Zn	low					
La	low					
Th	low					
Se	low					
Sn	low	high	low	high	low	low
Ti	low				low	
Co	low	high				low
Ge	low					
Sb	low	low	low	low		

61

Fig. 1. Mole merit number of metal compounds for the oxidizer velocities in the range of 50 cm/s to 60 cm/s (from [73]).

Fig. 2. Relative inhibitor effectiveness. Additive effectiveness is presented in coefficients of efficiency relative CF₃Br . The considered compounds are mostly liquids or solids [78].
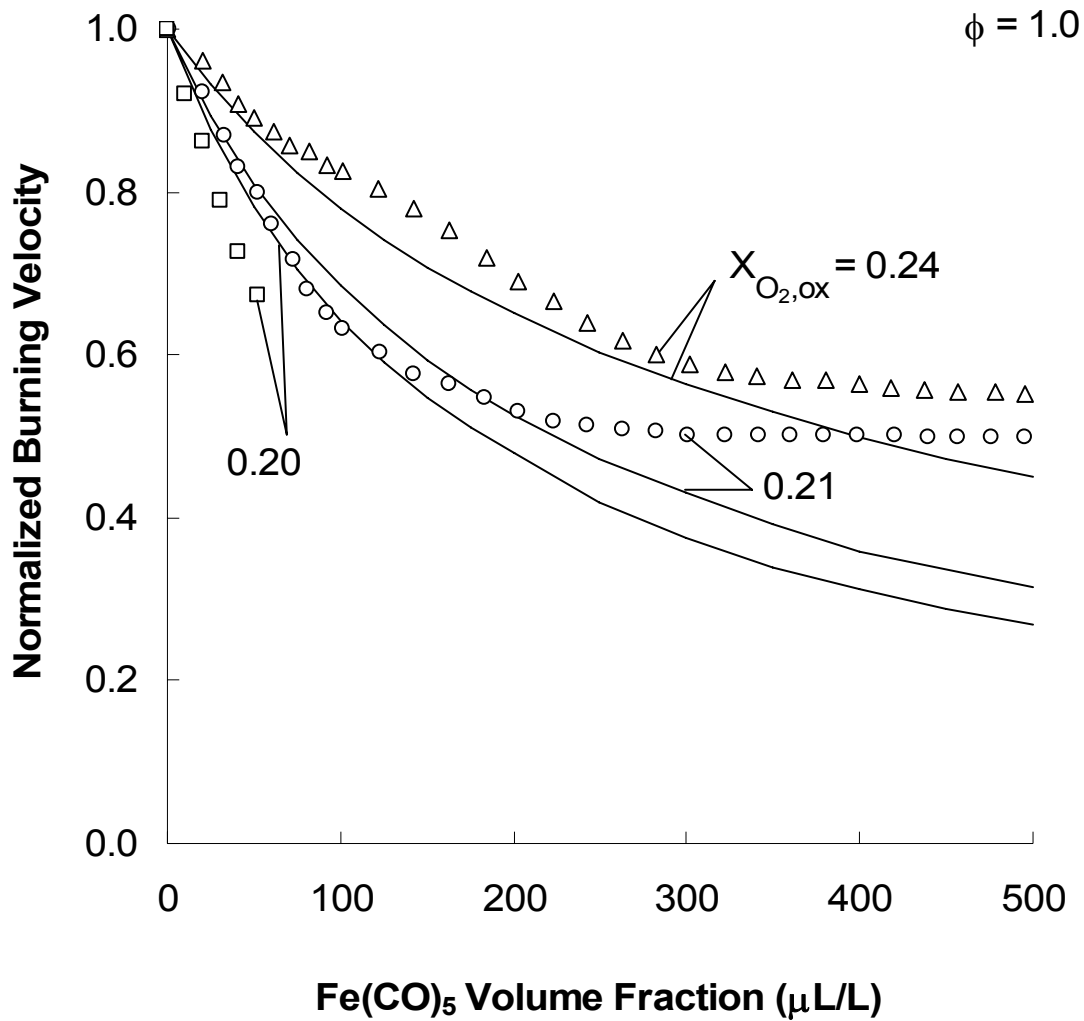
Fig. 3. Normalized burning velocity of premixed CH$_4$-air flames with added Fe(CO)$_5$ at varying $X_{O_2,ox}$.
(Points: experimental data; lines: 1-D numerical predictions with gas-phase inhibition chemistry) [9].

\home\greg\paper archive\Combustion and Flame\CNF Numerical Modeling Paper\PREPAPERnew.xls
Sheet:PECS Fe Xo2
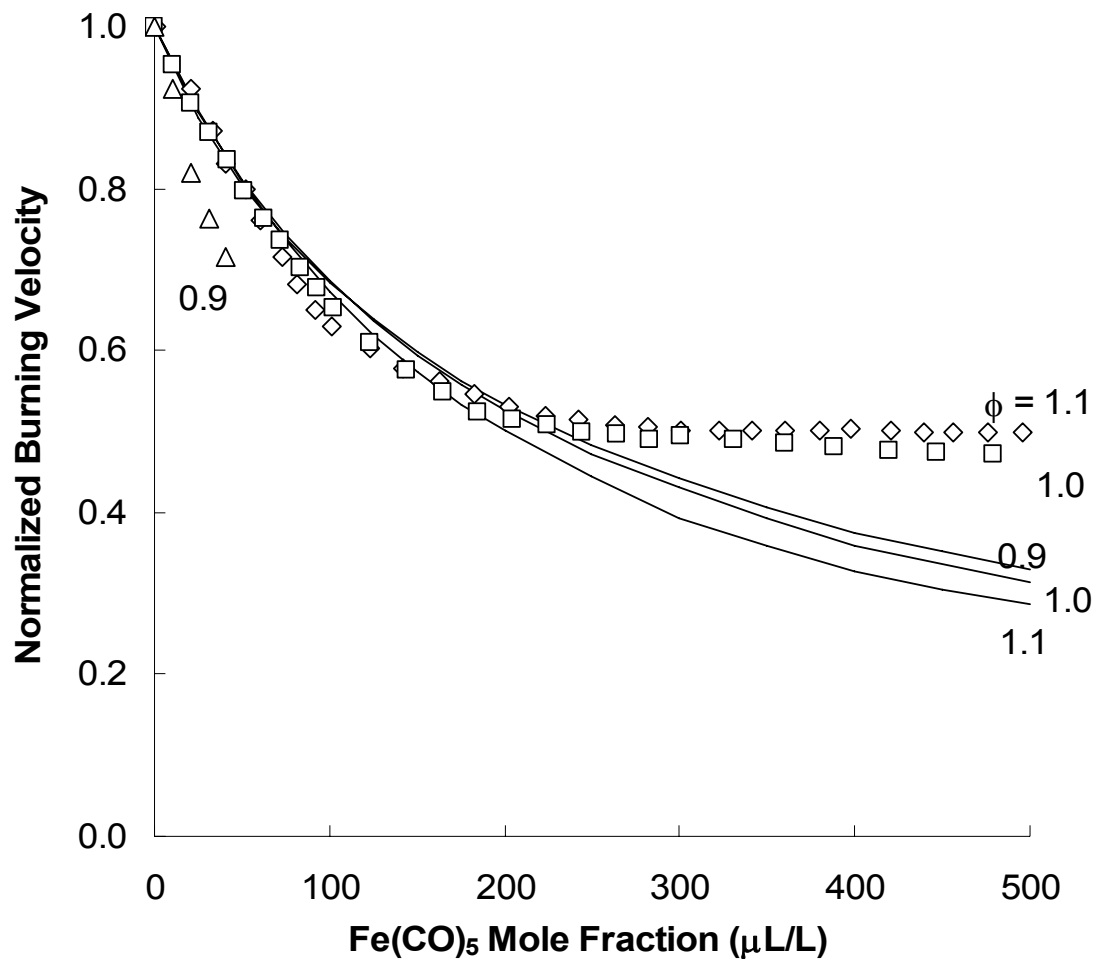
Fig. 4. Normalized burning velocity of premixed CH4-air flames with added Fe(CO)$_5$ at varying ϕ. (Points: experimental data; lines: 1-D numerical predictions with gas-phase inhibition chemistry) [9].

\home\greg\paper archive\Combustion and Flame\CNF Numerical Modeling Paper\PREPAPERnew.xls\Sheet:PECS Fe phi
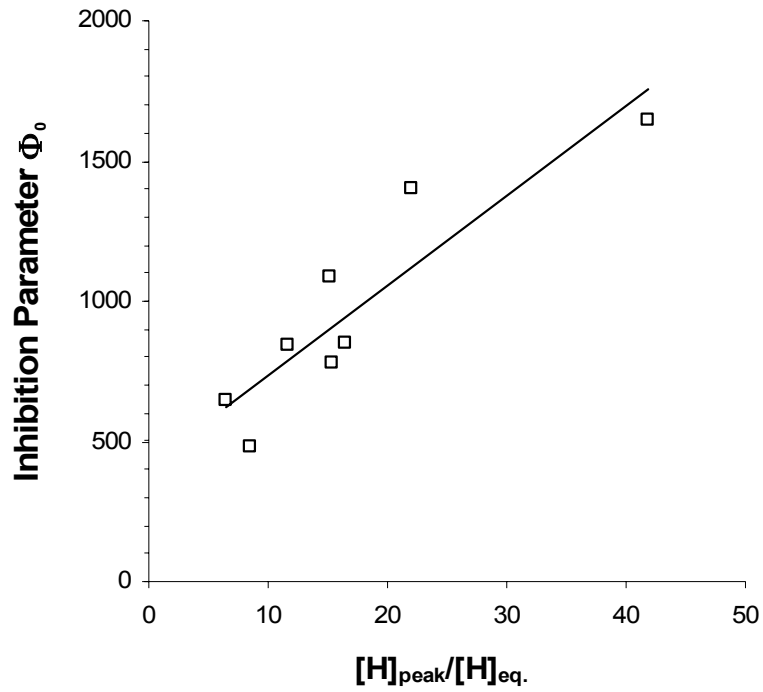
Fig. 5. Variation of inhibition parameter Φ_0 [124] with degree of H-atom super equilibrium in premixed methane-air flames with added $Fe(CO)_5$ (line: linear curve fit) [9].

\home\greg\paper archive\combustion symposium (international)\26th symp FECO5\SE_vs_PHI.xls\ sheet: sheet 1
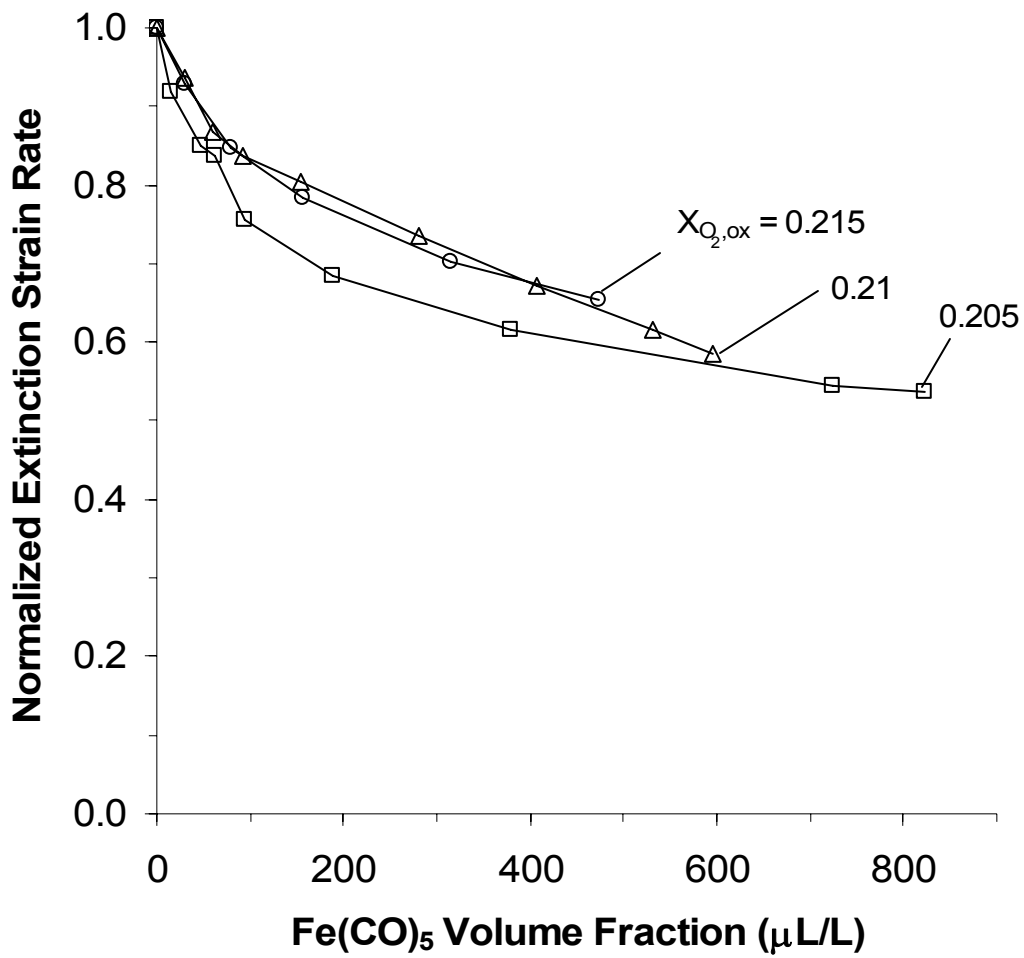
Fig. 6. Normalized extinction strain rate for CH$_4$/O$_2$/N$_2$ flames with added Fe(CO)$_5$ in the oxidizer stream having $X_{O_2,ox}$= 0.205, 0.21, and 0.215 (lines and points: experiments) [9].

..\..\Past Research\Metals\FECO5\CF\FECO5\feco5xo2.xls Sheet: a vs Xi var XO2
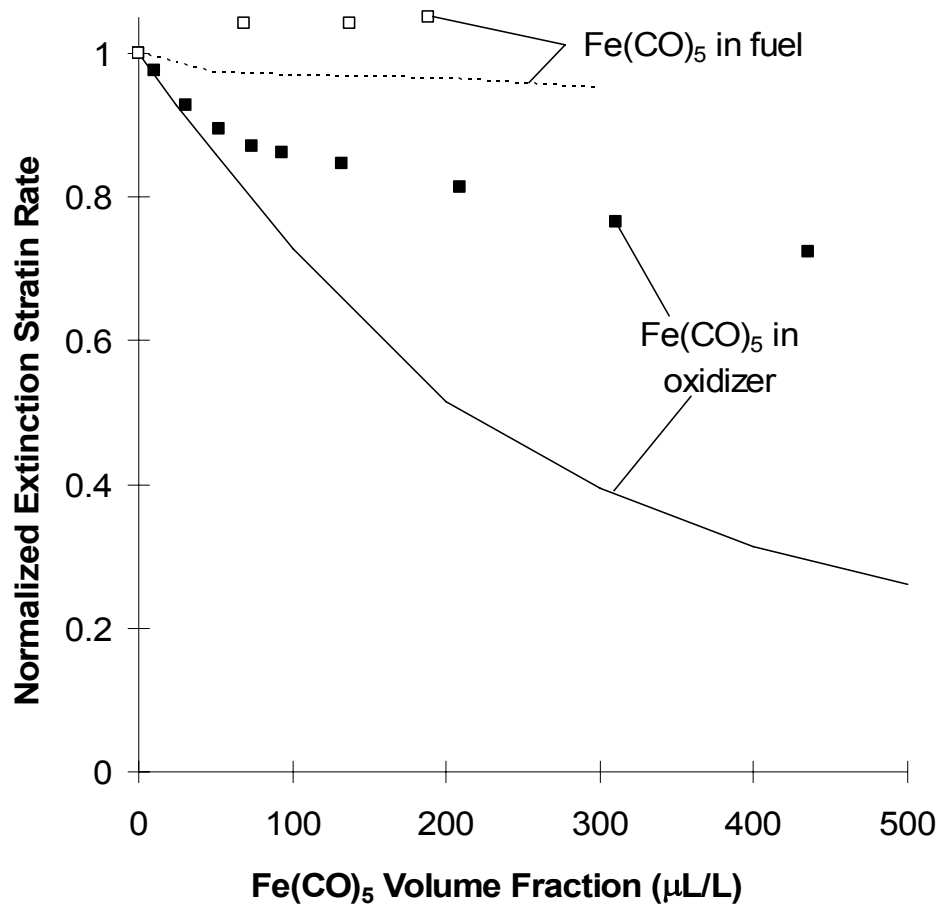
Fig. 7. Normalized extinction strain rate for $CH_4/O_2/N_2$ flames with added $Fe(CO)_5$ in the oxidizer stream or fuel stream (points: experiment; lines: numerical calculation) [9].

..\..\Paper Archive\Combustion and Flame\CNF Counterflow Particles\Excel files\Extinction Strain Rates for CH4 Flames.xls **sheet:**
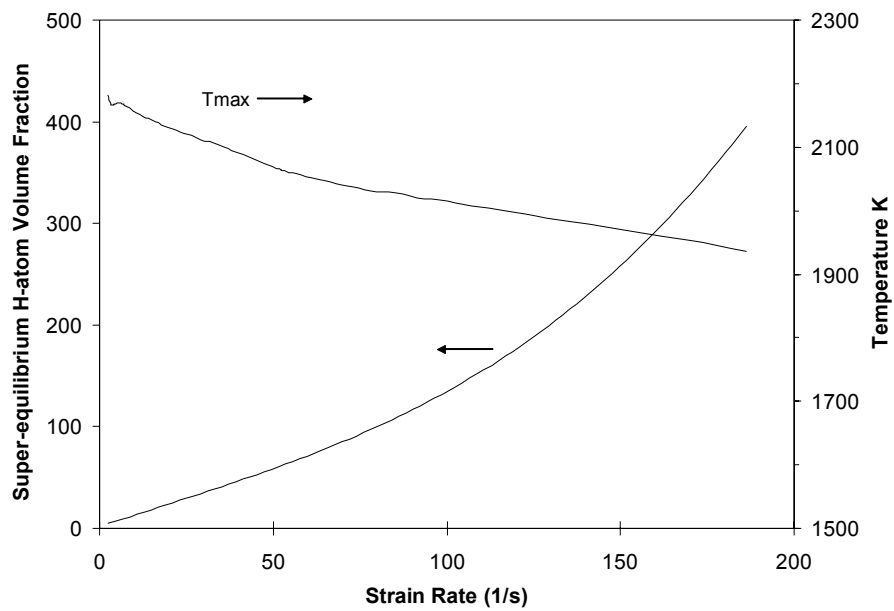
Fig. 8. Super-equilibrium ratio and temperature variation with strain for counterflow CH₄-air flames [151].
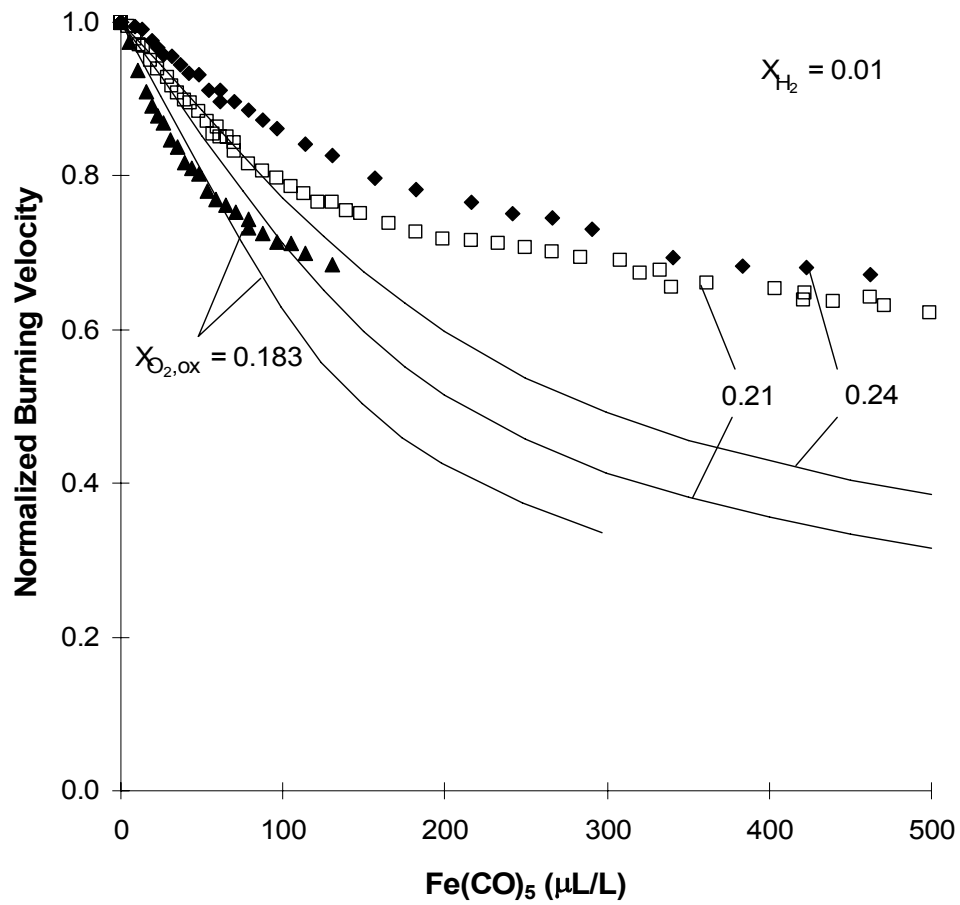
Fig. 9. Normalized burning velocity for $CO/O_2/H_2/N_2$ flames with added $Fe(CO)_5$ with X_{H_2}=0.01 and varying $X_{O_2,ox}$ (points: experiments; lines: numerical calculations) [74].

\home\greg\Paper Archive/Combustion and Flame\CNF Fe(CO)5 in CO Flames\Zipped up files\New CO-H2 with Fe(CO)5.xls\sheet:PECS vary XO2
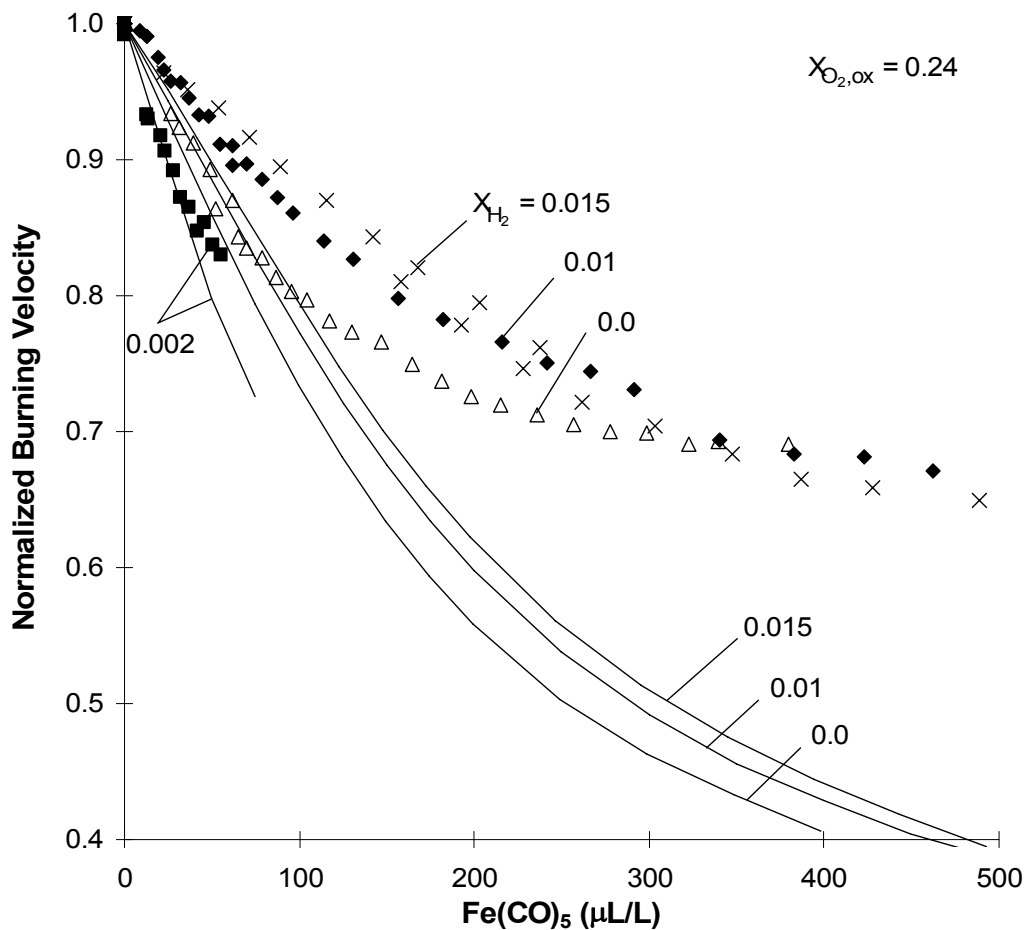
Fig. 10. Normalized burning velocity for $CO/O_2/H_2/N_2$ flames with added $Fe(CO)_5$ with $X_{O_2,ox} = 0.24$ and varying X_{H_2} (points: experiments; lines, numerical calculations) [74].

\home\greg\Paper Archive/Combustion and Flame\CNF Fe(CO)5 in CO Flames\Zipped up files\New CO-H2 with Fe(CO)5.xls\sheet:PECS vary XH2
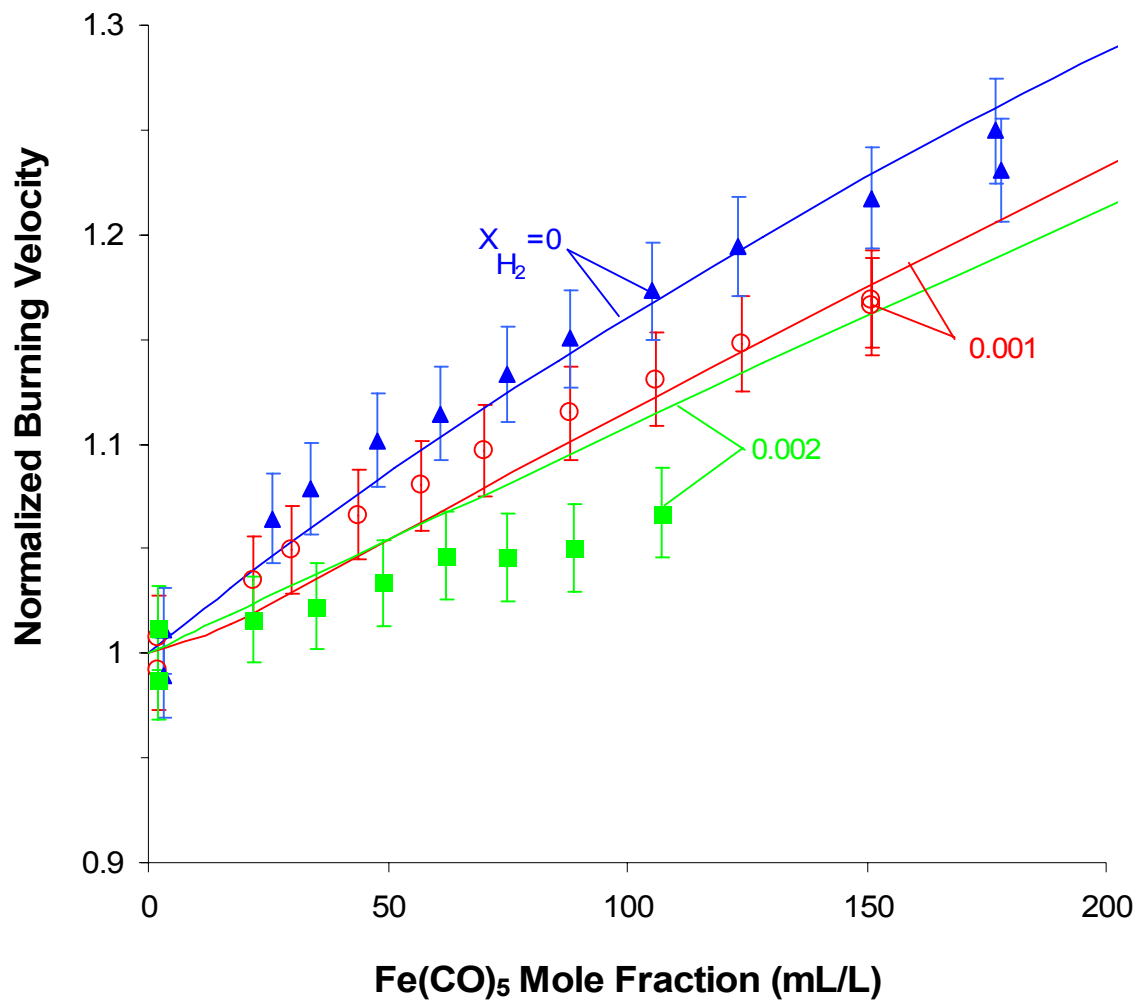
Fig. 11. Normalized burning velocity of premixed CO-N$_2$O flames with varying hydrogen content, as a function of Fe(CO)$_5$ volume fraction (points: experiments; lines: numerical calculations) [103].

..\..\Paper Archive\Combustion and Flame\CNF Fe(CO)5 in CO-N2O Flames\Excel Files\con2ov16.xls sheet: PECS CO-N2O V0
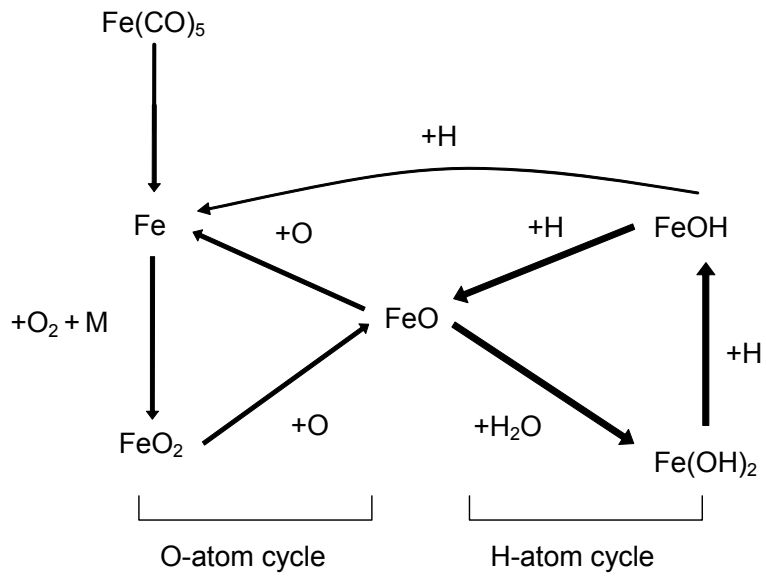
Fig. 12. Schematic diagram of radical recombination reaction pathways in found to be important for CO-H$_2$-O$_2$-N= flames. Thicker arrows correspond to higher reaction flux. Reaction partners are listed next to each arrow [74].
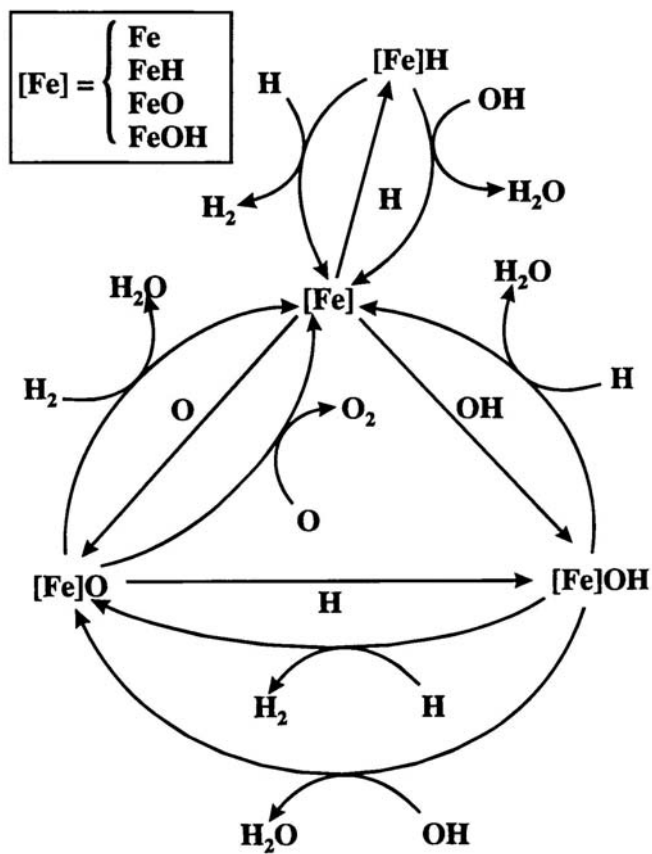
Fig. 13. Schematic representation of different classes of reactions which-may contribute to iron's super-efficient flame suppression ability through the catalytic recombination of radical species [111].
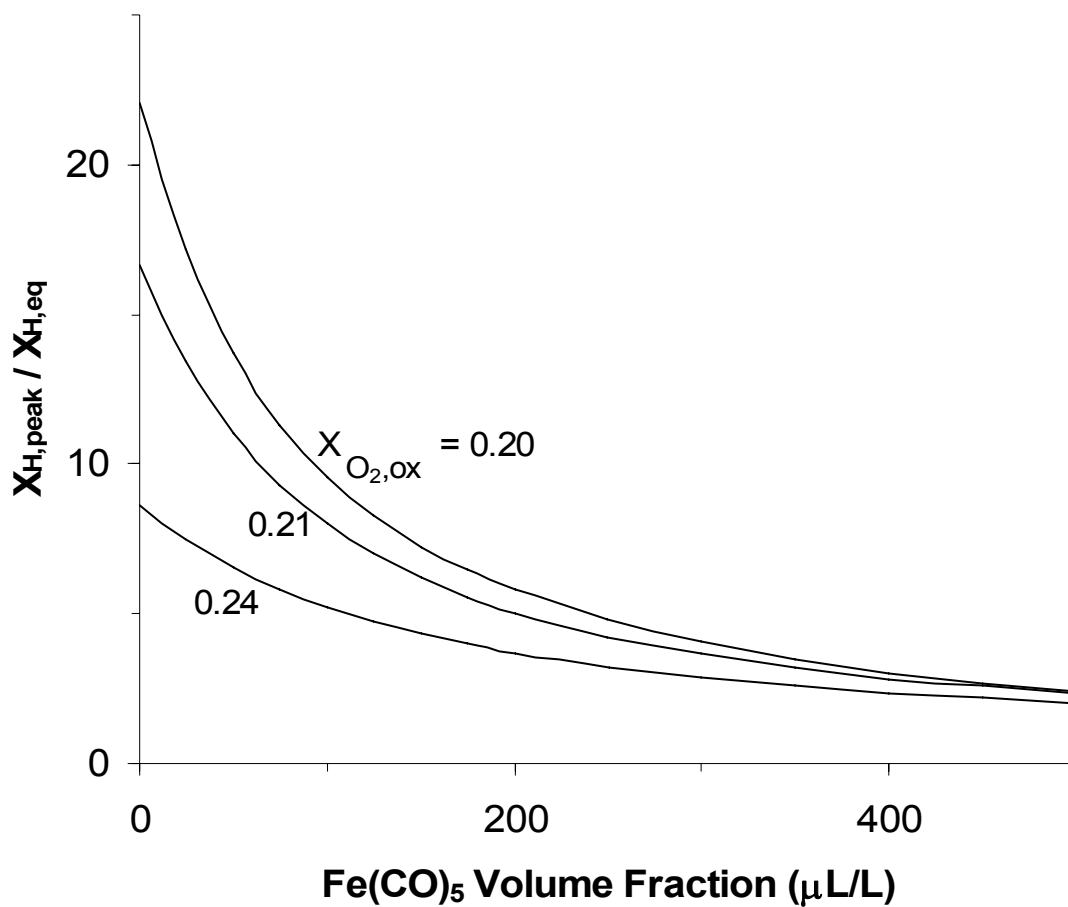
Fig. 14. Calculated ratio of peak and equilibrium values of [H] in premixed $CH_4/O_2/N_2$ flames with added $Fe(CO)_5$ at different $X_{O_2,ox}$. [42]

..\..\Paper Archive\Combustion and Flame\CNF Numerical Modeling Paper\PREPAPERnew.xls
sheet: PECS Peak-final (O2)
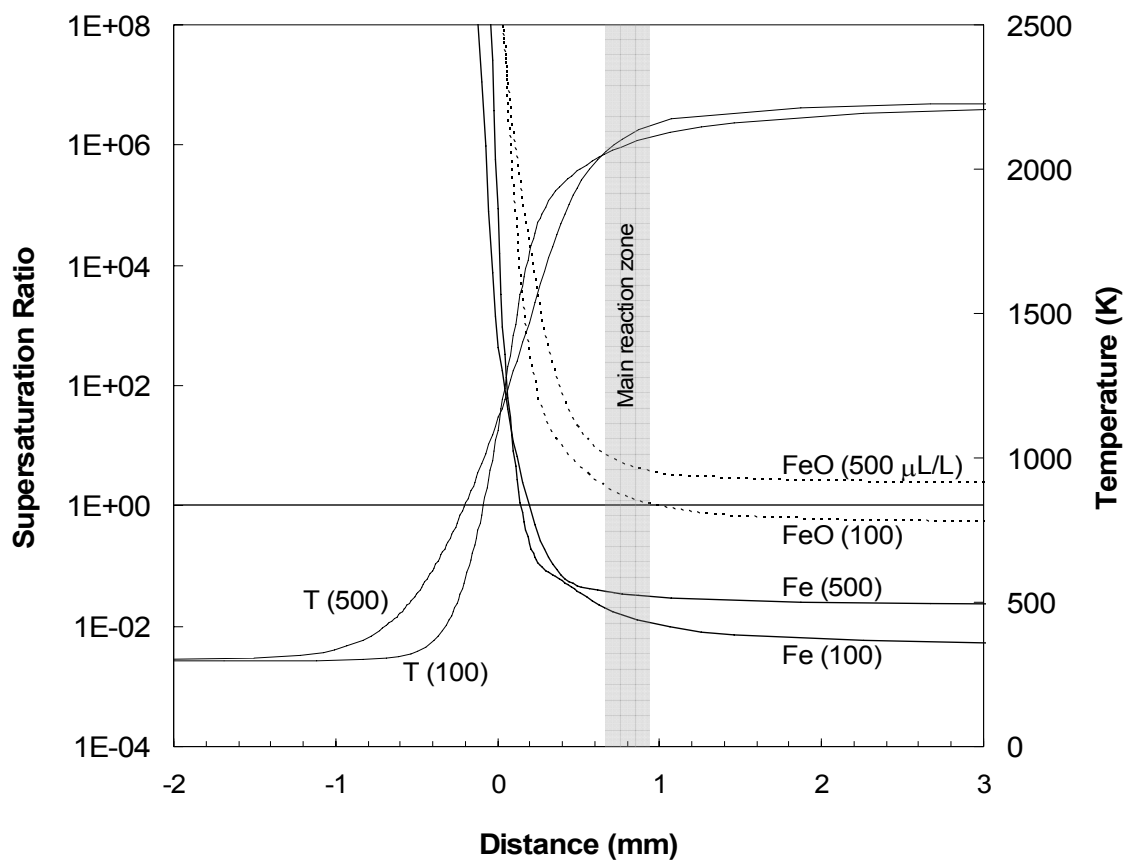
Fig. 15. Temperature and supersaturation ratio of Fe and FeO as a function of position through a premixed CH₄-air flame with Fe(CO)₅ added at 100 μL/L or 500 μL/L [9].

..\..\Paper Archive\Combustion and Flame\CNF Numerical Modeling Paper\PREPAPERnew.xls **sheet: PECS supersat**
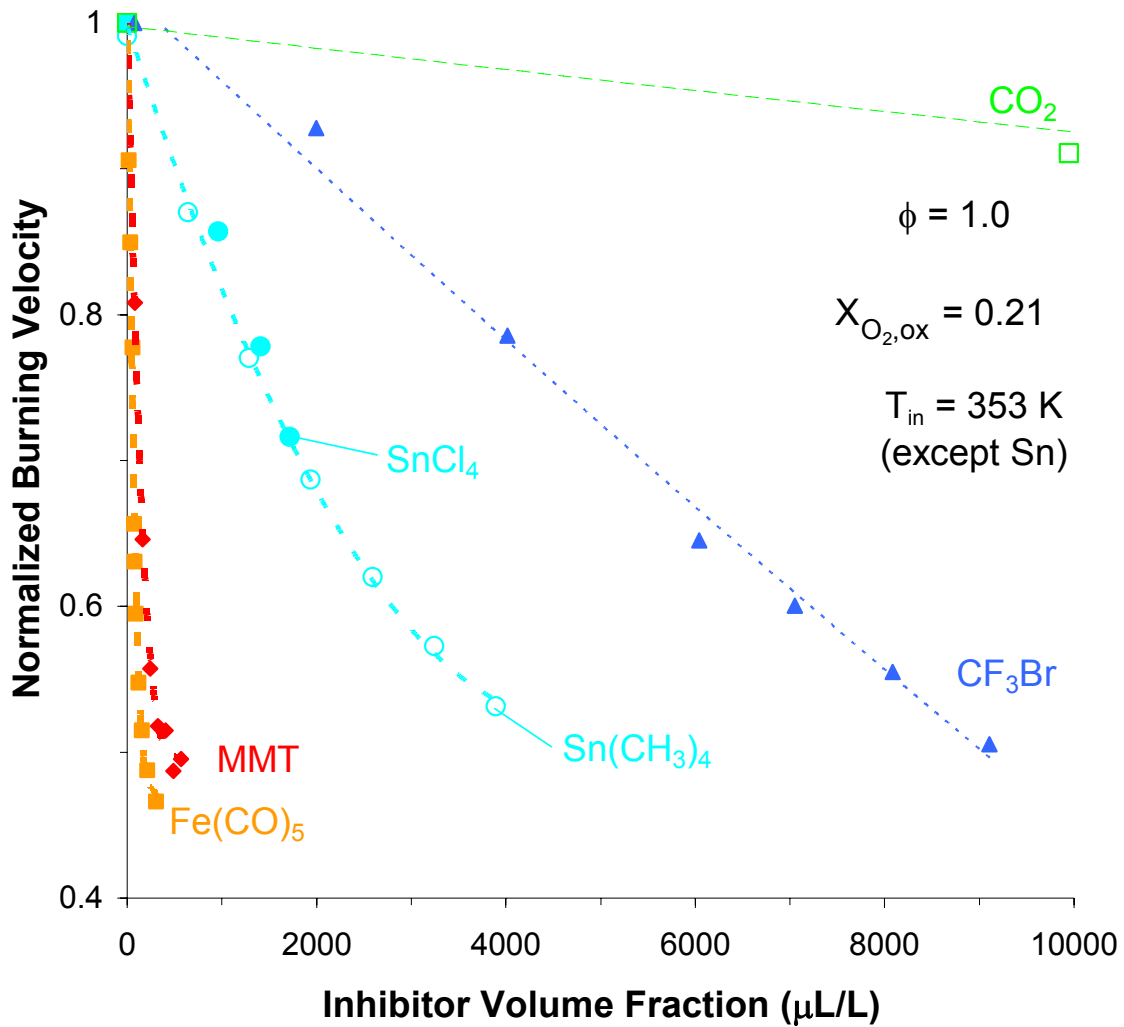
Fig. 16. Normalized burning velocity of premixed $CH_4/O_2/N_2$ flames inhibited by CO_2, CF_3Br, $Sn(CH_3)_4$, $SnCl_4$ [49], MMT, and $Fe(CO)_5$ (T_{in} = 353 K for all data except $Sn(CH_3)_4$ and $SnCl_4$ which are at 298 K). (Points: experiments; lines: curve fits) [10].

I:\Home\Greg\Paper Archive\Combustion and Flame\CNF Premixed Mn,Sn Paper\Excel Files\manganese.xls sheet: All Metals Norm PECS
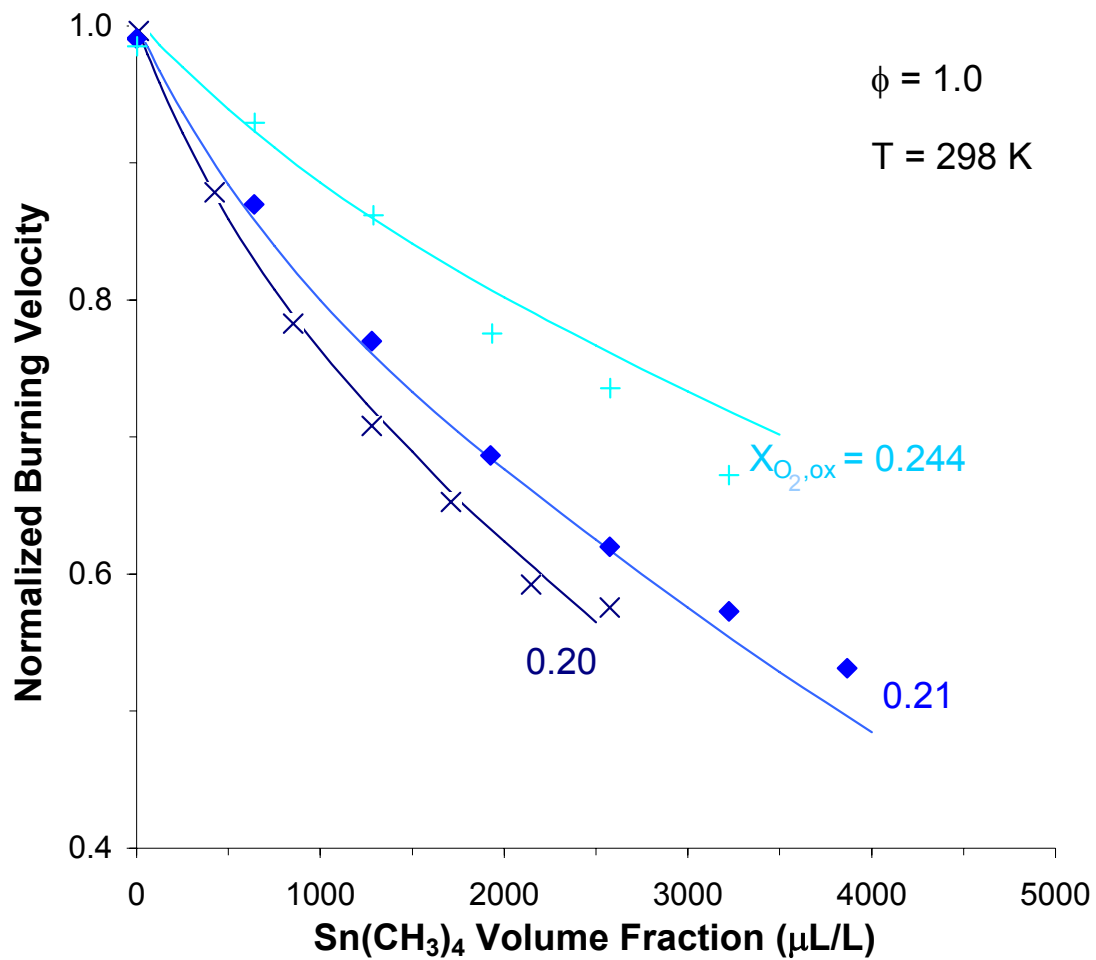
Fig. 17. Normalized burning velocity of premixed CH$_4$/O$_2$/N$_2$ flames inhibited by TMT, with ϕ=1.0 and X$_{O2,ox}$=0.20. 0.21, and 0.244 (points: experiments; lines: numerical calculations) [10].

I:\Home\Greg\Paper Archive\Combustion and Flame\CNF Premixed Mn,Sn Paper\Excel Files\tin01.xls sheet Var'n with XO2 - norm
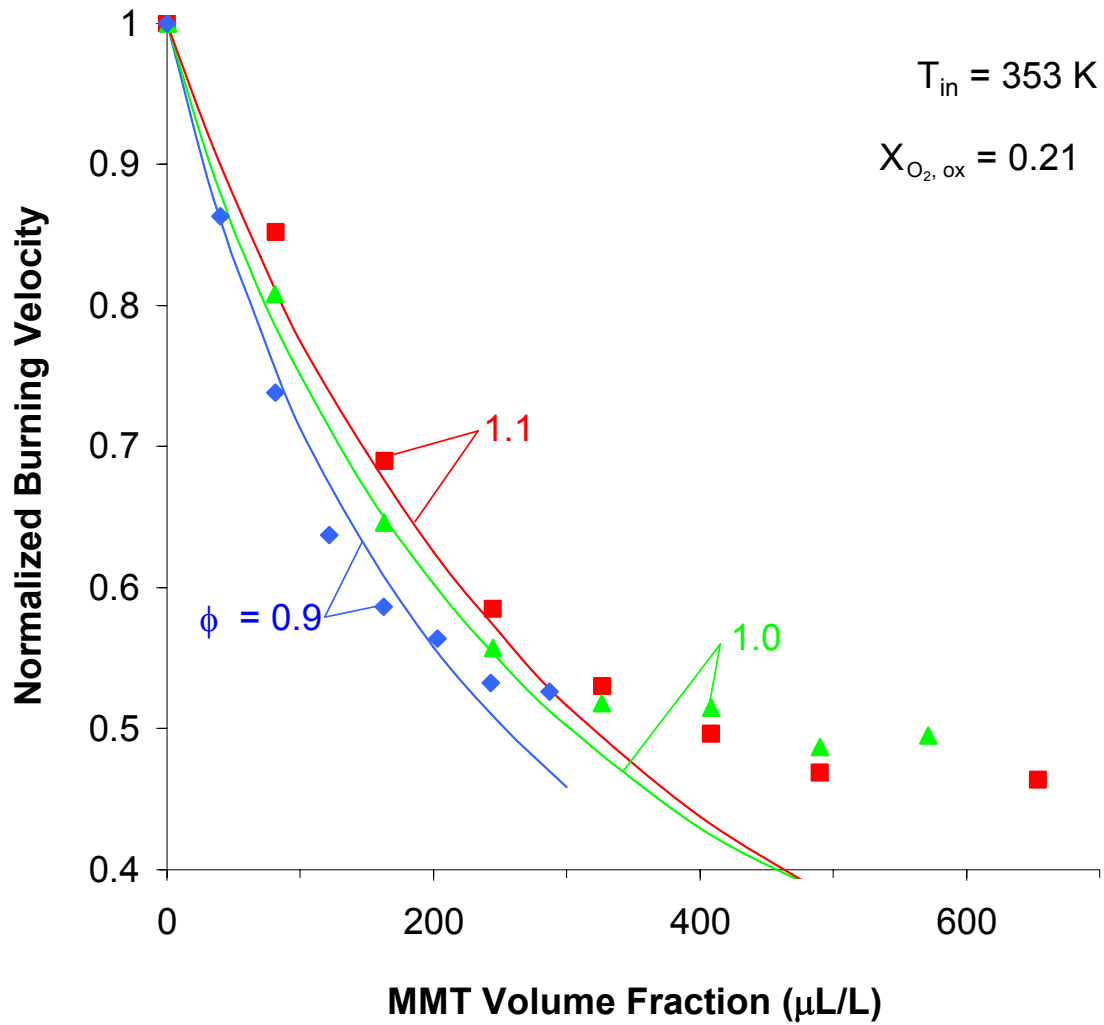
Fig. 18. Normalized burning velocity of premixed CH$_4$/O$_2$/N$_2$ flames inhibited by MMT with $X_{O2,ox}$=0.21 and ϕ=0.9, 1.0, and 1.1 (points: experiments; lines: numerical calculations) [10].

I:\Home\Greg\Paper Archive\Combustion and Flame\CNF Premixed Mn,Sn Paper\Excel Files\Manganese.xls sheet: vary Phi norm PECS

Sn

+ O₂ +(M) (4)

+ O₂ (95)

SnO₂

+ H (15)

+ H (63)
CO (16)
O (5)

+ OH (46)
H (43)
CH₃ (5)
O (5)

+ CO (4)

SnO

SnOH

+ H + M (86)
HCO (9)

Mn

+ O₂ +(M) (96)

MnO₂

+ H (43)
O (37)
CO (15)
OH (5)
H +M (3)

+ H (66)
O (14)
OH (13)
CH₃ (3)

MnO

+ H₂O (95)

MnOH

Mn(OH)₂

+ H (100)

Fe

+ O₂ +(M) (92)

FeO₂

+ O (94)
H (4)

+ H (2)
O (1)
H₂ (1)

+ H (76)
O (13)
CH₃ (4)
OH (3)

FeO

+ H₂O (95)

FeOH

Fe(OH)₂

+ H (100)
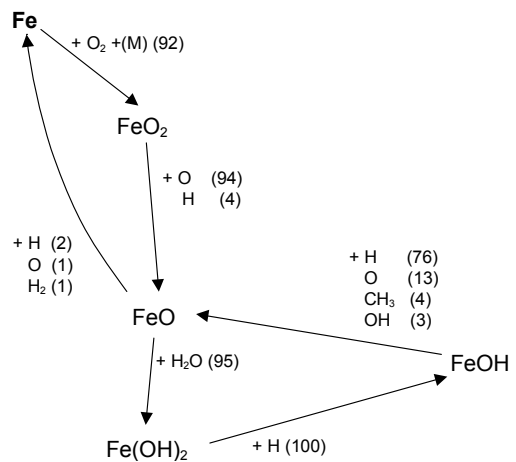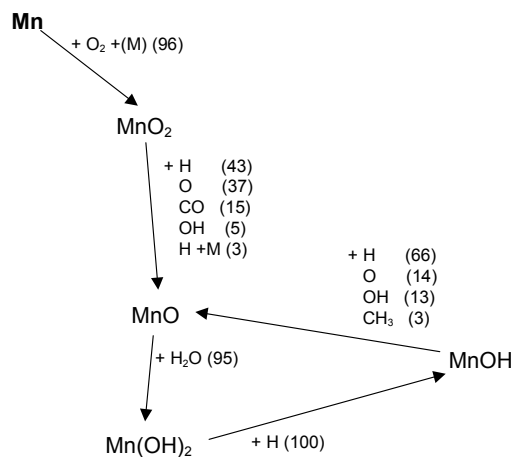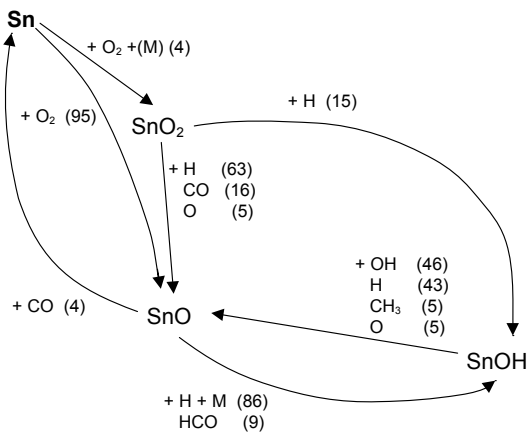
Fig. 19. Reaction pathways for Sn, Mn, and Fe in a premixed methane-air flame ($\phi=1.0$, $X_{O_2,ox} = 0.21$, Tin=353 K). TMT, MMT, and Fe(CO)₅ present at (1963, 128, or 105) μL/L, respectively. The numbers in parentheses are the fractional consumption (percent) of the reactant molecule

80
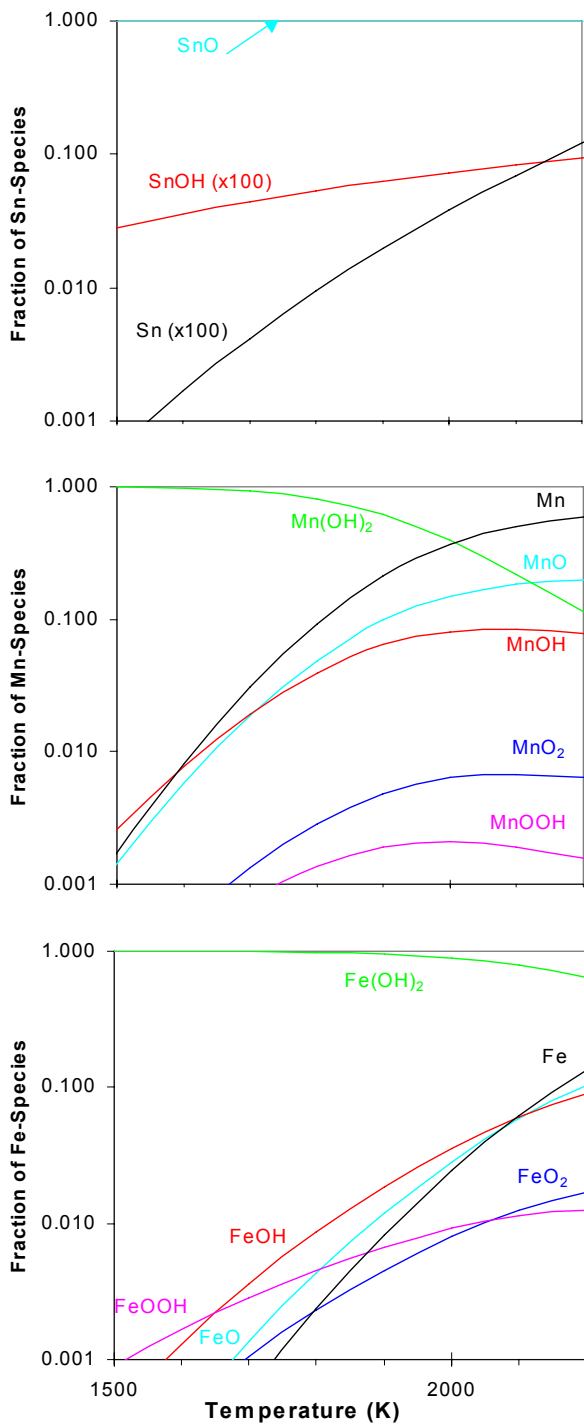
Fig. 20. Fraction of Sn-, Mn-, and Fe-species at equilibrium in methane-air flames as a function of temperature.
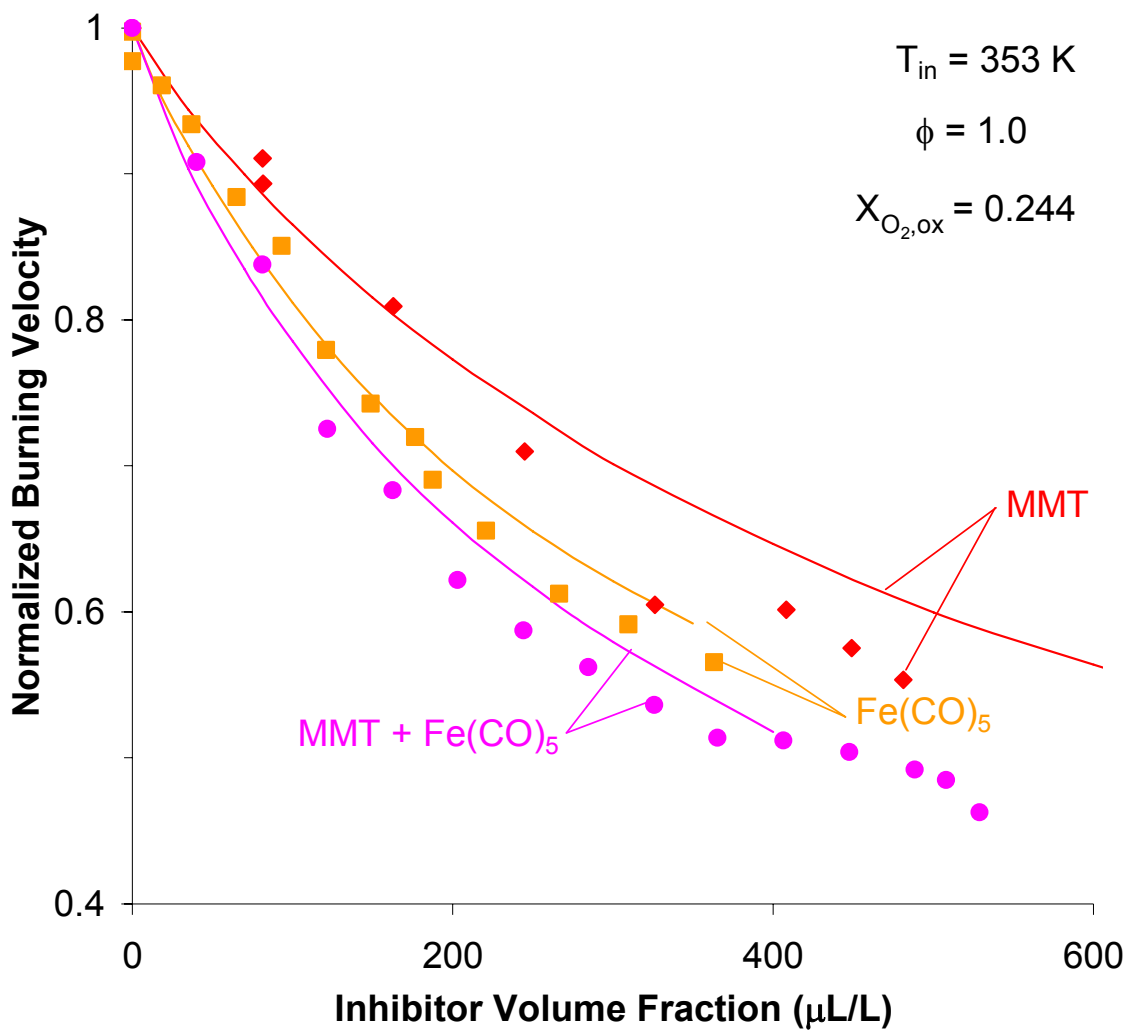
Fig. 21. Normalized burning velocity of premixed CH$_4$/O$_2$/N$_2$ flames inhibited by pure MMT and Fe(CO)$_5$, and by a blend of the two (points: experiments; lines: numerical calculations) [10].

I:\Home\Greg\Paper Archive\Combustion and Flame\CNF Premixed Mn,Sn Paper\Excel Files\Manganese.xls sheet: Simult. Norm PECS
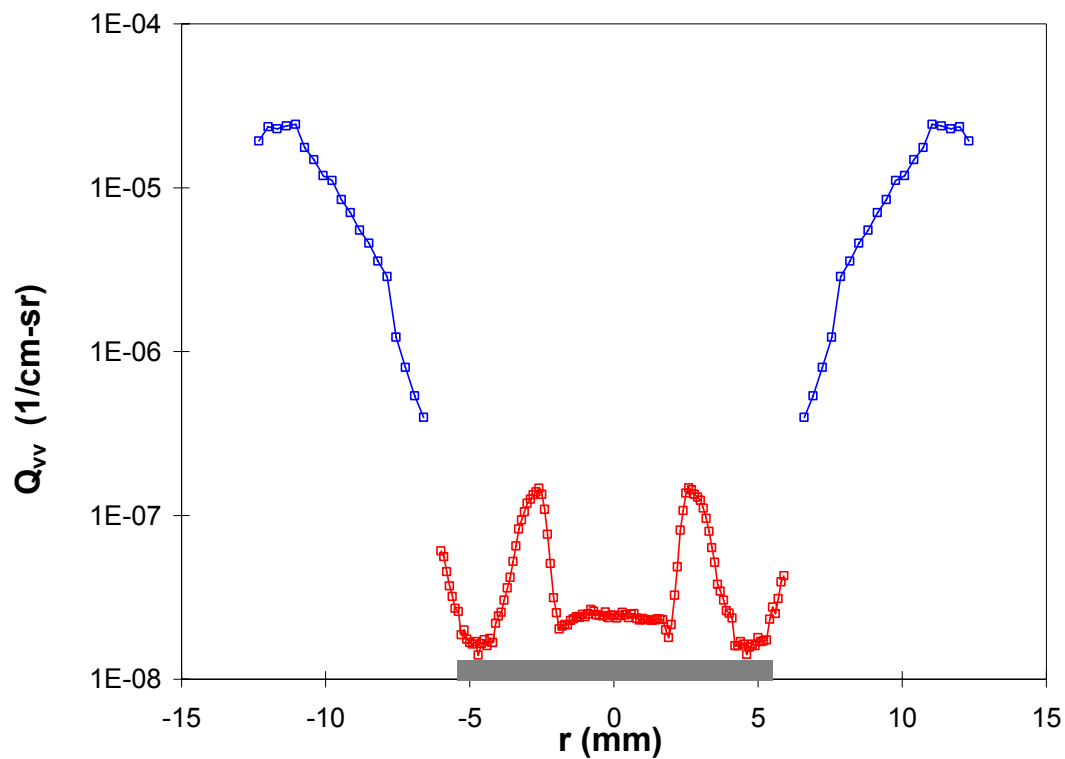
Fig. 22. Scattering cross section Q_{vv} as a function of the radial distance r from the burner centerline at 7 mm height in stoichiometric CH$_4$-air flame with 200 µL/L of Fe(CO)$_5$ (from [41]).
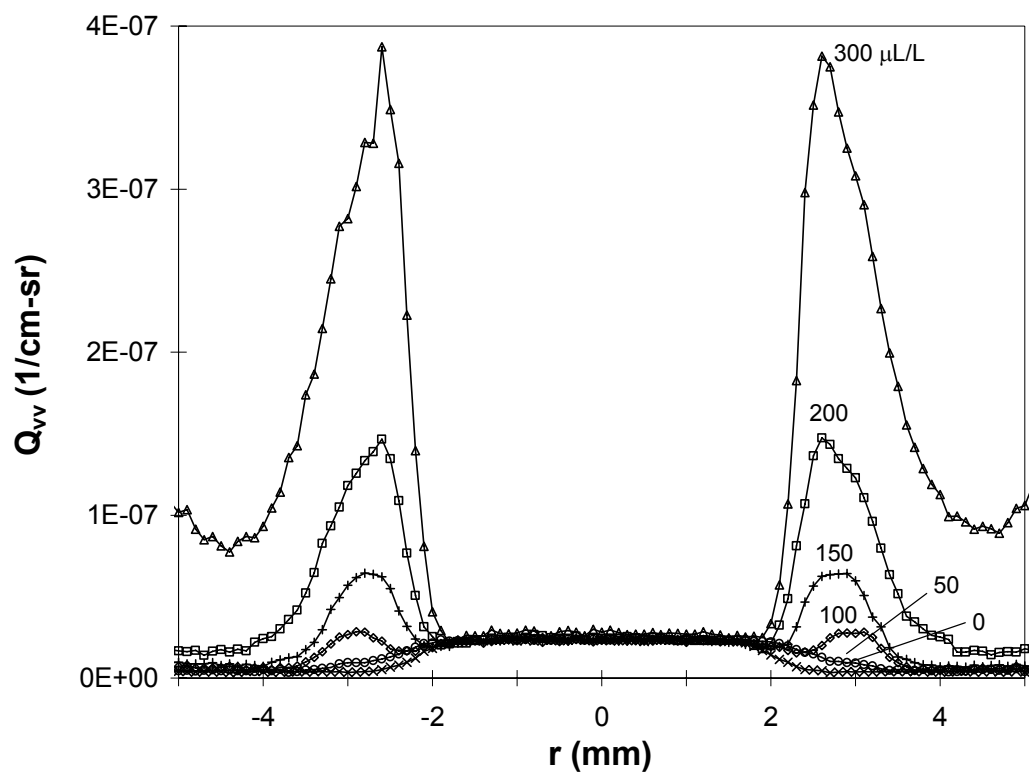
Fig. 23. Measured scattering cross section through a stoichiometric CH$_4$-air flame 7 mm above the burner rim at various inhibitor volume fractions (from [41]).
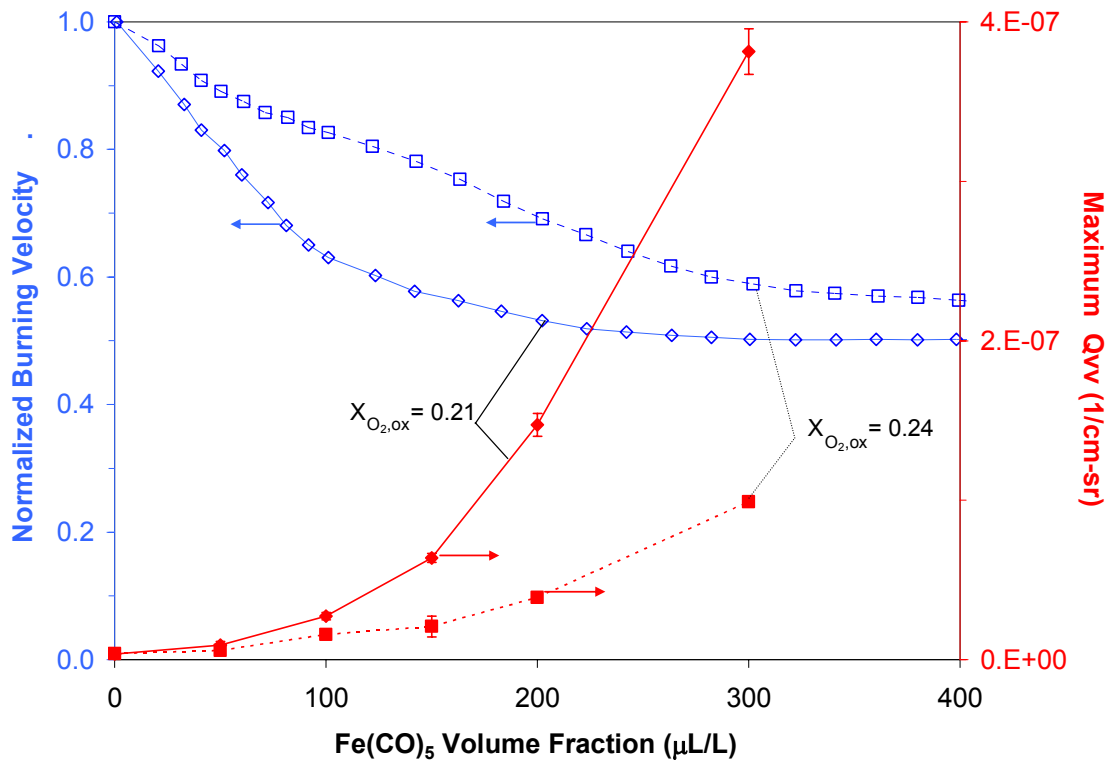
Fig. 24. Normalized burning velocity [9] and maximum Q_{vv} for ϕ=1.0 CH$_4$ flame with $X_{O_2,ox}$ = 0.21 and 0.24 [41].

Fig. 25. Maximum scattering signal and normalized burning velocity [74] for CO-H$_2$ flames as Fe(CO)$_5$ concentration varies [41]).
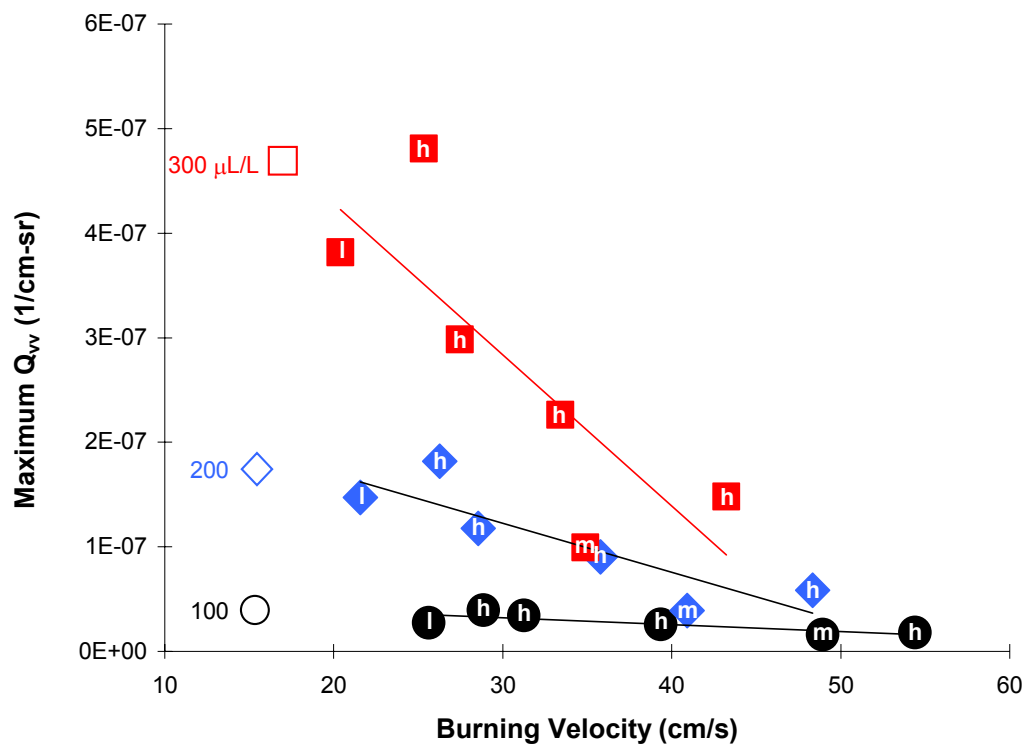
Fig. 26. Maximum Q_{vv} for flames of CH_4 (open symbols) and CO (closed symbols) as a function of the burning velocity. The letters correspond to the adiabatic flame temperature (<u>l</u>ow, <u>m</u>edium, and <u>h</u>igh, 2220, 2350, and 2470 K), while the symbol shape (square, diamond, and circle) corresponds to the loading of $Fe(CO)_5$: (100, 200, and 300) $\mu L/L$ [41].

:\Home\Greg\Paper Archive\Combustion and Flame\CNF Particles in Premixed Flames with Fe(CO)5\Calculations\ Data of 032999 CH4-air.xls **Sheet: Qvv vs. SL newcolor**
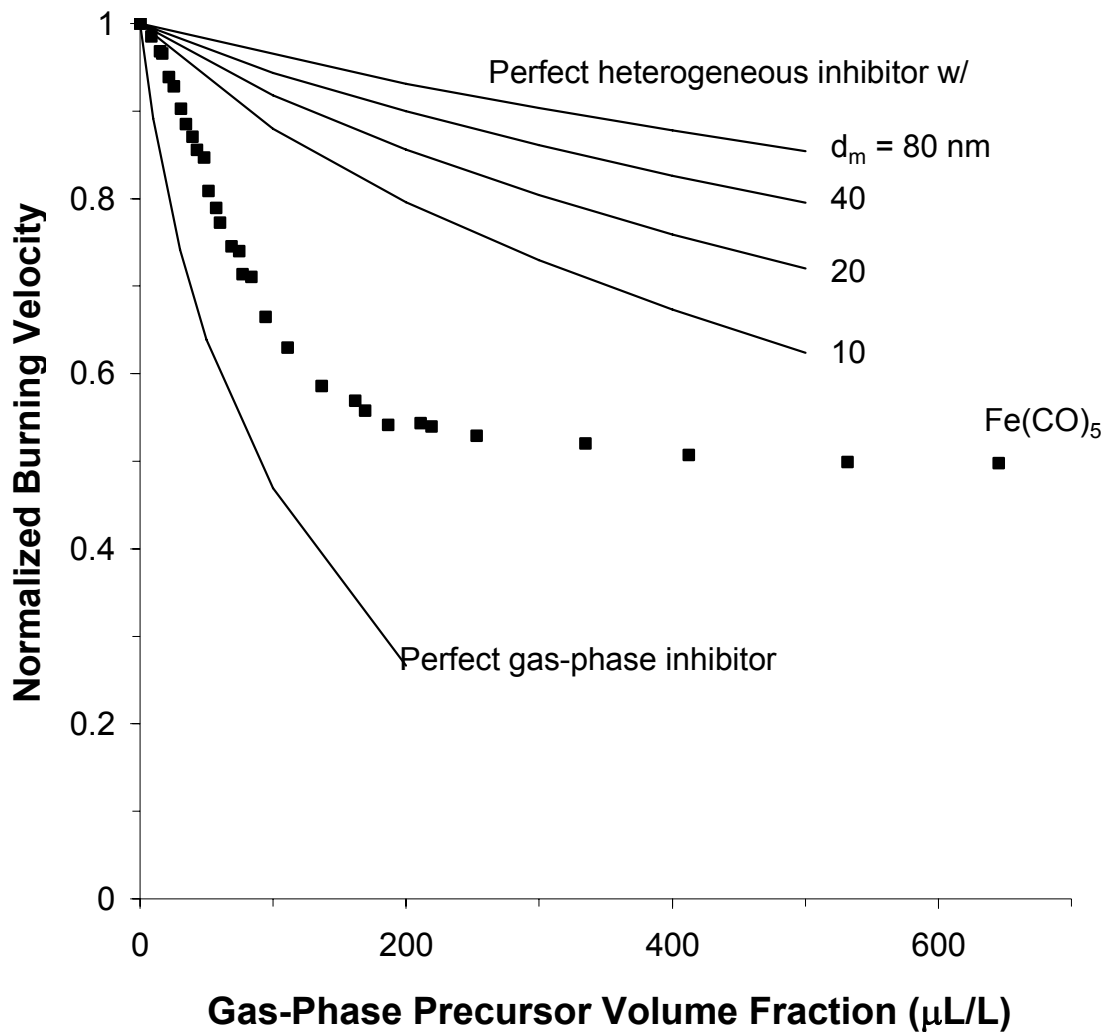
Fig. 27. Calculated normalized burning velocity for several diameters d_m of ideal heterogeneous inhibitor. Also shown are $Fe(CO)_5$ data and calculated normalized burning velocity using the perfect gas-phase inhibitor mechanism [41].

..\..\Paper Archive\Combustion and Flame\CNF Particles in Premixed Flames with Fe(CO)5\Calculations\Perfect Heterogeneous Inhibitor.xls
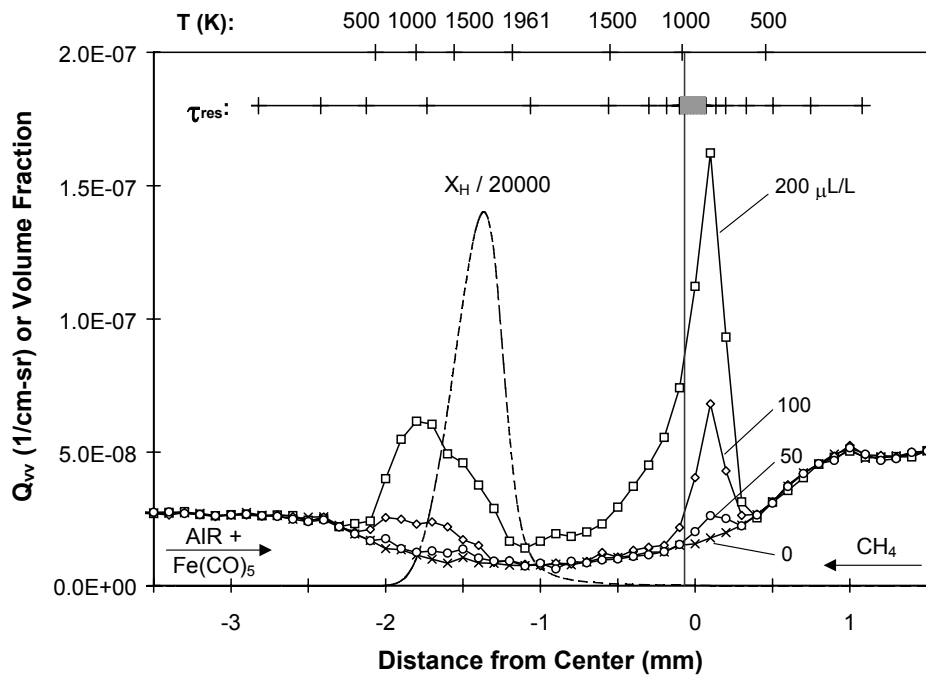
Fig. 28. Methane-air counterflow diffusion flame with inhibitor in the oxidizer. Shown are the calculated temperature (upper scale), stagnation plane location (vertical line), and H-atom volume fraction (dashed line) for the uninhibited flame, and the measured scattering profiles (connected points) for $Fe(CO)_5$ volume fractions of (0, 50, 100 and 200) µL/L in the air stream ($a = 330$ s^{-1} , which is 50 % of a_{ext} for the uninhibited flame and 77 % of a_{ext} for $X_{in} = 200$ µL/L). The estimated residence time for 5 nm particles is shown as 10 ms intervals in the hatched line near the top [45].
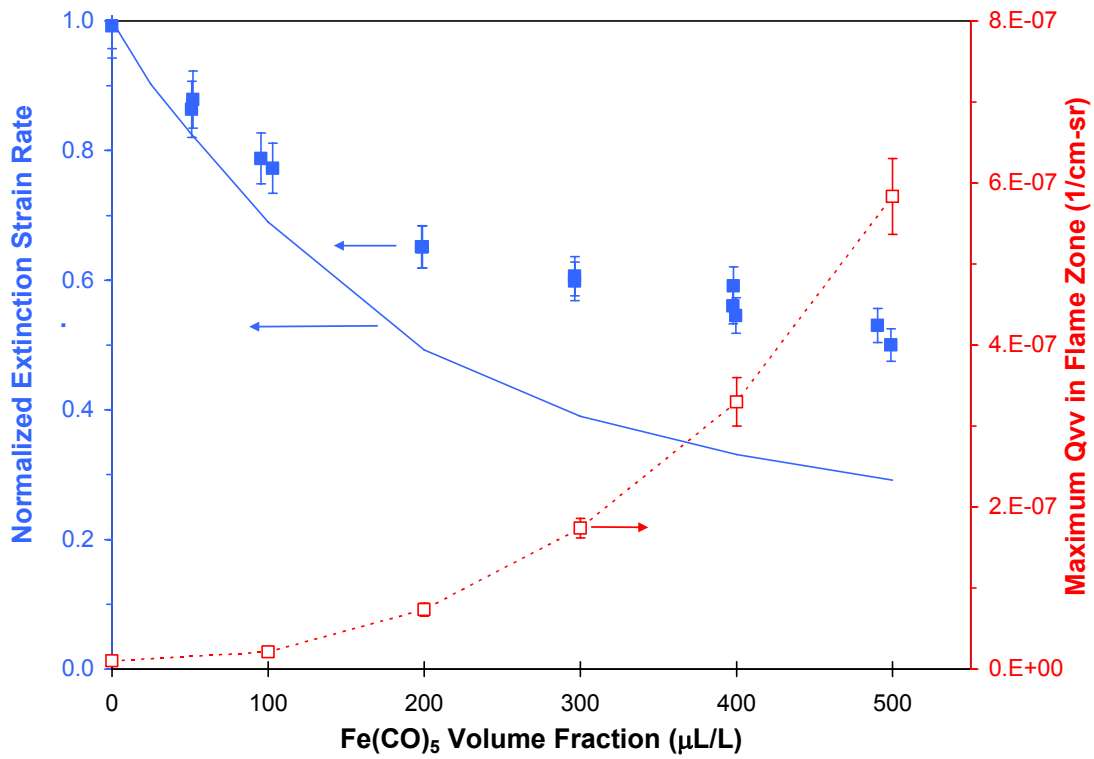
Fig. 29. Correlation between inhibition effect and maximum Q_{vv} . Filled points are experimental normalized a_{ext} , solid line is calculated a_{ext} ([43]). Open symbols connected by dotted lines are maximum measured Q_{vv}. Particle data collected at 75 % of a_{ext} [45].

I:\Home\Greg\Paper Archive\Combustion and Flame\CNF Counterflow Particles\Excel files\Data of 022499 FO-IO 75% scatter sheet: FO-IO wss
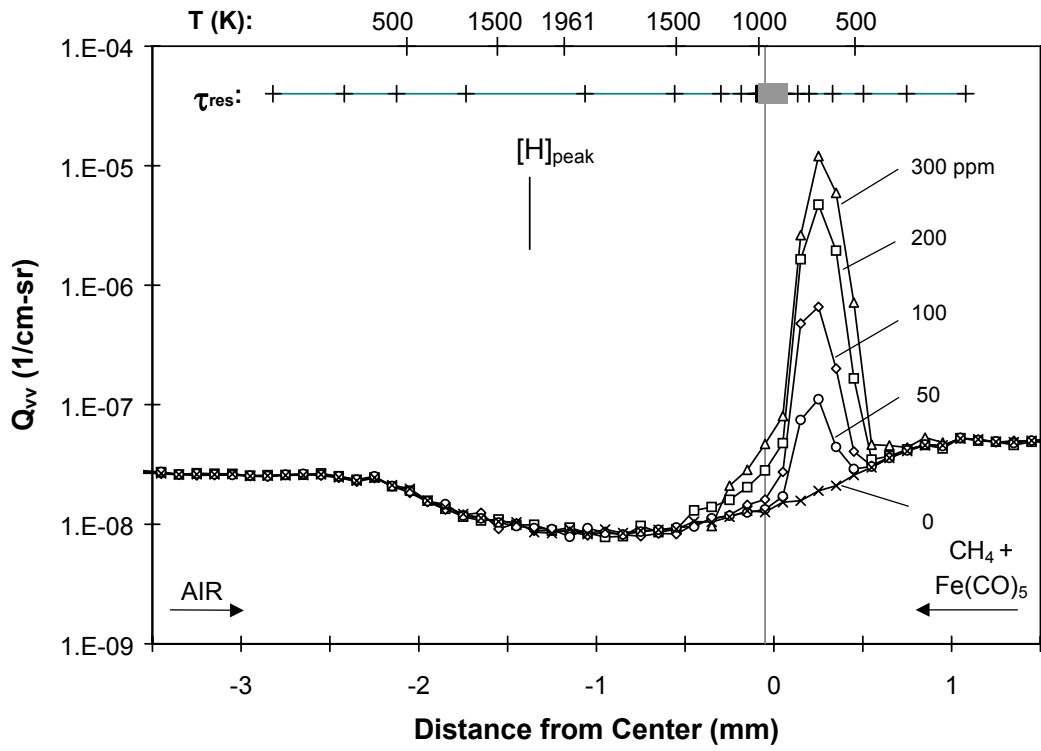
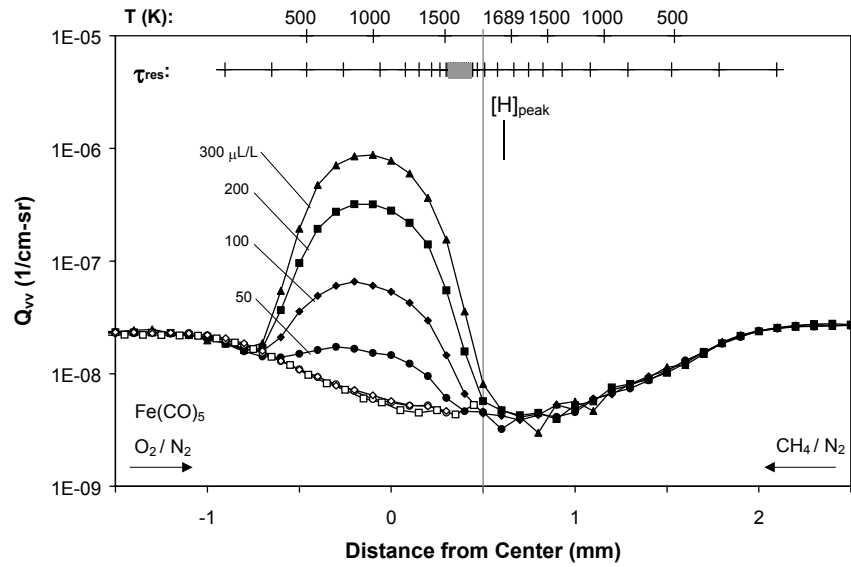**Fig. 30. Measured scattering profiles in CH$_4$-air counterflow diffusion flame with inhibitor in the fuel. The calculated temperature and point of peak H-atom mole fraction are marked on the upper x-axis, and the vertical line denotes the calculated location of the stagnation plane. Strain rate = 330 s^{-1} [45].**
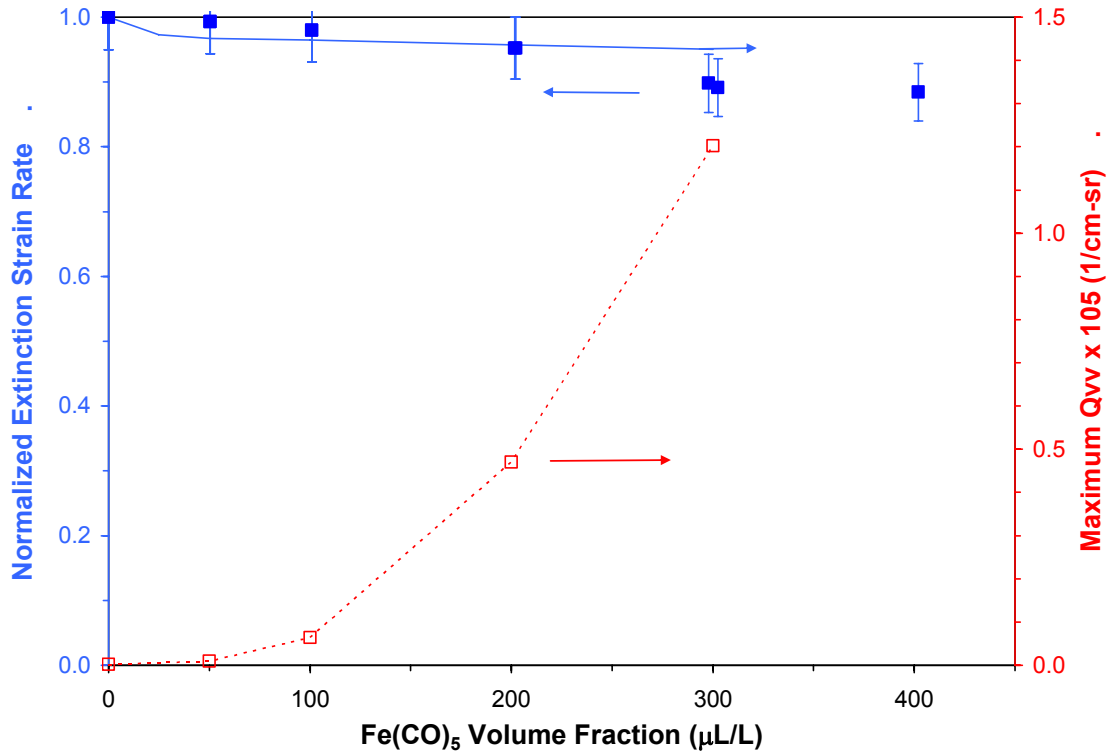
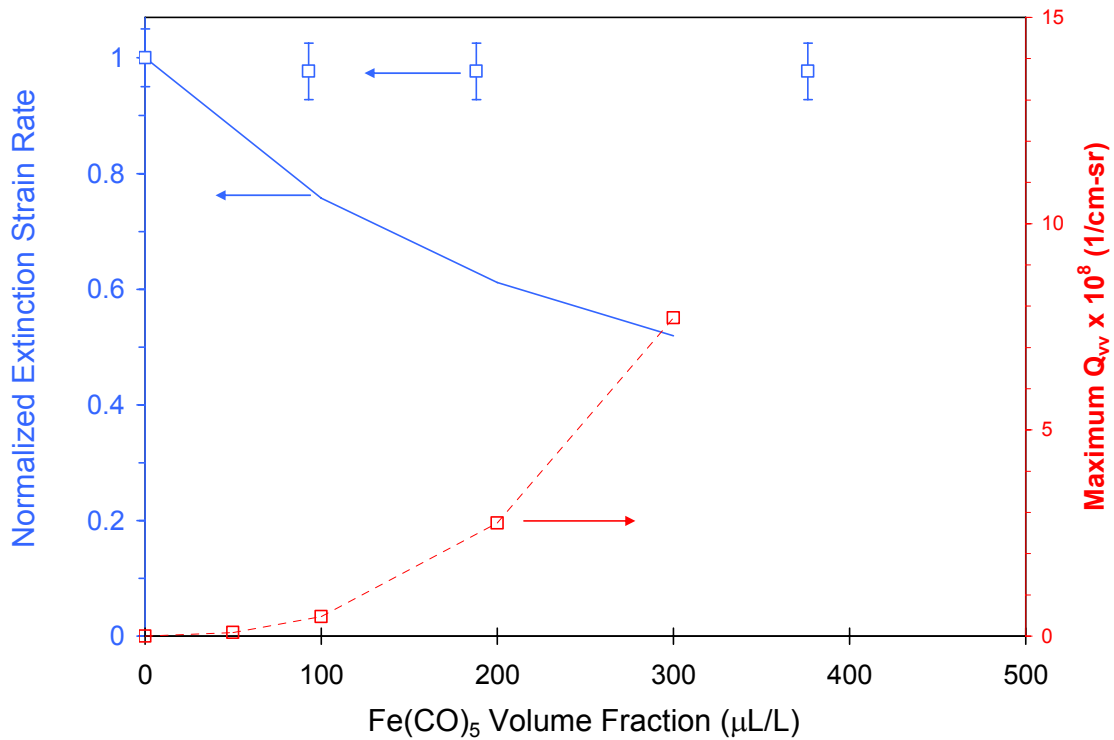**Fig. 31. Effect of Fe(CO)$_5$ added to the fuel stream of a methane-air counterflow diffusion flame. The experimentally measured and numerically calculated normalized extinction strain rate [43] are shown (left axis) as a function of Fe(CO)$_5$ volume fraction in the fuel stream. The maximum scattering cross section (right axis), obtained from the results in Fig. 30 is also shown for increasing X$_{inh}$.**

I:\Home\Greg\Paper Archive\Combustion and Flame\CNF Counterflow Particles\Excel files\Data of 022299 FO-IF Scatter.xls sheet: FO-IF wss
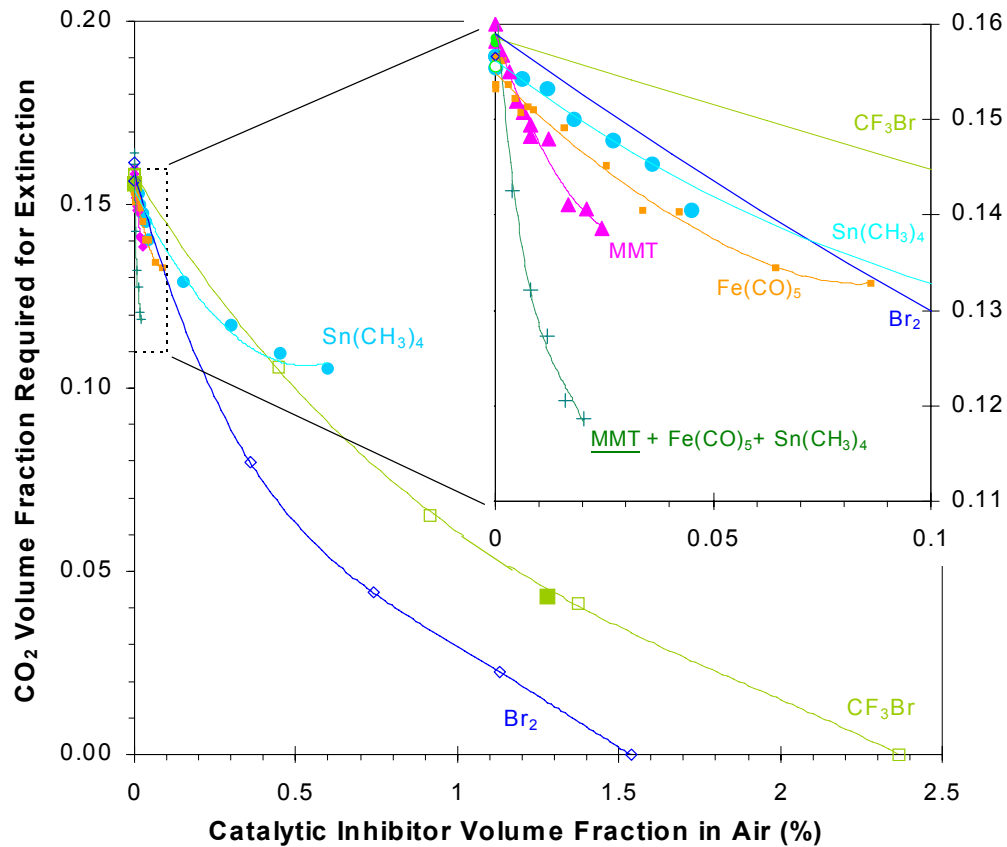
Fig. 32. Scattering profiles through a counterflow diffusion flame of 30 % O_2/70 % N_2 and 80 % CH_4/N_2. The calculated temperature and point of peak H-atom mole fraction are marked on the upper x-axis, and the vertical line denotes the calculated location of the stagnation plane. $Fe(CO)_5$ is added to the oxidizer stream at the indicate volume fraction. The estimated residence time for 5 nm particles is shown as 10 ms intervals in the hatched line near the top [45].

Fig. 33. Effect of Fe(CO)$_5$ added to the air stream of a diluted methane-air counterflow diffusion flame. The experimentally measured (points) and numerically calculated (solid line) normalized extinction strain rate [43] are shown (left axis) as a function of Fe(CO)$_5$ volume fraction in the air stream. The maximum scattering cross section (right axis), obtained from the results in Fig. 30 is also shown for increasing X$_{inh}$ [50].

I:\Home\Greg\Paper Archive\Combustion and Flame\CNF Counterflow Particles\Excel files\Data of 020199 FF-IO, IF, 75% scatter.xls sheet: FF-IO plot wss

Fig. 34. Volume fraction of CO_2 required for extinction ($X_{CO_2,ext}$) of methane-air cup burner flames as a function of the volume fraction of catalytic inhibitor added to the air stream. Inset shows region in dotted box with expanded scales (Points: experiments; lines: curve fits) [113].
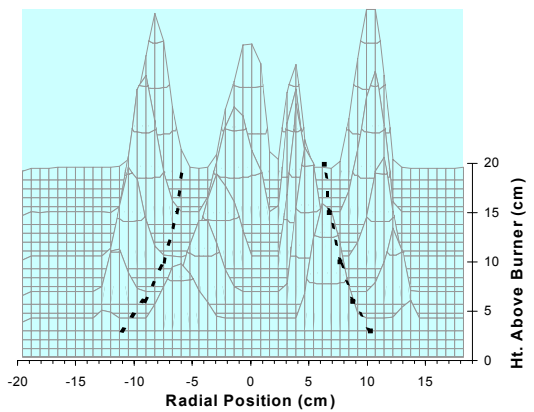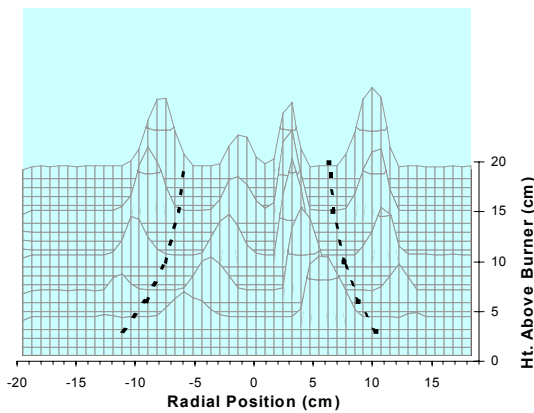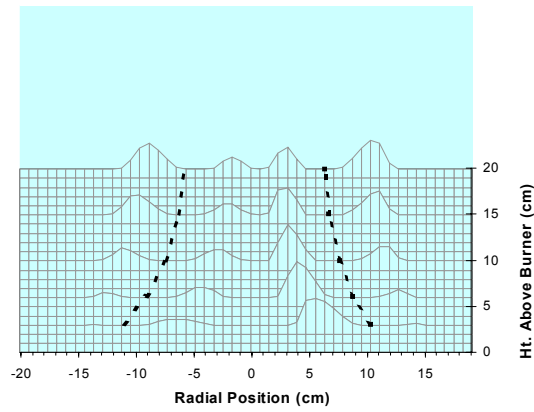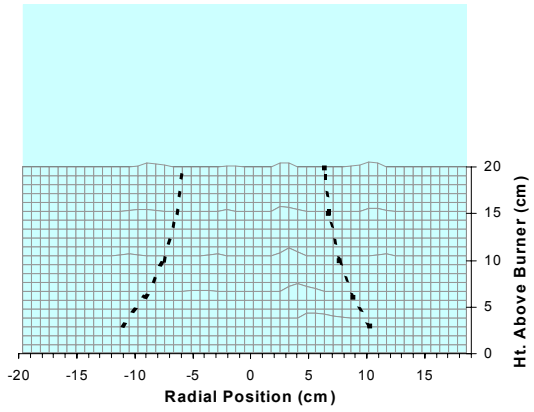
Fig. 35. Scattering cross section for laser light at 488 nm as a function of radial position and height above burner in methane-air cup-burner flame with 8 % CO_2 and $Fe(CO)_5$ in air at specified volume fraction . Dotted lines show flame location from a digitized video image of the uninhibited flame [113]. Top to bottom frames have (100, 200, 325, and 450) $\mu L/L$ of $Fe(CO)_5$, respectively.
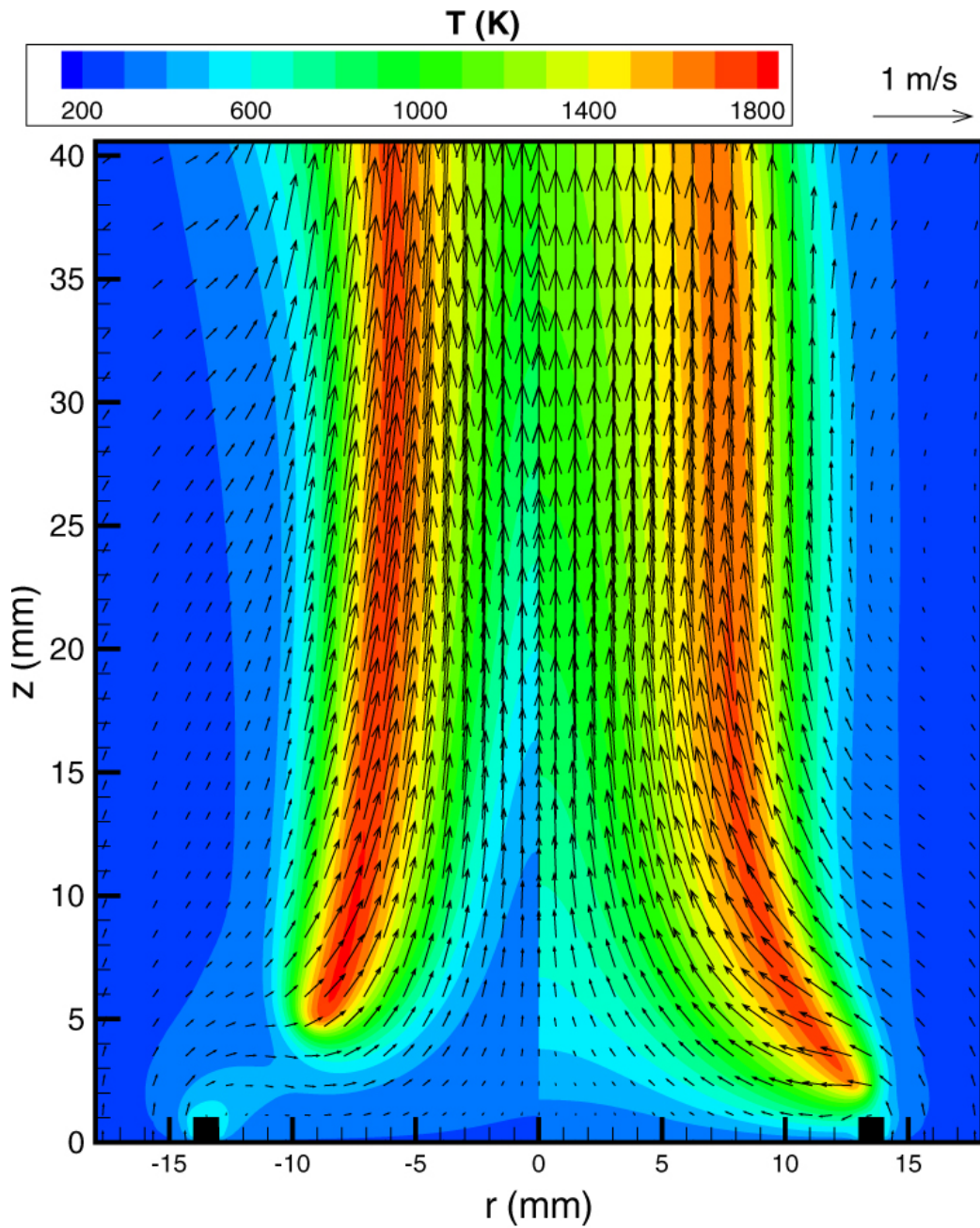
.

Fig. 36. Calculated temperature (color scale) and velocity vectors (arrows) for methane-air cup-burner flame with an oxidizer stream CO_2 volume fraction of 10 %, with (left) and without (right) an added $Fe(CO)_5$ volume fraction of 100 μL/L [113].
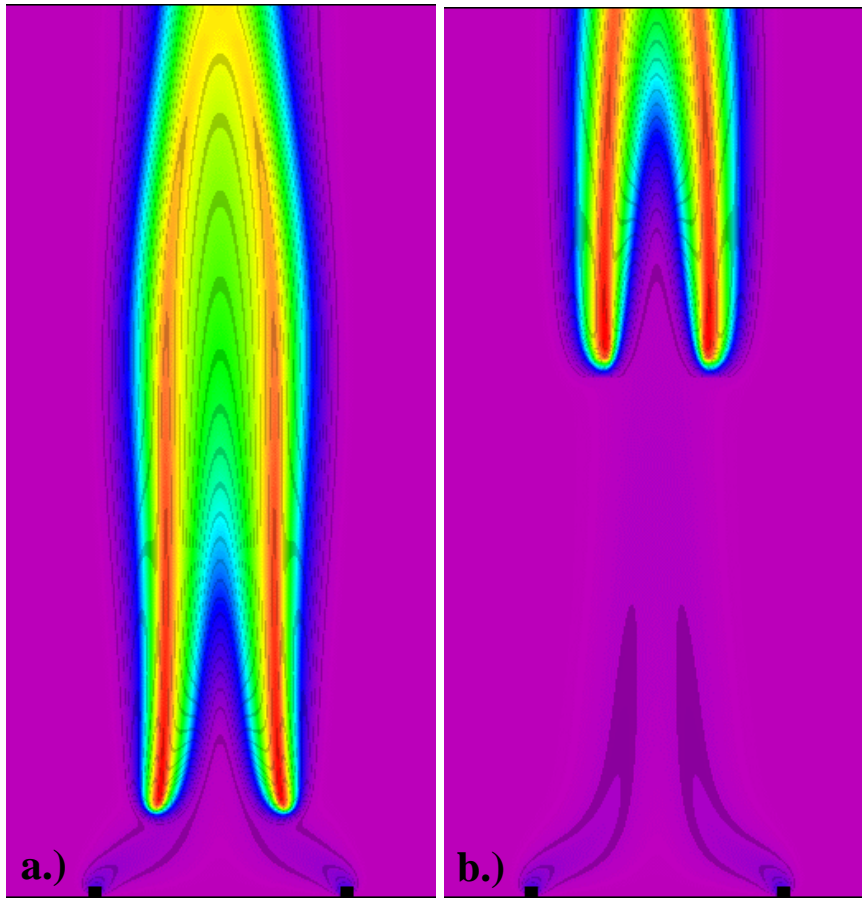
Fig. 37. Two-D color map of calculated temperature in cup-burner methane-air flames with 10 % CO_2 in the oxidizer stream, and a.) 0.011 and b.) 0.012 % $Fe(CO)_5$ volume fraction in the air stream, illustrating the blowoff phenomenon [113].
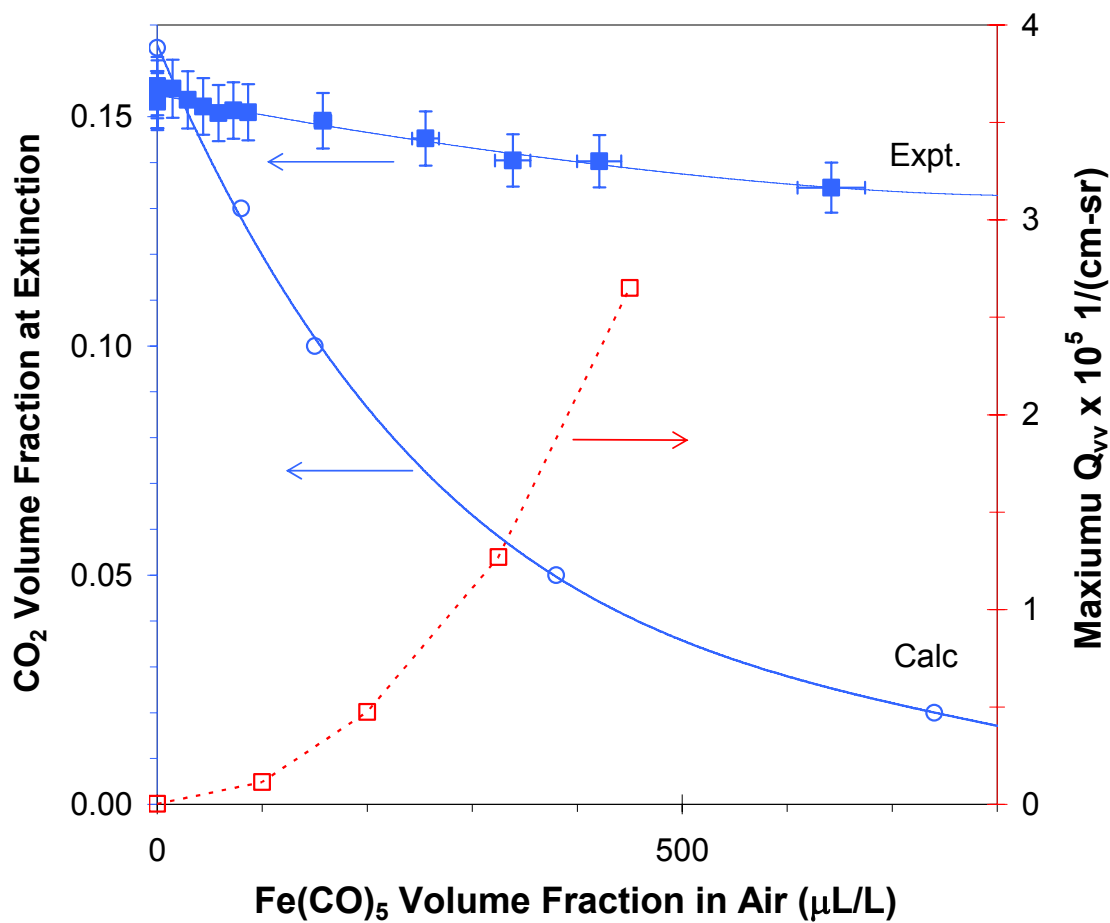
Methane-Air Cup Burner

Fig. 38. Experimental and numerically predicted extinction volume fraction of CO_2 (left axis) and peak measured scattering cross section (right axis), as a function of the volume fraction of $Fe(CO)_5$ in the air stream; [113,138].
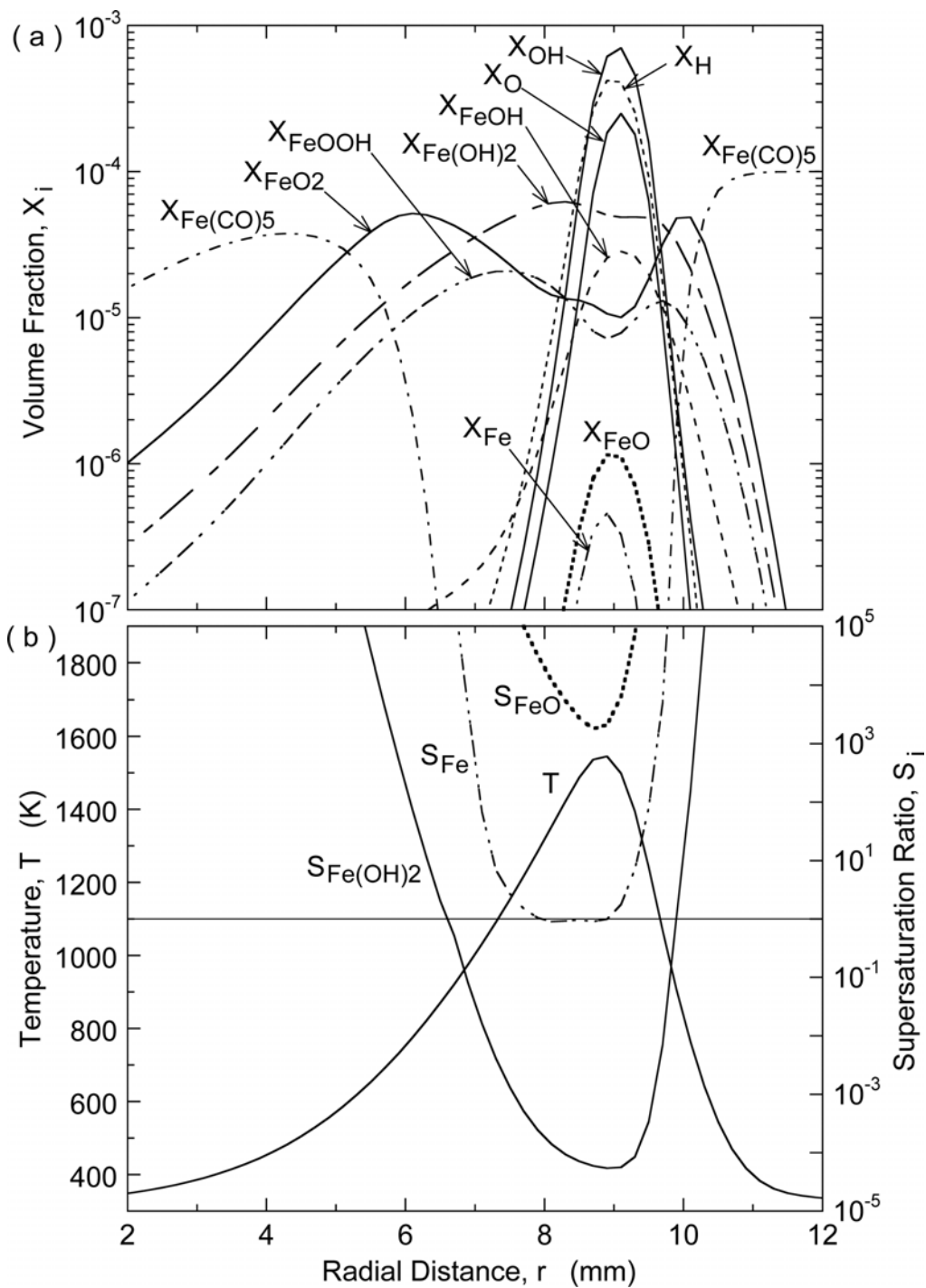
Fig. 39 a). Calculated iron-containing and major species volume fraction X_i as a function of radial position at the height above the burner of 4.8 mm (corresponding to the location of the reaction kernel in the flame base); and b). the super-saturation ratio, S_i, for Fe, FeO, and Fe(OH)$_2$ [113].
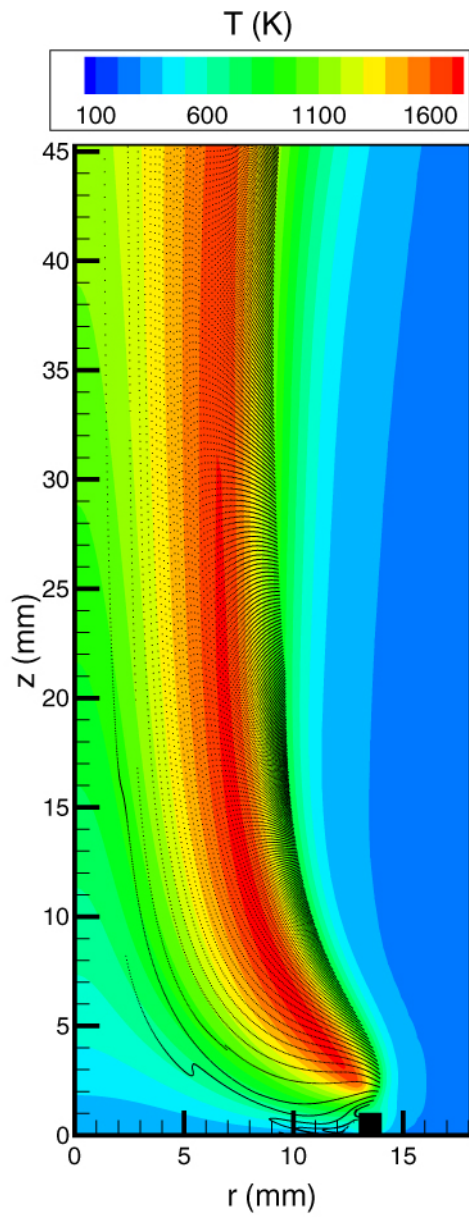
Fig. 40. Calculated particle trajectories for free-molecular-regime particles in a CH4 – air flame with 10 % CO_2 in the oxidizer stream [113].
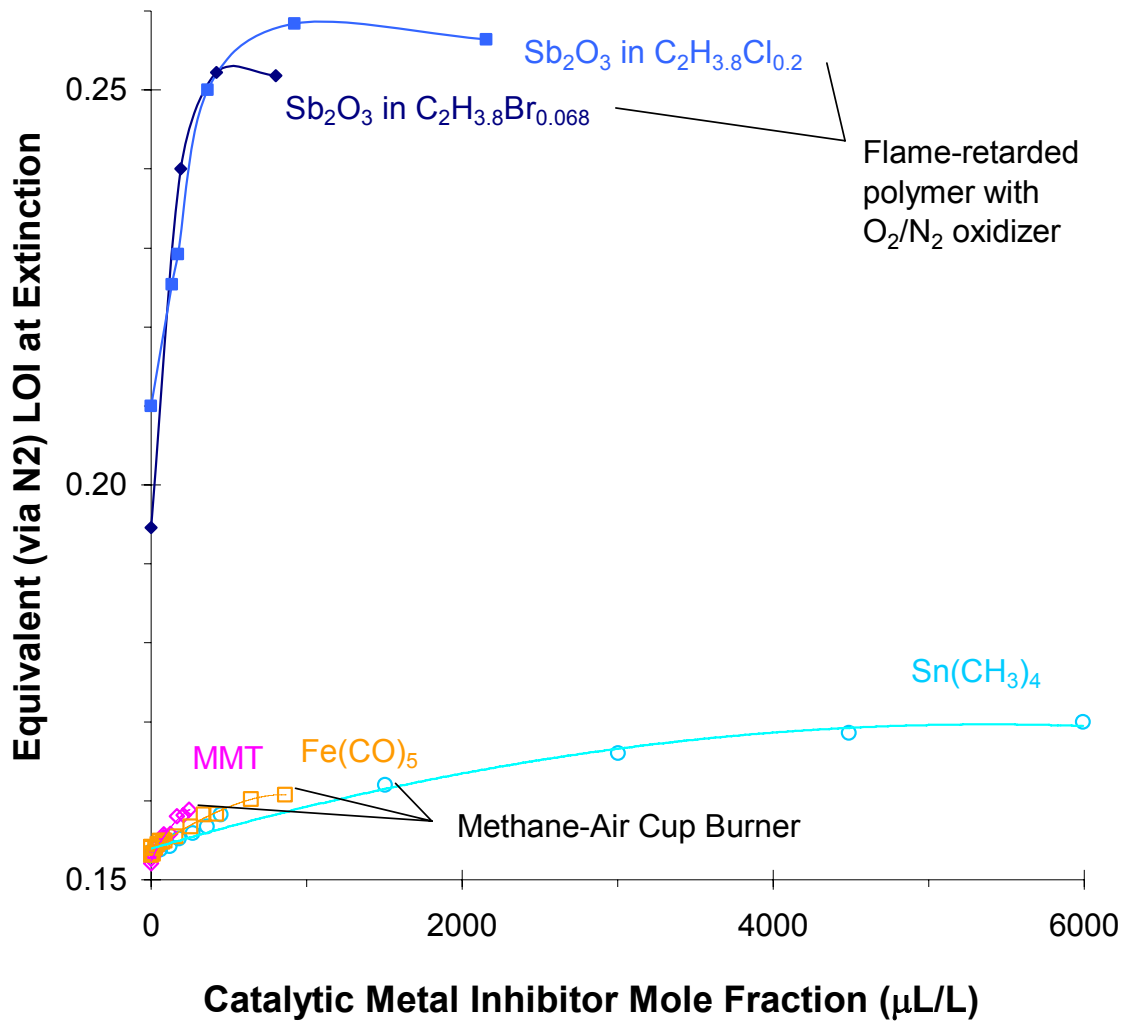
Fig. 41. Equivalent N_2/O_2 limiting oxygen index for extinction of polyethylene (PE) halogen blends or methane-air cup burner flames with MMT, $Fe(CO)_5$, and $Sn(CH_3)_4$ [152].

I:\Home\Greg\Current Research\Tania's cup Burner\cupburner.xls
sheet: Sb2O3 PECS